UNIVERSIDAD DE INVESTIGACIÓN DE TECNOLOGÍA EXPERIMENTAL YACHAY

ESCUELA DE CIENCIAS QUÍMICAS E INGENIERÍA

FOOD PACKAGING FILMS PREPARED FROM BIOPOLYMER REINFORCED AND LOADED WITH SILVER NANOPARTICLES

Trabajo de titulación presentado como requisito para la obtención del título de Máster en Ciencias Químicas con mención en Ciencia e Ingeniería de los Materiales

Autor

Quím. Araceli Granja Alvear

Tutor:

PhD. Floralba López

Co-Tutor:

PhD. Juan Pablo Saucedo

Urcuquí, septiembre 2024

Autoría

AUTORÍA

Yo, **GRANJA ALVEAR LOURDES ARACELI**, con cédula de identidad 1003444039, declaro que las ideas, juicios, valoraciones, interpretaciones, consultas bibliográficas, definiciones y conceptualizaciones expuestas en el presente trabajo; así cómo, los procedimientos y herramientas utilizadas en la investigación, son de absoluta responsabilidad del autor del trabajo de titulación.

Así mismo, me acojo a la normativa interna de la Universidad de Investigación de Tecnología Experimental Yachay.

San Miguel de Urcuquí, abril 2024

Firmado electrónicamente por:
**LOURDES ARACELI
GRANJA ALVEAR**

_____
Lourdes Araceli Granja Alvear
CI: 1003444039

Autorización de Publicación

AUTORIZACIÓN DE PUBLICACIÓN

Yo, **LOURDES ARACELI GRANJA ALVEAR,** con cédula de identidad 1003444039, cedo a la Universidad de Tecnología Experimental Yachay, los derechos de publicación de la presente obra, sin que deba haber un reconocimiento económico por este concepto. Declaro además que el texto del presente trabajo de titulación no podrá ser cedido a ninguna empresa editorial para su publicación u otros fines, sin contar previamente con la autorización escrita de la Universidad.

Asimismo, autorizo a la Universidad que realice la digitalización y publicación de este trabajo de titulación en el repositorio virtual, de conformidad a lo que dispone la Ley Orgánica de Educación Superior

San Miguel de Urcuquí, julio 2024

Firmado electrónicamente por:
LOURDES ARACELI
GRANJA ALVEAR

Lourdes Araceli Granja Alvear
CI: 1003444039

Dedicatoria

Este trabajo va dedicado a mi familia, por todo el apoyo incondicional que he recibido para poder culminar este paso académico, principalmente a la niña que motiva cada cosa que hago; mi hija Dannita, a mi esposo Víctor por ser un gran apoyo en todos los sentidos; A mi mami, a mi hermana Lore, por estar siempre con un consejo y cuidándome, a mi hermana Diany por estar para mí para cualquier cosa y en cualquier momento. Y una dedicatoria especial para mi abuelita Piedacita, que me hace tanta falta y que estoy segura que se sentiría muy orgullosa de mi.

Araceli Granja Alvear

Agradecimiento

Resumen

En este proyecto de investigación se estudió el desarrollo de nuevas películas de empaque de alimentos utilizando biopolímeros, como pectina y carboximetil celulosa (CMC), los cuales fueron químicamente modificados y cargados con nanopartículas de plata (AgNPs). Estas nanopartículas fueron sintetizadas mediante métodos de química verde utilizando extracto de corteza de canela como agente reductor, con el propósito de garantizar sostenibilidad del material preparado. Este estudio pretende generar soluciones de empaque que extiendan la vida útil de frutas de la región, aprovechando además las propiedades antimicrobianas de las nanopartículas de plata. La investigación incluye la preparación y caracterización de diversas formulaciones de películas. Los nanocompositos obtenidos se sometieron a análisis y caracterización química para determinar sus cambios estructurales, también se sometieron a ensayos físicos para determinar sus propiedades mecánicas y permeabilidad al vapor de agua. Los principales hallazgos destacan el potencial de estas películas para servir como materiales de empaque de alimentos efectivos, ofreciendo mejoras significativas en la estabilidad térmica, propiedades mecánicas y de barrera y la eficacia a antimicrobiana que se encuentra debido a que las AgNPs inhibieron efectivamente el crecimiento de bacterias Gram-positivas y Gram-negativas. La adición de AgNPs y albúmina de huevo también mejora la estabilidad térmica de las películas, según los análisis TGA, donde las películas con AgNPs mostraron una mayor resistencia a la degradación térmica. Las formulaciones combinadas de pectina y CMC presentaron mejores propiedades de barrera al vapor de agua, con valores de WVP más bajos en comparación con las películas de pectina pura, lo que demuestra una mejor barrera contra la humedad. Las pruebas de vida útil mostraron que las frutas recubiertas con las películas con nanopartículas de plata embebidas se mantuvieron frescas por un período más prolongado.

Palabras Clave:

Nanocompositos, Empaques de Frutas, Nanopartículas de plata, Canela, Cinamaldehído Propiedades Antibacteriales.

Abstract

This research project studied the development of new food packaging films using biopolymers, such as pectin and carboxymethyl cellulose (CMC), which were chemically modified and loaded with silver nanoparticles (AgNPs). These nanoparticles were synthesized by green chemistry methods using cinnamon bark extract as a reducing agent, with the purpose of guaranteeing sustainability of the prepared material. This study aims to generate packaging solutions that extend the shelf life of fruits of the region, also taking advantage of the antimicrobial properties of silver nanoparticles. The research includes the preparation and characterization of various film formulations. The nanocomposites obtained were subjected to analysis and chemical characterization to determine their structural changes, they were also subjected to physical tests to determine their mechanical properties and water vapor permeability. The main findings highlight the potential of these films to serve as effective food packaging materials, offering significant improvements in thermal stability, mechanical and barrier properties, and antimicrobial efficacy found because the AgNPs effectively inhibited the growth of Gram-positive and Gram-negative bacteria. The addition of AgNPs and egg albumin also improves the thermal stability of the films, according to TGA analyses, where films with AgNPs showed greater resistance to thermal degradation. The combined pectin and CMC formulations presented better water vapor barrier properties, with lower WVP values compared to pure pectin films, demonstrating a better moisture barrier, shelf life tests showed that the Fruits coated with these films stayed fresh for a longer period.

Key Words:

Nanocomposites, Food Packaging, Silver Nanoparticles, Cinnamon, Cinnamaldhyde, Antibacterial

Contents

TABLES

FIGURES

1 INTRODUCTION

1.1 Problem Statement

Ecuador is among the 17 most megadiverse countries in the world, according to the United Nations Educational, Scientific, and Cultural Organization (UNESCO, National Geographic 2024).[1] Despite being a very small country, its privileged geographical location and extraordinary diversity of endemic species, impressive landscapes, and lush vegetation it houses make Ecuador the most biodiverse country per unit of surface area in the world.[2] Its natural wealth includes exotic fruits such as, naranjilla, golden berry, banana-passion fruit, and sapote, to name a few. Internationally, Ecuadorian bananas and cocoa have gained widespread acceptance, becoming the country's most exported traditional products. However, other fruits have not yet entered the foreign market.

According to the Boletín de Cifras de Comercio Exterior, Ministry of Production, Ecuador for February 2024, there has been significant growth in the top 10 non-traditional products, highlighting the leadership of other fruits.[3] In 2023, fresh dragon fruit exports from Ecuador reached a historic milestone, exceeding USD 172 million, according to the Banco Central del Ecuador (BCE).[3] This achievement has consolidated dragon fruit as one of the main non-traditional products exported by the country, according to the Ministry of Production of Ecuador. The United States is the primary market, absorbing 80% of Ecuadorian production, followed by Hong Kong, Spain, Peru, and Canada. Dragon fruit production is essential for about 15,000 families in Ecuador, especially in the Morona Santiago Province. This fruit holds certifications of Denomination of Origin, Good Agricultural Practices, and international certifications such as Global Gap.[3]

The record in exports reflects the potential and quality of the Ecuadorian agricultural sector and its capacity to satisfy the demands of the international market with high-quality and value-added products. However, it also highlights the significant challenges that this sector must overcome, given the strict national and international certification requirements for products like dragon fruit to enter these markets. One of the most important challenges that must be solved to further improve the export quality of agricultural products is the preservation of product quality, which is threatened by different factors during transport and storage. The most common factors contributing to food spoilage are oxidation, bacterial, and fungal contamination, each operating through distinct mechanisms. To overcome the challenges posed by these spoilage processes, it is

crucial to use materials that can effectively safeguard food from these threats, thereby extending its shelf life and preserving product quality.

1.2 Justification

One of the strategies to protect foods from physical and chemical damage is their coating with biocompatible films with antimicrobial activity. For this purpose, several studies have been developed on new composite materials, and they are constantly growing. For example, in 2022, Macieja and co-workers reported the preparation of films based on bioactive carboxy methyl cellulose (CMC) modified with melanin and silver nanoparticles (AgNPs),[4] they explored the effect of CMC substitution on the in-situ synthesis of AgNPs and the functional properties of the films, with promising applications in food packaging. In 2023, Akyüz and co-workers reported research on the use of locust bean gum coatings loaded with silver nanoparticles to extend the shelf life of fruits.[5] Their study concluded that coating fruits with an AgNPs-LBG solution has significant potential for use in the fruit industry to extend the shelf life of the products.

This study is aimed to produce biocompatible food packaging films based on AgNPs/pectin/CMC with enhanced mechanical and antimicrobial properties.

1.3 Objectives

General Objective

The purpose of this study is to develop biopolymer-based films loaded with silver nanoparticles to be used as food packaging for regional fruits.

Specific Objectives

- Develop formulations for films incorporating biopolymers (pectin and CMC) and reinforcing additives with convenient mechanical properties for food packaging.
- Synthesize silver nanoparticles by green chemistry methods using cinnamon bark extract as a dual function reducing and capping agent, characterizing their morphological and antibacterial properties.
- Load silver nanoparticles into the optimized film formulations to impart antimicrobial properties.

- Characterize the resulting nanocomposite materials by analyzing their properties, composition, structure, and behavior.
- Verify the efficacy of the prepared antimicrobial nanocomposite films on regional fruits by comparing the shelf life of two covered and uncovered specimens.

2 THEORETICAL BACKGROUND

2.1 Food Packaging

Different types of packaging are used for fruits and vegetables, each tailored to meet specific requirements depending on the type of product and its destination.[6,7] Boxes for fruits and vegetables are widely used for their transport and storage due to their high rigidity, resistance to tearing and low moisture absorption, making them ideal for products such as cherry tomatoes, cucumbers, peppers, apples, strawberries and endives. Some fruits and vegetables require plastic, mesh or jute bags for enhanced protection and preservation. Selecting packaging materials many factors should be considered, including cost, quality of products, and their ability to maintain product freshness. A few common materials used in food packaging are plastics, paper, glass, and metals. Among these, a wide variety of plastics are used in rigid or flexible food packaging.[7,8] Various alternatives have been proposed based on the required functionality, because of research focused on the food industry, considering basic requirements such as low environmental impact and low production cost.[6,8]

Plastic bags, often made of low-density polyethylene and sometimes with micro perforations to allow breathing are used for both whole fruits (such as strawberries, apples or carrots) and cut fruits (salads, sliced cucumber, etc).[9] Various types of packaging satisfy different needs in the fruit and vegetable industry. These materials are often petrochemical-based non-degradable plastics that if disposed of in landfills will impair the ecosystem.[6,8]

Regarding packaging and coatings for export fruits, there are several options to guarantee the quality and safety of the products during transport and storage. Heat-shrink packages offer enhanced protection for individual fruits or small groups, helping to maintain freshness and reduce dehydration.[10–12] Flexible packaging with multi-layer films and oxygen barriers protects against oxygen entry and moisture loss, especially suitable for delicate fruits such as grapes, berries and kiwis.[5,13] Pouch bags for vacuum packaging extend the shelf life of cut or whole fruits, while cold-resistant polyethylene freezer bags maintain the quality of fruits intended for export as frozen products, maintaining quality and preventing the formation of ice crystals.[12] Watering bags, plastic bags filled with water, are strategically placed around the fruits to maintain moisture and freshness during

transport. Additionally, light barrier mulches not only protect fruits during growth and harvest, but also contribute to weed control and soil moisture retention.

Growing global concern about pollution from plastic uses has driven the development of green technologies for food packaging, including biodegradable polymers, edible films and coatings, as well as smart packaging.[8,14] A variation has been noted during the year 2023 and so far in 2024, where there is a trend towards greater use of compostable materials in response to this ecological demand. For example, several companies in the sector have introduced bottles made from plant-based materials and edible packaging, which reduce environmental impact and offer attractive and innovative experiences for consumers.[15]

For producers it is important to explore new technologies but without forgetting about sustainability, for this they are increasing the use of recyclable or biodegradable products to create efficient, safe and sustainable packaging. For example, they are adopting 3D printing to create personalized packaging, in addition to using artificial intelligence to improve food traceability.[15]

2.2 Food Coating

Food coatings are thin, usually transparent layers applied to the surface of food for various purposes. Some studies have suggested the use of polysaccharides, lipids, proteins and biopolymers as precursors for food coating films, particularly fruits and vegetables, since in addition to being an eco-friendly alternative, it can improve food quality and extend shelf life.[8,16,17] These coatings serve as barriers against water loss and regulate gas exchange. They also act as antioxidants and antimicrobials, extending the shelf life of fruits, improving their visual appearance, and protecting them against physical damage and microbiological contamination. Widely used in both fresh and processed fruits, these coatings play an important role in preserving quality and freshness in the food industry.[8,13]

There are both edible and non-edible coatings available for fruits, each serving distinct purposes based on their application and function. Edible coatings are thin layers of food-grade materials applied directly onto the fruit surface. Their primary role is to protect the fruit by reducing moisture loss, and they can incorporate plant extracts for antimicrobial properties and UV protection, in addition to improving the fruit visual

appeal. In contrast, non-edible coatings are used on fruits not intended for human consumption, such as those used in floral arrangements or for decorative purposes. These coatings similarly act as a barrier and improve the appearance of the fruits, but they are not safe for consumption, and must be washed before use. In summary, edible coatings provide an effective alternative for fruits preservation, whereas non-edible coatings are tailored for specific non-consumable applications.

The growing environmental awareness is becoming standard practice in many countries, further driving interest in recyclable and bio-derived materials sourced from agricultural origins that are renewable and non-toxic. The use of agri-food waste and by-products as raw materials for producing biodegradable packaging is a highly attractive and sustainable option. These residues are commonly processed to obtain fibers and polymers used in food packaging, not only adding value to fruit peels, pulps, seeds, and stems but also promoting the production of biodegradable or compostable materials, thus contributing to environmental stewardship.[14]

Edible films and coatings primarily differ in the way they are applied to foods. Films are thin layers of material formed independently and placed on a smooth, flat surface, then removed and applied to the food.[18] On the other hand, the coating is applied directly to the surface of the food, either by immersion in a solution or by spraying.[19]

2.3 Preparation of Edible Coating Films

Fruit coating involves the incorporation of a thin layer of chemical or biological material on a substrate by deposition in either the liquid phase (solution) or the solid phase (powder or nanoparticles) to create a partial barrier and prevent gaseous exchange, thus retarding the ripening process. In general terms, the procedure for forming edible films and coating for food includes the following steps:

1. Preparation of an initial solution by uniformly mixing components such as polymers, solvents, plasticizers, and additives, ensuring a homogeneous material.

2. Degassing and defoaming processes, which are carried out to remove air and microbubbles formed during the previous step. For this, vacuum or ultrasound degassing techniques are used,[20] adjusting the parameters according to the specific formulation.

3. Solvent drying, which is performed using techniques such as casting, thermal gelation, electrospray, and microfluidization. This final step is crucial as it defines the process of preparing films and coatings.[14]

The forming solution is dissolved in a solvent, such as water, ethanol, or acetic acid, which contains additives like plasticizers, crosslinking agents, or solutes. Subsequently, the solvent is removed, resulting in the formation of a thin layer that dries and can be separated. In the solvent removal process, a molecular structure is formed and stabilized through physical and chemical interactions, which conditions the properties of the material. The different methods to carry out prepared to thin films preparation are described below:
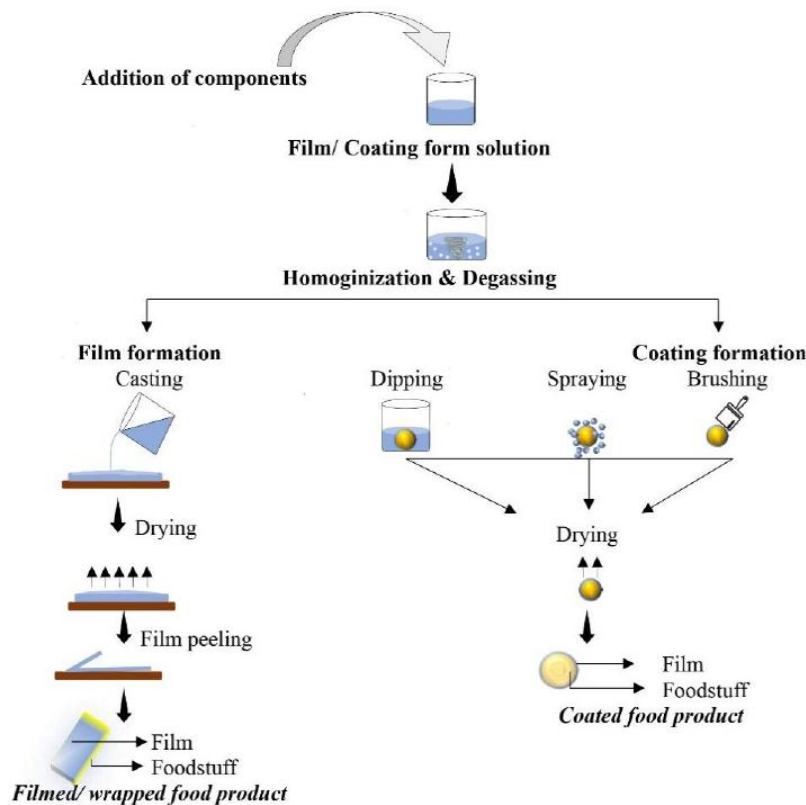
Figure 1 Schematic representation of films food packaging and coating for food. Taken from Nair 2023[14]

Thermal Gelation: This method involves the application of thermal treatment to form a stable gel with a rigid structure, typically used in protein-based films and coatings. During this process, thermal denaturation occurs, which destabilizes protein molecules, forming a stable network between particles.[21]

Solidification: The macromolecules dissolve together with the plasticizer and are homogenized before being poured into thin layers over molds. After a period of time, the solvent evaporates, and the material is removed.

Casting Method: This method involves the controlled deposition of a solution or suspension onto a flat surface. During this process, the solvent is gradually removed under precisely controlled conditions of temperature and humidity, enabling the uniform formation of a film.[22]

Electrospinning: This method atomizes a film-forming liquid using electrical forces. The liquid is expelled through a nozzle with a high electrical potential, producing extremely small droplets with particle sizes in the nanometer range, which can be controlled using electric fields.[13,23] This process allows produce ultrafine fibers with diameters in the nanometer range and offers versatility to use a wide variety of polymers.

Microfluidization: In this process, dispersions are channeled through microchannels to obtain nanoparticles that enhance the physical properties of the film. Subsequently, the casting method is used to form the final film.[21]

The main components used in the preparation of films for food packaging include polymers, lipids, polysaccharides, and proteins,[14] whose properties can be modified by the combination with plasticizers, crosslinking agents, and functional additives. Bio-based food coating films are becoming increasingly important due to their safe and environmentally friendly material. Their use is not considered new, since they have been used since ancient times, but their functionality and effectiveness are optimized with the development of new materials with suitable mechanical, antibacterial and permeability properties.[13,14,24] Due to their biodegradable properties and their ability to form flexible and durable films, biopolymers such as pectin, carboxymethyl cellulose (CMC), starch, and chitosan, have been widely used as precursor materials for coating films.[13,24,25] The use of plasticizers, such as glycerol and citric acid derivatives, has led to improving flexibility and reducing the brittleness of the films.[26] On the other hand, crosslinking agents are used to strength the films by forming bonds between polymer chains, thereby improving mechanical properties and thermal stability. Additionally, functional additives such as antioxidants and antimicrobial agents can be incorporated to extend the shelf life of packaged foods by inhibiting microbial growth and delaying oxidation.[13]

2.4 Components in biopolymer-based films for food packaging

Biodegradable polymers are materials designed to naturally decompose in the environment through biological processes, facilitated by the action of microorganisms, bacteria and enzymes. This contrasts with conventional plastics, which persist in the environment as pollution, harming wildlife and contributing to global pollution.[27–30] To mention some figures in the year 2021, 139 million metric tons of single-use plastic were used globally, up from 133 MMT in 2019, this includes plastic wrappers and envelopes.[8,31] In response to these environmental challenges, there has been increasing interest in the development of bio-based and biodegradable polymers for food packaging.[6,29,32] These materials offer sustainable alternatives that reduce environmental impact, aligning with consumer preferences for eco-friendly solutions in packaging technology.

Several types of biodegradable materials offer a more sustainable alternative, as they break down into simpler components and do not generate long-term waste accumulation. Some of these biodegradable materials includes polylactic acid (PLA), polyhydroxyalkanoates (PHA), polyethylene oxide (PEO), poly(caprolactone) (PCL), polyethylene glycol (PEG), among others as, which are frequently seen in some single-use products.[33] A recent trend of packing materials using biodegradable precursors include whey proteins, casein, wheat gluten, gelatin, polysaccharides such as starch, pectin, carrageen, alginate, gill, gum, chitosan, cellulose and its derivatives, fatty compounds, such as plant fats, animal fats, and waxes are used for the development of edible films and coatings.[34–36]

In the field of fruit coating and fruit packaging, several biodegradable biopolymers have been used. Some of the most used biopolymers include polysaccharides, Figure 2 which are known for their complex structure and functional diversity. The linear structure found in some polysaccharides, such as 1,4-β-D-glucan (in cellulose), 1,4-α-D-glucan (in amylose), and 1,4-β-D-glucoside (in chitosan), provide hardness, flexibility, and transparency to certain films.[14] These films are also resistant to fats and oils. For instance, the crosslinking of chitosan with aldehydes makes the film tougher, insoluble in water, and highly resistant.[37,38]
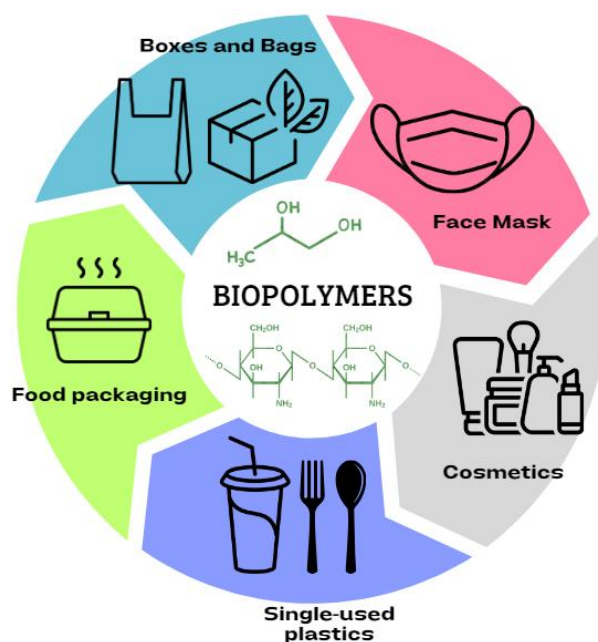
Figure 2 Biopolymers and some applications

Since cellulose is the most abundant biopolymer in nature, it would be wise to take this into account. However, its limited solubility in water makes it difficult to process, as well as the generation of homogeneous coatings. Nevertheless, water-soluble cellulose derivatives provide a more practical alternative due to their more convenient functional properties. As an example, carboxymethyl cellulose (CMC) could be considered which has excellent film forming properties, making it ideal for fruit coating, protecting them from physical damage and moisture loss. It is a cellulose derivative, completely biodegradable, reducing environmental impact compared to synthetic polymers.[39] CMC is food-safe, approved by regulators like the Food and Drug Administration of the United States of America, and widely used in food applications, offering good oxygen barrier properties, which helps extend the shelf life of fruits by reducing oxidation.[40] Subsequently, a more comprehensive description of CMC in food coating will be provided, because biopolymer is a central component of the coating films to be prepared in this project.

Starch and chitosan have been extensively used to create edible films and food coatings,[21,41] due to their properties and good functionality. Starch, especially from maize, is an abundant raw material with thermoplastic properties when subjected to molecular-level structural disruption. The 70% content of amylose in high-amylopectin maize starches gives the film a strong and flexible structure. The branched structure of amylopectin generally results in poor mechanical properties in the film.

Hydroxypropylated starches are used to preserve candies, raisins, nuts, and dates, preventing oxidative rancidity.[42] Copolymerization and grafting synthesis with monomers like acrylonitrile (AN) produce acrylic fiber precursors used in starch-polymer composites (starch-graft-PAN), which are also biodegradable.[38] Chitosan, on other hand, is a renewable biopolymer obtained from the valorization of agriculture-food industry waste. It holds significant potential in the field of food packaging, due to its excellent antimicrobial properties and film forming abilities.[27] This polycationic polysaccharide is soluble in acidic solutions and possesses film-forming capability. Moreover, its chemical structure grants it intrinsic antimicrobial activity.[8,21]

Various studies have evaluated the properties of films made from chitosan. These coatings and films extend the shelf life of foods and exhibit good optical properties such as color, gloss, and strength.[21,43] Their application has been focused on highly perishable foods like fruits such as: apples, grapes, and citrus fruits among others,[44] vegetables such as tomatoes,[45] and meats. Furthermore, recent developments incorporate natural products that impart multifunctional characteristics, including antimicrobial and antioxidant properties, as well as improvements in organoleptic and nutritional quality.[24] However, the low stability of films generated from starch, which tend to undergo retrogradation; a process that occurs in gelatinized starch during cooling and storage, can affect the mechanical properties and coating barrier performance. Regarding chitosan, its solubility in water requires acidic conditions, which can hamper its utilization and compatibility in some food products.

Pectin is another natural polysaccharide used in edible coating applications. This biopolymer is present in many fruits, therefore is safe for human consumption. Also, it has good gel-forming properties, helping to maintain the integrity of the coating and providing an effective barrier against moisture loss and microorganism entry.[46] Like CMC, it is completely biodegradable, contributing to a more sustainable packaging solution. Pectin is also compatible with other biopolymers like CMC, improving the mechanical and barrier properties of the coating. Knowing the chemistry of the components is essential to creating an effective coating. Due to the hydrophilic nature of carbohydrates, polysaccharides exhibit poor water barrier properties. Since polysaccharide coating will only increase the moisture content of the fruit surface, using polysaccharide alone may not be able to solve water loss problems. Therefore, incorporating functional additives can improve the features of the resulting films.

Carboxymethyl cellulose (CMC)

Carboxymethyl cellulose (CMC) is a modified derivative of cellulose widely used in various industries due to its unique properties. Figure 3 shown the chemical structure of CMC . It comes from cellulose, the most available natural polymer, which is found in the cell walls of plants. Due to its good film-forming properties, biocompatibility and biodegradability,[10,47–49] CMC, like most cellulose-based materials, can be used as an environmentally friendly substitute to petroleum-based polymers in the preparation of food packaging films to control the food quality.[49] As mentioned before, pure cellulose is not the best material to use for creating fruit coating films because of its limited water solubility and processing challenges.

Anionic ether cellulose, cellulose acetate, hydroxypropyl methyl cellulose (HPMC), methyl cellulose (MC), and carboxymethyl cellulose (CMC), and other cellulose derivatives, dissolve in water and are compatible with other biomolecules, improving the mechanical and barrier properties of the manufactured films.[39,50] Although CMC has many of the same advantageous qualities as cellulose acetate, HPMC, and MC, it is especially well-suited for food coating applications because of its unique processing ease, cost-effectiveness, non-toxicity, thickening efficiency, and ingredient compatibility. CMC can absorb oil from foods subjected to deep frying.[51] In addition, films made from yucca bagasse, CMC, and Kraft paper residues have shown high strength, an important property for manufacturing packaging like egg cartons and containers for fruits and vegetables.[52]

Furthermore, CMC improves the texture and consistency of liquids and semi-liquids and acts as an efficient thickening and stabilizing agent, making it possible to create extremely homogeneous precursor mixes.[17] The superior water retention qualities of CMC contribute to the preservation of moisture and the extension of food freshness. These properties extend the shelf life of fruits by forming barriers against moisture and oxygen and carbon dioxide. In addition, CMC is a versatile and sustainable material due to its biodegradability and compatibility with other components.
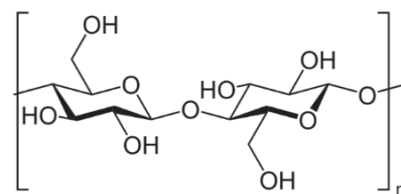
Figure 3 Structure of Carboxymethyl Cellulose (CMC)

CMC being the most important derivatives of cellulose, characterized by a backbone of β-(1-4) linked glucopyranose residues.[33] CMC is formed through the etherification of cellulose, specifically by substituting some of the hydroxyl groups (-OH) on the cellulose backbone with carboxymethyl groups (-CH$_2$-COOH).[49,53,54] Due to the presence of a hydrophobic polysaccharide backbone, CMC exhibits amphiphilic characteristics, generating a unique structure with high molecular weight chains.[47,49,53] This property allows CMC to be used as a filler in polysaccharide-based films.[49,55] Several studies have reported that the addition of CMC improves the mechanical and barrier properties of various polysaccharide-based films.[56,57]

Pectin (PEC)

Pectin is a natural polysaccharide found in the cell walls of plants, especially fruits, considered a complex anionic polysaccharide composed of α-(1-4)- linked D-galacturonic acid residues. It is a soluble dietary fiber that plays a crucial role in the texture, structure and quality of fruits and vegetables. Pectin is widely used in the food industry for its gelling, thickening and stabilizing properties. In food coating applications, pectin-based films have been proposed due to their excellent oxygen barrier and moisture barrier, although they generally do not show good mechanical properties and low efficiency as a moisture barrier through films.[36,58,59] To improve these properties, the pristine biopolymer can be subjected to chemical and enzymatic modifications, further enhancing its functionality and application potential, or it can be combined with other materials (precursors or biopolymers) to achieve a convenient synergistic effect.
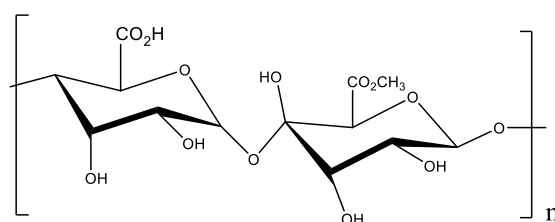
Figure 4 Structure of Pectin

Pectin, an anionic polysaccharide composed of β-1,4-D-galacturonic acid residues, as indicated in Figure 4, can be high-methoxyl pectin (HMP) or low-methoxyl pectin (LMP); HMP forms excellent films. Mixing citrus pectin and high-amylose starch as plasticizers provides stability and flexibility to the film, which is thermally stable above 180 °C. Pectin is also miscible with polyvinyl alcohol or glycerol in all proportions and can be used in film production through extrusion, compression, and other operations.[33]

Plasticizer agent

Plasticizers are additives used to increase the flexibility and reduce the fragility of films for food packaging and edible coatings. These compounds can be part of the internal polymer structure if they are chemically linked to the polymer chain. In addition, there are external plasticizers, which operate primarily by intercalating between polymer molecules, reducing intermolecular forces and increasing free volume, resulting in more flexible, elastic, and durable materials. External plasticizers operate primarily by intercalating between polymer molecules, reducing intermolecular forces and increasing free volume, resulting in more flexible, elastic, and durable materials.[13,60] However, this can also compromise the barrier properties of the films, since the greater molecular mobility facilitates the permeability of gases and vapors. Among the available plasticizers, glycerol is the most used due to its high efficiency in the plasticization of water-soluble polymers[14,60] standing out for its ability to reduce the fragility and rigidity of films, making them more manageable and easier to manipulate.

Glycerol: Also known as glycerin, is a trihydroxyl alcohol with the chemical formula $C_3H_8O_3$ (Figure 5). Glycerol is naturally found in lipids, such as triglycerides, and is industrially obtained as a byproduct of soap and biodiesel production. Glycerol acts as a plasticizer by incorporating into the polymer matrix, reducing the intermolecular forces between the polymer chains. This process has several effects: it reduces rigidity by interfering with the hydrophobic and hydrogen interactions between the polymer chains, thereby increasing the flexibility of the polymeric material; by decreasing the attractive forces between polymer chains, glycerol also increases their mobility, facilitating polymer deformation under mechanical stress; it enhances elasticity by allowing polymer chains to slide more easily over each other, improving the elasticity of the material.[61] Additionally, glycerol is biodegradable, non-toxic, low-cost, and

compatible with a wide range of natural polymers such as pectin, gelatin, and starches, improving their mechanical properties without compromising their biodegradability.

OH

HO⎯ ⎯OH
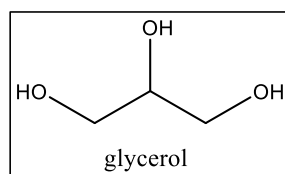
glycerol

Figure 5 Structure of glycerol

Cross-linking agents

The cross-linking agents for polymer matrices serve to join adjacent chains through covalent bonds, generally to obtain stronger and less permeable films, generally to obtain stronger and less permeable films. The cross-linking phenomenon can be achieved chemically or physically by subjecting the macromolecule to treatments that induce the formation of a three-dimensional network. There are various chemical, physical or radiative methods, such as exposure to gamma and ultraviolet B radiation, that can promote cross-linking, offering different advantages depending on the type of biopolymer and potential applications. Chemically, cross-linking is obtained by adding cross-linking agents, these agents can be enzymes, minerals, proteins, organic acids, amino acids, phenolic compounds, calcium chloride.[62,63] The cross-linking agents selected to be used in this project are presented below.

Citric Acid ($C_6H_8O_7$) is a tricarboxylic organic acid, its chemical structure is shown in Figure 6. It is widely known for its presence in citrus fruits like lemons and oranges. It is a biodegradable and non-toxic compound, making it ideal for various applications in the food, pharmaceutical, and materials industries. Citric acid acts as an efficient crosslinking agent due to its three carboxyl groups (-COOH) that can react with functional groups such as hydroxyls (-OH) or amines (-NH$_2$) present in polymers, primarily forming ester or amide bonds. These bonds formed through crosslinking with citric acid enhance the water resistance and thermal stability of biopolymers.[31] In general terms, crosslinking with citric acid improves the mechanical properties of biopolymers, such as tensile strength and elasticity.[25]
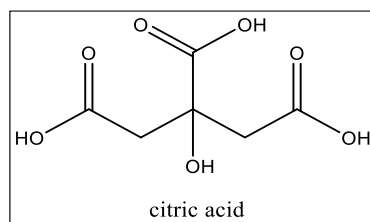
Figure 6 Structure of citric acid

Egg Albumin: is the main protein present in egg white. It constitutes approximately 60% of the total proteins in the egg and is known for its gelling, foaming, and emulsifying properties. Egg albumin is a water-soluble globular protein that denatures and coagulates when heated, forming a protein network that traps water and other components. Egg albumin has been used as a crosslinking agent in biopolymers since it can form covalent bonds between polymer chains due to its numerous functional groups, such as amine and carboxyl groups. The advantages of using egg albumin are that it improves the mechanical properties of the polymer, such as tensile strength and stability.[64] Figure 7 shows a representation of egg albumin.
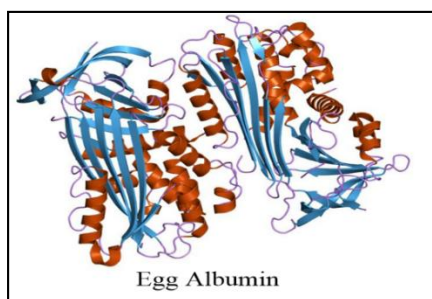
Figure 7 Structure of egg albumin

Functional additives for food coatings

In order to condition the properties of food coatings, additives such as antibacterial agents are incorporated, which control the proliferation of bacteria and therefore improve the effectiveness in protecting the coated products. Among these agents are essential oils from species such as oregano, thyme, and cinnamon, bioactive compounds from plants and fruits like flavonoids and phenols, as well as polymers that intrinsically contain this property. Some examples of these polymers can be mentioned; polyglycolic acid, polylactic acid, and chitosan organic acids, antimicrobial peptides and bacteriocins, enzymes, metal and metal oxides, metallic nanoparticles.[65]

16

2.5 Metallic nanoparticles in food packaging

Metals and metal oxides nanoparticles are frequently used as active additives in films to food packaging and coating. The main function of these additives is to provide antibacterial or antifungal or antiviral properties, thanks to their ability to penetrate bacterial cells due to their small size. Although the exact mechanism is not completely clear about the toxicity of nanoparticles, it is suggested that it involves the generation of reactive oxygen species (ROS) and free radicals, as well as direct contact with the bacterial surface, which damages the cell wall. e Interferes with the transport of electrons across the membrane. ROS cause oxidative stress, alter gene expression, and damage crucial cellular components such as DNA and proteins, affecting mitochondrial function and leading to bacterial cell death.[66] The antibacterial effectiveness of metal NPs is also related to the release of metal ions. Gram-positive bacteria exhibit greater resistance to NPs compared to Gram-negative bacteria, due to their additional layers of peptidoglycan and teichoic acids, which can more effectively trap negatively charged NPs.[65]

Silver nanoparticles

Among metallic nanoparticles, one of the most prominent are silver nanoparticles due to their exceptional optical, magnetic and electrical properties, as has been widely reported.[67–69] In addition, the well-documented antibacterial activity associated with silver has led to the integration of silver nanoparticles into numerous applications, with the aim of addressing the challenges posed by the post-antibiotic era. This has encouraged the development of new agents capable of fighting pathogenic microorganisms without favoring the emergence of new resistance mechanisms. In Figure 8 are indicated some applications of silver nanoparticles.
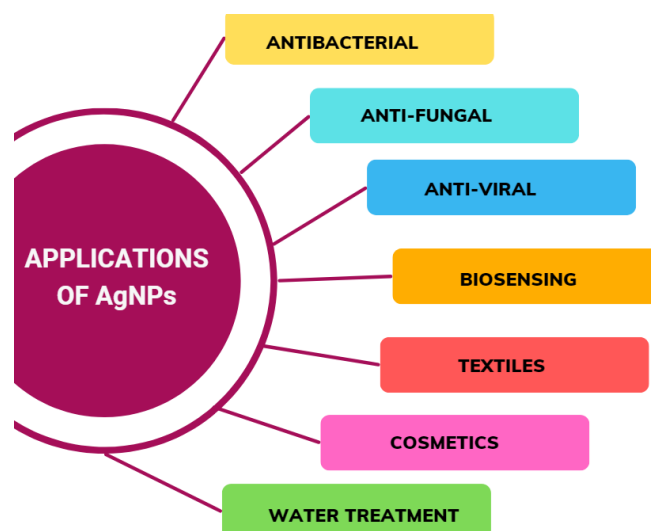
Figure 8 Some applications of silver nanoparticles.

Nanomaterials can be obtained through top-down and bottom-up methods. Top-down methods involve the destruction of the sample to adjust the shape and size of the nanostructure, while bottom-up methods use specific chemical substances and compounds. Depending on the formation mechanism involved, various shapes can be obtained such as spheres, rods, wires, and prisms.[68]

Bottom-up methods are better at controlling the size and shape of nanostructures, since stabilizing agents, layering agents and reducing agents are used to help control the synthesis, these bottom-up methods can be chemical methods: such as chemical reduction, electrochemical methods, microemulsion, or biological methods known as green methods. in which plants, bacteria or fungi are used as reducing agents and which in turn serve as capping and stabilizing agents.[70]

Green Synthesis of silver nanoparticles

The green synthesis of silver nanoparticles from biocompatible natural sources is a suitable approach, especially for food coating applications. This method offers the additional benefit of perhaps giving the resulting nanomaterials an antibacterial action thanks to the use of biopolymers as reducing agents, microbial cells or through the use of plant extracts from leaves, stems, roots or fruits.[71–73]

Several alternative and effective synthetic routes to obtain silver nanoparticles have been studied, in which the use of different natural extracts has been evaluated for their ability to reduce silver ions and promote the formation of nanostructures with different sizes and morphology.[45] They have been used as reducing agents *Cinnamomum*

18

zeylancium, Cocous, Tea, and *Nelumbo nucifera*, *Premna herbacea*, *Pistacia atlantic*, *Allium sativum leaves, Acalypha indica, Centella asiatica*, and *Citrus sinensis,*[37,72,74] obtaining silver nanoparticles with diameters that vary between 8 and 50 nm. Likewise, nanoparticles with spherical and triangular shapes were obtained from the *Aloe Vera* extract, with sizes varying between 25 and 80 nm.[75] On the other hand, using extracts of *Memecylon edule or Eclipta postrate*, triangular and hexagonal shapes were achieved, with sizes in the range of 16 to 40 nm.[37,76] Spherical and face-centered cubic (fcc) shapes were obtained from *Vitex negundo*,[37] with sizes of approximately 5 nm and from 10 to 30 nm the *Datura metel* extract produced almost linear superstructures with sizes between 16 and 40 nm.[77] Cinnamaldehyde, the predominant chemical component extracted from the bark of cinnamon, belonging to the *Cinnamomum* genus of the *Laureceae* family, has a wide range of beneficial properties, including analgesic, antiseptic, insecticidal and parasiticide effects, standing out for its antimicrobial effectiveness against various infections.[78]

Antibacterial mechanism of silver nanoparticles

A large number of studies have demonstrated the bactericidal capacity of silver nanoparticles, which present several mechanisms of action simultaneously. The results indicate that smaller nanoparticles show greater bactericidal activity, mainly due to their greater surface area available to interact with bacterial membranes.[66,73] This interaction causes alterations in the membrane, which ultimately leads to the death of the bacteria. Such alterations include protein dysfunction, oxidative stress and DNA damage, affecting vital functions such as permeability and respiration, resulting in bacterial death.

One of the mechanisms for DNA modification involves the action of silver ions. These ions can hinder protein synthesis, deactivate respiratory enzymes, and generate reactive oxygen species, interfering with the production of adenosine triphosphate (ATP). The nanostructures most likely to release silver ions are the smallest and with spherical or quasi-spherical shapes, due to their greater surface area.[72] However, optimizing capping agents and adjusting the pH of the medium can expedite the release of silver ions.

The incorporation of phytochemical agents, such as organic compounds or antibiotics, together with silver nanostructures, has demonstrated a synergistic effect against pathogenic bacteria.[66] This novel approach of combining phytochemicals with metallic nanomaterials has appear as a promising strategy to respond to the urgent need

for effective antibacterial agents and to address the challenge of multidrug resistance.[78,79] The bioavailability of phytochemical agents has improved with the use of nanostructures due facilitating their controlled release at the desired target site or tissue. This results in increased stability, antimicrobial efficacy and reduced toxicity to the host.

Recent research also demonstrates that antibacterial activity may occur due to the generation of reactive oxygen species. These species cause damage to both the membrane and the bacterial lipases, causing leakage of intracellular contents and, consequently, the death of the bacteria.[66] The Figure 9 shows a schematic of the bactericidal mechanisms of silver nanoparticles, illustrating: the disruption of the cell membrane, DNA damage, enzyme inactivation, and the generation of reactive oxygen species, among others.
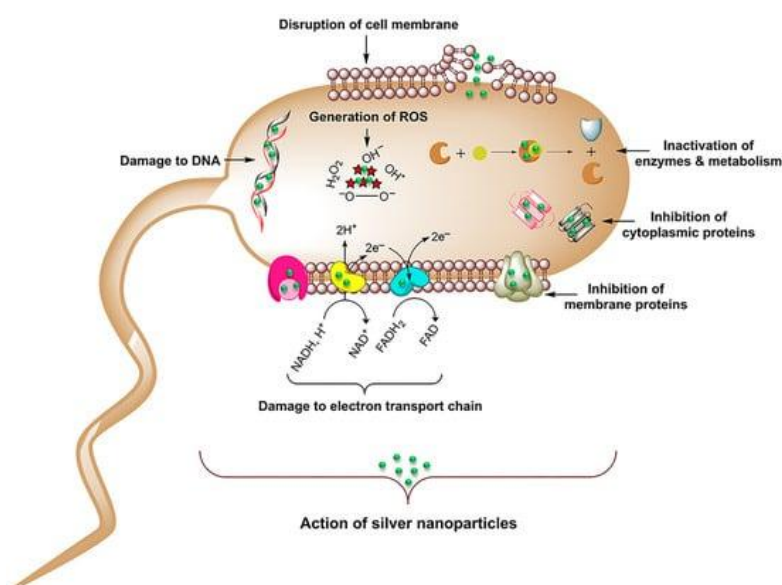
Figure 9 Schematic diagram illustrating fabrication and bacterial process of AgNPs-green synthesis. Taken from Menicheti 2023[66]

3 EXPERIMENTAL METHODOLOGY

3.1 Chemical Reagents, Bacteria and Materials

Chemicals used in this project were acquired from Loba Chemie and Sigma Aldrich-Merck, while pectin and cinnamon bark extract were acquired form local stores, as is indicated below:

Loba Chemie: Carboxymethyl cellulose (CMC).

Sigma Aldrich – Merck: Silver nitrate (AgNO$_3$), citric acid (C$_6$H$_8$O$_7$).

Local stores: Pectin (PEC) food-grade, cinnamon bark extract.

Bacterial strains used for antibacterial analysis: *Escherichia coli* (DH5α), *Klebsiella pneumoniae* (KpCL17), *Pseudomonas aeruginosa* (PAO1), *Acinetobacter haemolyticus* (AN54), *Escherichia coli* (C7230), *Klebsiella pneumoniae* (KpE52), *Pseudomonas aeruginosa* (PE52), *Acinetobacter* (AN2) and *Staphylococcus aureus* (29213), came from Puebla-Mexico from the Pediatric Hospital of the city. In addition, some analyses were developed using *Escherichia coli* (25922) strain obtained from Laboratory of School of Biological Science and Engineering of Yachay Tech University.

3.2 Cinnamon bark extract

To obtain the cinnamon extract, the steam distillation equipment is first assembled, cinnamon bark is placed in distilled with water for 3 hours. A whitish emulsion was obtained. To characterize the cinnamon extract, several techniques were used, including UV-Vis spectroscopy, Fourier-transform infrared spectroscopy (FTIR), High-Performance Liquid Chromatography (HPLC), Gas Chromatography-Mass Spectrometry (GC-MS). Phytochemical tests were carried out, particularly a biological activity screening, for the identification of bioactive compounds in the cinnamon extract.

UV-Vis spectroscopy

The UV-Vis spectrum can provide information about the presence of aldehyde groups in cinnamon extract. The chromophore group for these compounds (aldehydes, ketones, acids, and derivatives) is the carbonyl (C=O) group. Because oxygen has lone pairs of electrons, the lowest-energy transition is n→π∗, although this transition is forbidden (€max=15) due to the lack of orbital overlap. The next lowest-energy transition is π→π∗, observable at λmax=290 nm, with a molar absorptivity of 900.[80] UV-Vis

determinations in solution were performed in a Diode Array Analytic Jena Spectracord S200 spectrophotometer in the range of 190 to 800 nm using a standard 1 cm quartz cell.

FTIR spectroscopy

Infrared spectroscopy (FTIR) was used to identify the main compounds obtained from cinnamon extraction and to analyze the structural changes occurring in these compounds after the synthesis of silver nanoparticles (AgNPs). FTIR spectra also helped identify structural changes in the modified biopolymers (pectin and CMC). The FTIR analysis was conducted using a Perkin Elmer/100 FTIR spectrophotometer, operating in the range of 500 to 4500 cm^{-1}.

HPLC

HPLC analysis was performed using a Thermo UltiMate 3000 system, which is equipped with a diode-array detector (DAD) and a Hypersil GOLD™ C-18 column for HPLC (150 mm × 4.6 mm, 5 μm particle size). The mobile phase used was an acetonitrile:water mixture in a 60:40 ratio, with a flow rate of 1 mL/min at room temperature. A sample volume of 5 μL was injected, and the detection wavelength was set at 210 nm.

GC-MS

To demonstrate the presence of cinnamaldehyde in the cinnamon extract a GC-MS analysis was performed using a Waters SYNAPT-G2Si Mass spectrometer, this spectrometer is coupled to an Agilent 7290A Gas Chromatograph, which is equipped with an Agilent DB5-MS column, 30 m in length, 0.25 mm internal diameter, and 0.25 μm (5% phenyl and 95% polydimethylsiloxane). The volumetric flow of helium, used as carrier gas, was 1.5 mL/min, and for the analysis a temperature range of 70 °C to 300 °C (5 °C/min) was used.

Phytochemical Analysis

Several qualitative colorimetric tests were used to determine the secondary metabolites present in the cinnamon extract. They are mentioned below:[81]

- Flavonoids determination was carried out by the test with concentrated H_2SO_4 and the Shinoda test, using concentrated sulfuric acid, magnesium and concentrated hydrochloric acid, respectively.

- Phenolic compounds detection was achieved by the iodide test, for which dilute iodine solution and the ferric chloride test with 5% ferric chloride solution were used.

- Tannins detection was carried out by the test with 10% NaOH, using a sodium hydroxide solution, and the Braymer test with a 10% ferric chloride solution.

- Coumarins detection was carried out with the NaOH test, using 10% sodium hydroxide solution and chloroform.

- Alkaloids detection was carried out by the Wagner's Dragendorff tests with Wagner's reagent and the Lugol test were used,

- Protein determination was performed using the Biuret test.

3.3 Green Synthesis of Silver Nanoparticles

To prepare the silver nanostructures, 2.5 mL of a 1 mM silver nitrate solution and 2.5 mL of cinnamon extract were mixed. The mixture was stirred for approximately 20 minutes at 40 °C. The onset of silver nanostructure formation was evidenced by the pink-orange color change of the colloidal dispersion, as shown in Figure 10. The nanoparticles synthesized by this method are denoted as AgNPs-c.

Figure 10 Scheme of synthesis of silver nanoparticles using cinnamon bark extract

In order to characterize the silver nanoparticles (AgNPs-c), UV-Vis spectroscopy, FT-IR spectroscopy, Scanning Electron Microscopy, Transmission Electron Microscopy, Dynamic Light Scattering were used to evaluate their chemical and morphological properties.

UV-Vis spectroscopy: Surface Plasmon Resonance analysis

Surface plasmon resonance is a characteristic phenomenon of metallic nanoparticles. The free electrons in the conduction band of these nanoparticles, like the electrons in the orbitals of silver atoms, are affected by an external electromagnetic field, such as incident light with a wavelength longer than that of the nanoparticles, resulting in a strong interaction between the light beam and the nanoparticles. This light resonates with the plasmon oscillation near the surface, causing the free electrons to oscillate. In simple terms, conduction electrons collectively move to detect the disturbed charge distribution in the plasmon oscillation. As the light wave progresses, the electron density on the particle's surface polarizes and oscillates in resonance with the light frequency, leading to a continuous and characteristic oscillation. Figure 11.

The interaction of radiation with the surface electrons of metallic nanoparticles depends crucially on their shape, size, chemical composition, and surrounding environment. When the shape and size vary, the surface geometry also changes, intensifying the electric field density on the surface. This alteration in geometry leads to a change in the oscillation frequency of the electrons, generating various optical properties such as absorption and dispersion. This phenomenon is essential for the detailed characterization of metallic nanoparticles in terms of their morphology and optical behavior. In the visible light spectrum, the wavelengths associated with this phenomenon are typically between 400 and 700 nm. For example, silver nanoparticles exhibit an absorption band around 445 nm,[82,83] while gold nanoparticles typically display a band near 520 nm.[83]
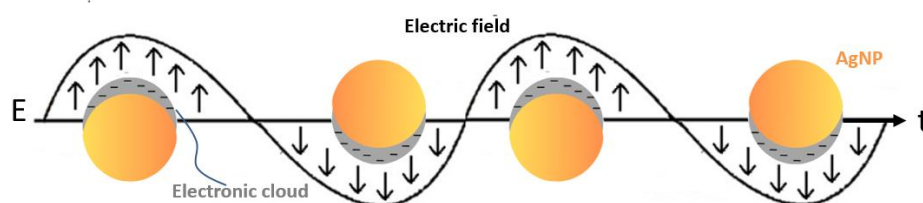
Figure 11 Surface Plasmon Resonance of metallic nanoparticles

FT-IR Spectroscopy

In order to carry out the SPR analysis of the silver nanoparticles obtained in this project, the UV-Vis spectrometer was utilized. FT-IR Spectroscopy

Once a green synthesis of silver nanostructures is achieved, it is important to identify the chemical systems that were modified, either because they are reduced or oxidized. Fourier-transform infrared spectroscopy (FTIR) provides detailed information about structural chemical changes that cinnamaldehyde undergoes after the oxidation process while reducing silver.

Scanning Electron Microscopy (SEM) and Electron Microscopy Transmission Electron Microscopy (TEM)

Electron Microscopy is a powerful and indispensable material characterization technique, which uses an electron beam to study objects on a very small scale. On one hand, Transmission Electron Microscopy (TEM) allows the study of internal structures, based on several phenomena generated during the inelastic interactions of electrons with the sample. One of the main advantages of TEM is its ability to provide high-resolution images at the atomic level, allowing detailed analysis of the crystalline structure, defects, and interfaces within materials.

The electrons are accelerated by a potential difference that can range between 50 and 30,000 volts, to take advantage of their wave behavior, resulting in their acceleration in the microscope column. These accelerated electrons travel through a gun and are focused by a condenser and objective lens, there the image of the filament is reduced so that the electron beam is very thin. This fine electron beam scans the sample point by point.[70,84,85]

The formation of the image in SEM corresponds to signals produced by the interactions of the sample's atoms with the electron beam impacting the sample. These interactions can be elastic (the energy lost by electrons when colliding with the sample can cause other electrons to be ejected and produce secondary X-ray electrons) and inelastic (electrons that bounce like billiard balls). Thanks to their high resolution and imaging speed, SEM and TEM microscopy have established themselves as standard methods for direct imaging and dimensional measurements of microstructures and nanostructures.

The shape and structure of the AgNPs-c were determined by Transmission Electron Microscopy (TEM) using a Tecnai G2 Spirit Twin microscope, equipped with an Eagle 4k HR camera. (This equipment is in ESPE University of Sangolqui Ecuador)

The solid samples were resuspended in absolute ethanol, on a Copper F/C TEM grid 5 μL of each suspension was placed. Images were acquired at different magnifications by operating the microscope at 80 kV. In addition, the evaluation of the morphology was performed using a TESCAN model MIRA 3 field emission scanning electron microscope (FEG-SEM). Images were obtained at various magnifications operating at 10 kV. The samples were placed one by one on a scanning electron microscopy peg and fixed with a double layer of double-sided carbon tape.

Dynamic Light Scattering (DLS)

Dynamic Light Scattering (DLS) is a widely used technique for measuring the dimensions of nanoparticles based on the observation of particles suspended in a liquid phase. This technique uses the temporal variation of light scattered by particles undergoing Brownian motion, allowing for the determination of their hydrodynamic size distribution. Brownian motion, caused by constant collisions with solvent molecules, is slower in larger particles, while smaller particles move more quickly due to their smaller size and higher energy from the surrounding molecules.[86,87]

To conduct this analysis, it is crucial to maintain a precise and constant temperature, as it is necessary to know the viscosity of the medium. Temperature fluctuations can generate convection currents that interfere with the correct interpretation of particle size. The speed of Brownian motion is related to the translational diffusion coefficient, which in turn is associated with particle diameter through the Stokes-Einstein equation (1):

$$(1) \quad d_H = \frac{k_B T}{3 D \pi \mu}$$

where d_H is the hydrodynamic diameter, D is the translational diffusion coefficient, y is the viscosity of the medium, k_B is the Boltzmann constant, and T is the absolute temperature at which the experiment was carried out. [52,87]

In addition to determining nanoparticle diameter, DLS equipment is also used to evaluate the zeta potential, which measures the electrical potential on the surface of the nanoparticle. This technique is useful for assessing the stability of colloidal suspensions,

as it describes the intensity of the static electric field at the particle-liquid interface, which is closely related to suspension stability and particle surface morphology.[88]

The DLS analysis was performed by pouring the silver nanoparticle sample into a quartz cuvette, which was then introduced into the DLS equipment. For an optimal analysis, it is necessary to have information about the medium in which the AgNPs-c are dispersed, following information is used.

$$\text{Refractive index for silver} \rightarrow \text{RI: 1.333}$$
$$\text{Viscosity} \rightarrow \mu = 0.8772 \text{ cP}$$

Antibacterial Analysis of Silver Nanoparticles

This area around a disk impregnated with antibiotics or bactericides shows inhibition of bacterial growth, providing a qualitative analysis of bacterial susceptibility to the substance being tested. This method is one of the most used[89] and offers a quick way to determine the effectiveness of various antibiotics and bactericides against different bacterial strains, being used to evaluate the antibacterial properties of the prepared AgNPs-c.

To examine the bactericidal activity of AgNPs-c, Gram-negative bacteria, both resistant and sensitive, were used and this was done using the methods: disk diffusion and the broth dilution method. The disk diffusion method, known as the Kirby-Bauer method, consists of inoculating a standard amount of microorganisms in a petri dish in Muller Hinton medium (MHB), forming a bacterial lawn. This procedure involves determining the zone of inhibition of each genus, where the effectiveness of antibiotics or bactericides against specific bacterial strains is estimated; for this, the measurement of the zone is carried out.[90] This area around a disk impregnated with antibiotics or bactericides shows inhibition of bacterial growth, providing a qualitative analysis of bacterial susceptibility to the substance being tested. This method is one of the most used and offers a quick way to determine the effectiveness of various antibiotics and bactericides against different bacterial strains, being used to evaluate the antibacterial properties of the prepared AgNPs-c. This zone is the area of the contour of a disk impregnated with the bactericidal or antibiotic sample where the inhibition of bacterial growth is clearly seen, therefore, this method provides an analysis or evaluation of bacterial susceptibility to the substance under test. This disk diffusion method is widely

used and provides ready information to determine the efficacy of various antibiotics and bactericidal samples and can be used against different bacterial strains.

To evaluate the antibacterial properties of prepared AgNPs-c. were used resistant bacterial cultures *Pseudomona aeruginosa* (PE52), *Acinetobacter haemolyticus* (AN54), *Escherichia coli* (C7230) and *Staphylococcus aureus* (29213).

The sensidiscs were prepared inside a laminar flow hood, for this 1 cm diameter filter paper disks were impregnated with 10 μL of various samples of antibacterial agents, including silver nitrate which is blank 1 (B1) and extract cinnamon as blank 2 (B2); and the AgNPs-c suspensions were concentrated 2, 3, 5 and 10 times their initial concentration. These impregnated disks were then placed in Petri dishes containing inoculated bacteria and then incubated at 37 °C. Three replicates were made for each sample.

In a 38 g/L Mueller Hinton (MHB) culture medium, the different bacteria were inoculated, which were previously diluted in an isotonic 85.9% NaCl solution until obtaining a turbidity comparable to 0.5 McFarland (~105 UfC/mL).[90] The sensidisks impregnated with the bactericidal agents were placed on the inoculated culture medium, pressing them gently on the agar to ensure that they were sufficiently impregnated on the surface. An adequate distance between sensidisks was maintained so that the halos did not overlap each other, and they were separated from the edge of the plate by a minimum distance of 15 mm. The plates were inverted so that the agar was on top and then placed in a 37 °C oven for 18 to 24 hours. After the incubation time, the inhibition halos were removed and measured.

On the other hand, the broth microdilution method consists of the preparation of a liquid broth with different concentrations of the antimicrobial agent. The microorganisms are introduced and, after incubation, growth is observed. During this procedure, bacterial strains were standardized to 0.5 on the McFarland scale.[90] 100 μL of Luria-Bertani (LB) culture medium was poured into the properly labeled wells, adding 100 μL of the corresponding AgNPs-cinnamon samples and 10 μL of bacterial inoculum. The incubation process was carried out at 37 ºC for 20 hours. *Klebsiella pneumoniae* (KpCL17), *Pseudomona aeruginosa* (PAO1) and *Acinetobacter haemolyticus* (AN54) Gram negative sensitive bacteria were used, also *Escherichia coli* (C7230)*, Klebsiella pneumoniae* (KpE52), *Pseudomona aeruginosa* (PE52) and *Acinetobacter* (AN2) were

used to evaluate the antibacterial capacity of the AgNPs-c resistant bacteria were used to evaluate the antibacterial capacity of AgNPs-c by this method.

3.4 Films preparation

Given the rising demand for food preservation, the use of sustainable materials for fruit coatings and packaging, as mentioned above, has a significant positive environmental impact. The final application, precursors availability, cost, and processing conditions all have a role in the selection of materials to be utilized in the development of these coatings or packaging. Given these considerations, CMC and PEC biopolymers were the materials used in this project for fruit coating films preparation.

It is important to consider the need for structural and chemical modifications to provide these biopolymer-based edible films with the appropriate mechanical properties for their intended use. As already noted, it can be made more effective by combining antimicrobials and antioxidants with functional additives such as plasticizers, emulsifiers and cross-linkers. Several formulations were conducted to achieve optimal composition conditions for fruit packaging.

Two different polymers were used to prepare the forming solutions: 2% CMC and 4% PEC. Citric acid (CA) was used as the first cross-linking agent, glycerol (G) as the plasticizing agent, and egg white (EW) as the second cross-linking agent to take advantage of the benefits of its main component, albumin, and improve the mechanical and protective barrier properties of the coating film. The composition proportions used are shown in Table 1.

For the preparation, a procedure similar to that described by Zhao et al. in 2023 was followed. Briefly, the polymer was combined with the plasticizing and cross-linking agents, and stirred for 30 minutes at 40 °C. After removing the mixture, it was homogenized for 2 minutes at 5000 rpm and filtered. The filtered liquid was allowed to stand for approximately 15 minutes to allow degassing. It was then poured into Petri dishes and left to gel for 12 hours at 50 °C in an oven.[63] This procedure is represented in Figure 12.
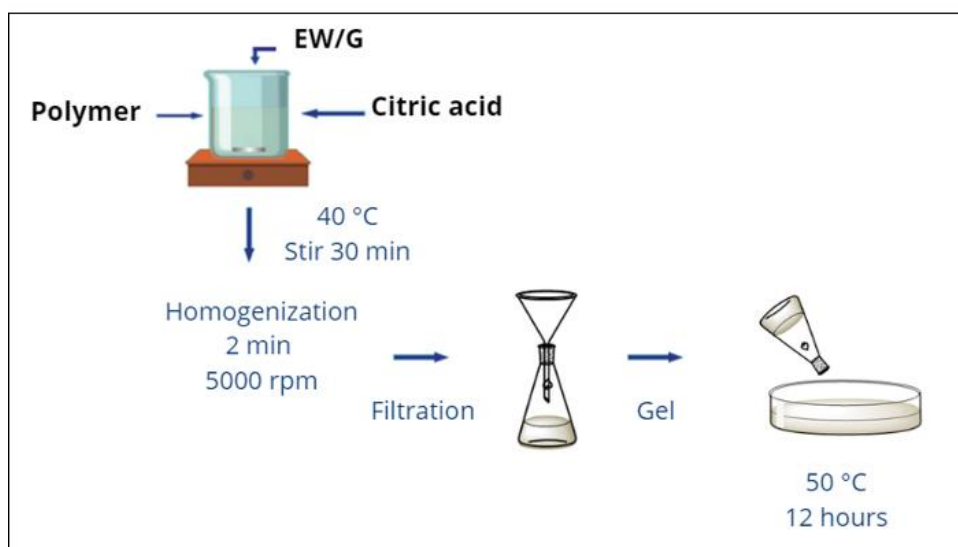
Figure 12 Scheme of films preparation

A second group of formulations was prepared from a combination of the two biopolymers, CMC and PEC, in a proportion of 1:1. The composition proportions for each component of the forming solution are given in Table 1.[47,70]

Table 1 Composition of different biopolymer based films for 100 mL of mixture

FILMS PREPARATION						
CODE	CMC (g)	PEC (g)	CA (g)	EW (g)	G(g)	AgNPs-c(mL)
CMC 0	2	0	1	0	0	0
CMC 0_2	2	0	1	0	5	0
CMC 1_1	2	0	1	2.5	2.5	0
CMC 2_0	2	0	1	5	0	0
CMC E	2	0	0	5	0	0
CMC E AgNPs-c	2	0	0	5	0	10
PEC 0	0	4	1	0	0	0
PEC 0_2	0	4	1	0	5	0
PEC 1_1	0	4	1	2.5	2.5	0
PEC 2_0	0	4	1	5	0	0
PEC 1_1	0	4	1	2.5	2.5	10
PEC CMC 0	2	4	1	0	0	0
PEC CMC 0_2	2	4	1	0	5	0
PEC CMC 1_1	2	4	1	2.5	2.5	0
PEC CMC 2_0	2	4	1	5	0	0
PEC CMC 1_1 AgNPs-c	2	4	1	2.5	2.5	10

Preparation of Nanocomposite for food packaging.

Nanocomposites, that is, the films loaded with silver nanoparticles, were prepared from the previously prepared formulations, but with the additional incorporation of silver nanoparticles. The procedure followed, similar to that previously described for the preparation of the forming solution, involved the combination of the biopolymer with plasticizing (G) and cross-linking (CA and EW) agents, under constant stirring for 30 minutes at 40 °C. Subsequently, silver nanoparticles were added in a relation of 10:1, and stirred for an additional 30 minutes without heating. After homogenization of the mixture for 2 minutes at 5000 rpm and filtration, the filtered liquid was left to stand for approximately 30 minutes to allow degassing. Then, the liquid was poured into Petri dishes and allowed to gel for 12 hours at 50 °C in an oven. A schematic representation of this process is shown in Figure 13. These nanocomposites are labeled as: PEC 1_1 AgNPs-c (pectin films), CMC AgNPs-c (CMC films); and PEC CMC AgNPs-c for the combination of the two polymers.
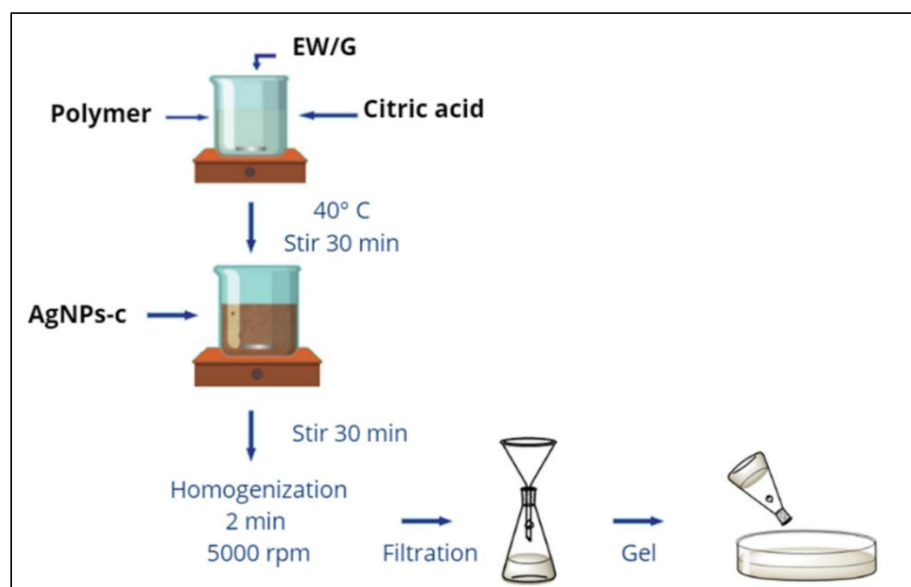
Figure 13 Scheme representing the different steps in the Films preparation

Chemical and structural characterization of prepared films

The mechanical properties of the prepared films were determined using a uniaxial tensile test conducted on a CellScale BioTester 5000. For this, specimens (5 per sample) were prepared, and their thicknesses were measured with a digital micrometer. The elongation speed was set at 10 mm/min using a 50 kN load cell at room temperature.

From the obtained the Young's modulus, strain at break, elongation at break, and ultimate tensile strength were determined.

3.1.1.1 X-ray Diffraction (XRD)

X-ray diffraction is used for the analysis of food packaging films, this technique is used to determine the presence of crystalline components in the films, which can determine their mechanical and barrier properties. In addition, it measures the degree of crystallinity, which influences the rigidity and permeability of the films, and studies how the polymer and additive components of the film interact internally, affecting its general structure. This technique is important to ensure that the structural properties of the films are suitable for use in food packaging.

For the XRD analysis, a Rigaku Miniflex 600 X-ray diffractometer for polycrystalline samples was used, equipped with a 600W X-ray tube, a Bragg-Brentano goniometer with an 8-position autosampler, a D/teX Ultra detector, and SmartLab Studio II software. Operated at 40 kV and 15 mA, the radiation source was CuK(alpha) (sealed tube). For data collection, a Theta/2Theta scanning axis was employed, with a step width of 0.0025°, a scanning range from 10 to 70° in 2Theta, at a speed of 10°/min, and a D/teX Ultra2 detector in 1D scanning mode.

3.1.1.2 FTIR spectroscopy

Infrared spectroscopy is a very useful characterization tool in the field of material science, since by identifying functional groups, it allows evaluating the changes in its chemical structure that result from the modifications to which it was subjected. Consequently, conclusions regarding the relevant molecular interactions could be drawn.

In order to verify the changes in the modified biopolymers, and to evaluate the influence of the additives, Fourier Transform Infrared Spectroscopy (FTIR) was used.

3.1.1.3 Thermogravimetric Analysis (TGA)

By this analysis, it is possible to suggest proposals for thermal decomposition mechanisms of sample, study the rate of the processes involved, and even to detect the presence of impurities. TGA has applications in the polymer industry, materials science, pharmaceuticals, and food industries, providing essential information on the thermal stability and composition of analyzed materials.[91,92]

TGA analysis, were performed with a thermogravimetric instrument model TGA 55, was used. This is equipped with an automatic loader, a Pt/Rh furnace, and a dual gas inlet collector (N_2 and Air). It operates within a temperature range from ambient to 1000 °C and can perform controlled heating rate modes, either linear (from 0.1 to 100 °C/min) or ballistic (> 600 °C/min). The sample containers are made of platinum and alumina, each with a maximum capacity of 1000 mg and a resolution of 0.1 µg.

For the measurement conditions, a heating ramp was set from room temperature to 600 °C at a heating rate of 10 °C per minute in an inert nitrogen atmosphere, using a platinum crucible with a 100 µL capacity. This setup ensures precise and accurate analysis of the thermal stability and composition of the pectin and CMC films.

3.1.1.4 Mechanical properties of prepared films

The mechanical properties of fruit packaging films and edible coatings generally depend on the interactions between the functional additives and the polymer matrix, as well as on chemical and physical conditions, such as temperature, which influence the film's stability and flexibility.[19] According to the ASTM D882-91 method,[91] these properties are characterized in terms of:

     (i)   Deformation at break (DAB): extension at the moment of rupture, mm.

    (ii)   Elongation at break (EAB): deformation divided by the initial sample length and multiplied by 100%.

   (iii)   Tensile strength (TS): Force at rupture divided by the film cross-section, MPa.

   (iv)   Elastic modulus (YM) slope of the force-deformation curve, N/mm.

The control (and adjustment) of these parameters is essential to ensure the suitability of the coating and protective films. Tensile strength (TS) elongation at break (EAB) are two of the most important tensile properties that describe an elastic material. These refer to the maximum force required per unit area before the film breaks and the degree of stretching it can withstand before breaking, respectively.

On the other hand, the Young's modulus (YM) indicates the material's flexibility or brittleness, with high YM values denoting more brittle films and low values indicating greater flexibility.[92]

Antimicrobial Analysis of the Films

The different preparations of silver nanoparticle films, namely PEC 1_1 AgNPs-c, PEC CMC 1_1 AgNPs-c and CMC 1_1 AgNPs, were evaluated against E. coli for their antibacterial properties. Initially, an analysis was performed using the Kirby-Bauer method. For this purpose, 10 µL of the film-forming solution was placed on the sensidisc, followed by 24 hours incubation period. Subsequently, the inhibition zone was measured. However, due to the high viscosity of the preparation, no significant results were obtained.

Another test was performed in which film discs were placed directly into a Petri dish with the inoculated bacteria and left to incubate for 16 hours. After this period, the films swelled due to the absorption of water vapor from the test, which prevented satisfactory results from being observed.

A final analysis was carried out by Diffusion per well, placing 50 µL of the film-forming solution with silver nanoparticles in each well. Ampicillin (Amp) was used as a positive control, and water H_2O was used as a negative control.

Water Vapor Permeability

Water vapor permeability measures the ease with which water vapor can pass through a material. The transfer of water vapor depends mainly on the hydrophobic portion of the components of the edible film or coating. This is due to the movement of vapor in the polymers regulating the transfer of moisture from the product to the environment, seeking to make this process as slow as possible. This process involves the relationship between water vapor permeability and the type of components of the film or coating.[19]

To determine the water permeability in the films Figure 14, the method described by Zhao and co-workers was used. Briefly, a cylindrical container was filled with 1g of calcium chloride, sealed with the prepared (and tested) film. The vessel was placed in a desiccator, which contained a saturated potassium chloride solution to create a relative humidity of 85% at 25° C. It was left for 7 days, after which the change in mass of the conical container was determined. For the water vapor permeability calculations, equation (2) is used, where Δm (in g) represents the mass change of the conical container, L (in mm) is the film thickness, A (in m^2) is the area covered by the film, t (in h) is the exposure

time of the sample to the saturated KCl solution, and ΔP (in kPa) is the pressure change on the film surfaces.[63]
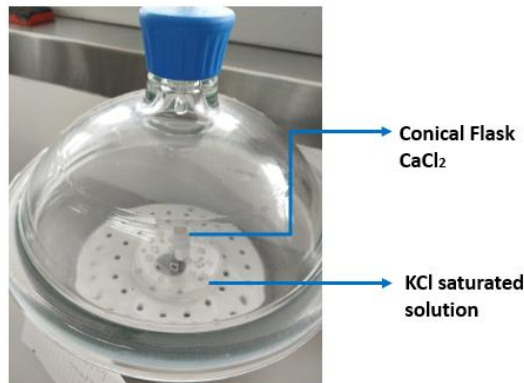
Figure 14 Water Vapor Permeability essay

(2) $\text{WVP}(\text{g mm/m}^2\text{h kPa}) = \dfrac{\Delta m \, x \, L}{A \, x \, t \, x \, \Delta P}$

Test to shelf life of fruits

To test the effectiveness of the developed films, local fruits such as golden berries and strawberries were chosen and coated with the formulation containing AgNPs-c. The coated and uncoated fruits were kept at room temperature for 10 days, and changes were documented after one day.

4 RESULTS

4.1 Cinnamon bark extract

A whitish emulsion was obtained from cinnamon extract, with the characteristic odor of cinnamon. The emulsion obtained suggests that hydrodistillate formation, containing other components than cinnamaldehyde. Therefore, for a characterization of the extract, eventually a purification of the extract was required.

UV-Vis spectroscopy

Steam distillated of cinnamon bark, was evaluated through UV-vis spectroscopy. In the obtained spectrum, shown in Figure 15, a peak at 292 nm, indicating $\pi \rightarrow \pi*$ transitions typical of the molecular structure of cinnamaldehyde

Figure 15 UV-Vis spectrum of cinnamon bark extract
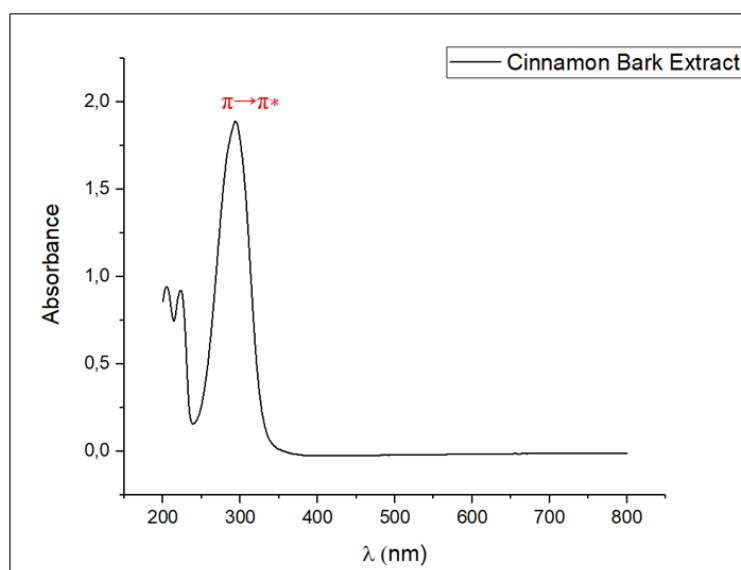
FT-IR spectroscopy

Figure 16 Cinnamon bark extract (left) cinnamon oil (right)

To obtain a good infrared spectrum, the cinnamon extract sample was decanted, and the liquid phase was separated from the oily phase, resulting in cinnamon oil. The

36

appearance of the resulting product is shown in Figure 16, from which the difference between the hydrodistillate and the purified cinnamon oil can be noted.

Figure 17 FT-IR spectrum of cinnamon bark extractshows the resulting FTIR spectrum for purified cinnamaldehyde. The most representative peaks of the spectrum can be attributed to the distinctive characteristics of cinnamaldehyde. At 3028, 3062 and 3069 cm^{-1} due to the aromatic and olefinic stretching vibration of the C-H groups. The C–H Fermi resonance of the aldehyde is observed at 2813 and 2742 cm^{-1}. The peak at 1673 cm^{-1} corresponds to the stretching of the C=O conjugated carbonyl group of the aldehyde. The peak at 1625 cm^{-1} is associated with the C=C stretching of the conjugated olefin. While the peak at 973 cm^{-1} is characteristic of out-of-plane (oop) C–H bending of a disubstituted trans-olefin group. The C=C vibrations in the aromatic structure are associated with the peaks between 1605 and 1451 cm^{-1}. Furthermore, the peaks with wave numbers at 744 and 688 cm^{-1} indicate a monosubstituted benzene aromatic structure. Finally, a peak can be seen at 1121 cm^{-1} due to the stretching of the alpha carbon-aldehydic carbon C-C bond.[93]
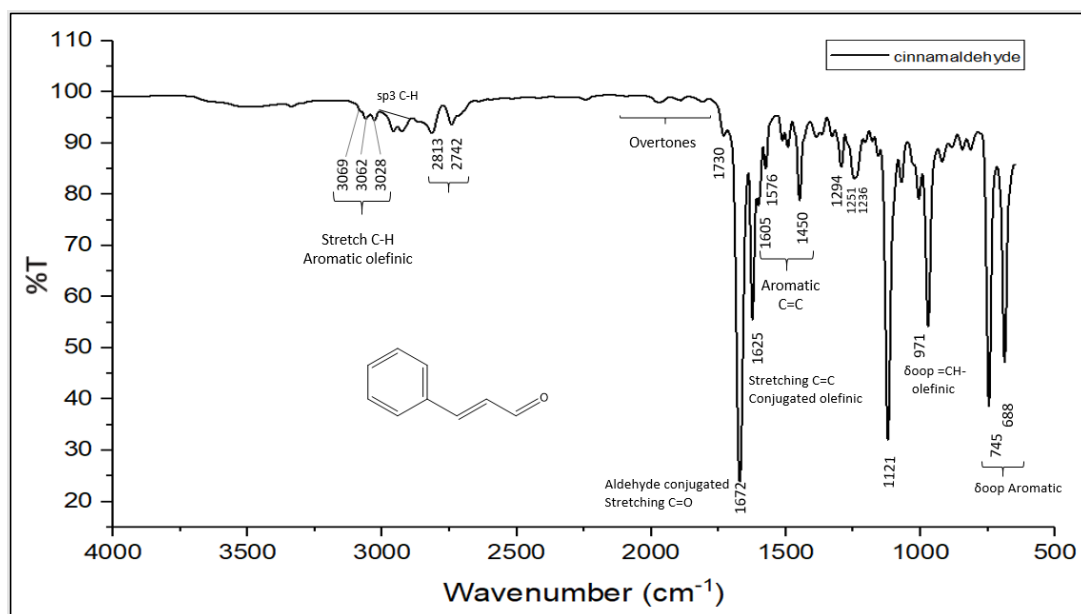
Figure 17 FT-IR spectrum of cinnamon bark extract

HPLC and GC-MS

The High Performance Liquid Chromatography (HPLC) analysis for cinnamon bark extract showed three peaks (Figure 18), with a main peak indicating a prominent

concentration of a species, whose retention time is 2.8 min. This peak is assigned to cinnamaldehyde, as it was compared with the retention time of a cinnamaldehyde standard. Based on the ratio of the intensities of the observed peaks, the purity of extract can be confirmed.
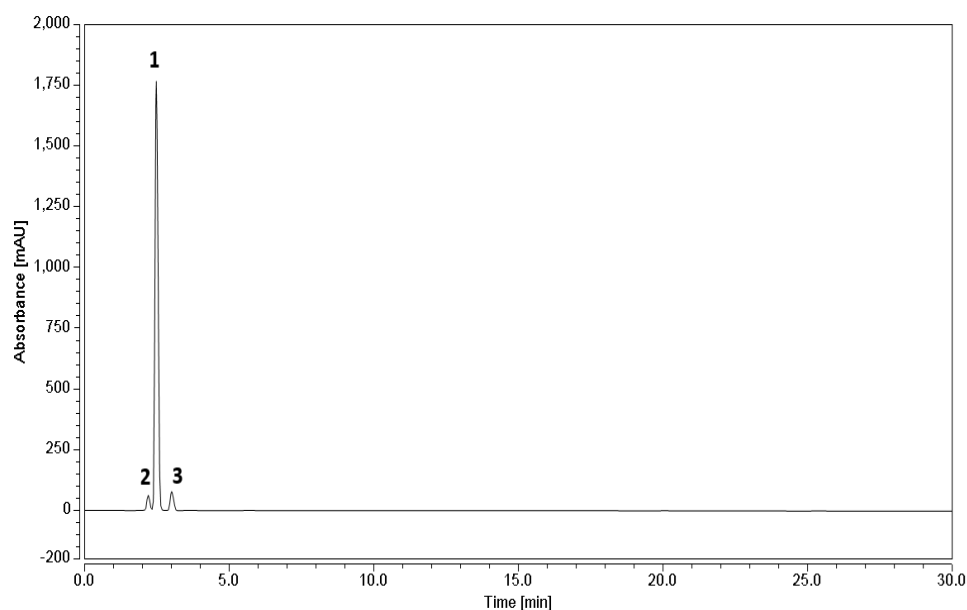
Figure 18 HPLC analysis of cinnamon bark extract

On the other hand, the presence of cinnamaldehyde was unambiguously determined by Mass Spectrometry (GC-MS). Mass spectrum from the peak at a retention time of 2.23 minutes (Figure 19) shows the presence of cinnamaldehyde molecular ion at m/z = 131 and its characteristic fragmentation pattern (m/z = 131, 103, 77, and 51). These values are comparable with the results found in the literature.
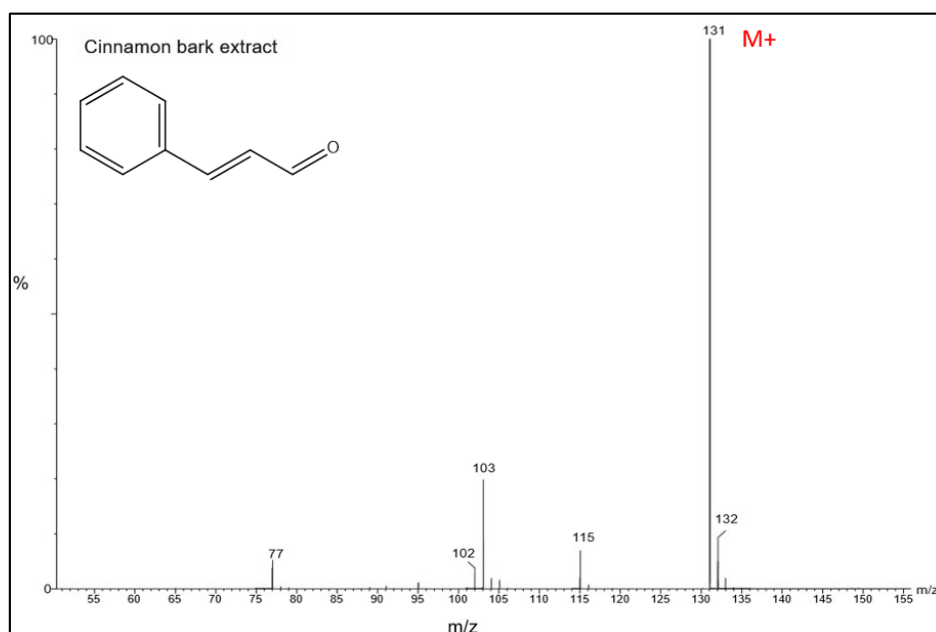
Figure 19 Mass Spectroscopy of cinnamon bark extract

38

Phytochemical Analysis

A qualitative screening for secondary metabolites in cinnamon extract was conducted through various colorimetric tests, following the established and widely known procedures.[50] In Table 2 is shown the information for each test, where the protocol reference and the respective results are indicated. In Figure 20 are shown the different colorations achieved from tests.

From tests results it can be confirmed that the presence of flavonoids was confirmed by the positive outcome of the concentrated sulfuric acid test, which resulted in an orange-red solution. However, the Shinoda's Test yielded a negative result, as there was no observable pink to crimson color change. Simple phenolic compounds were not detected, as evidenced by the negative outcomes in iodide test, Lugol's test and the ferric chloride test, with no transient red or bluish black/dark green color changes, respectively. Tannins, coumarins, and proteins also showed negative results in their respective tests.

Alkaloids were positively identified through the Dragendroff's test and Wagner's test, where reddish-brown precipitates formed. Lastly, the presence of ammonium was confirmed by the positive outcome of the Nessler test, with the solution turning yellow. The presence of nitrogen-containing species indicates that, despite the high purity of the extract, functional groups other those of cinnamaldehyde are present. It is important to note that these tests provide qualitative insights, and a more in-depth quantitative analysis is necessary for accurate concentration assessments of these secondary metabolites.
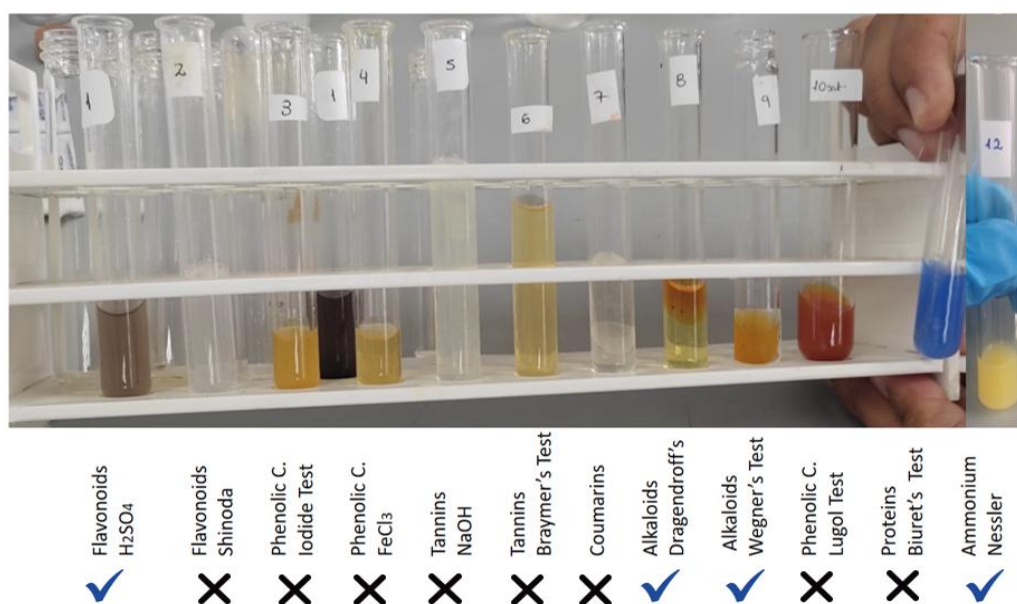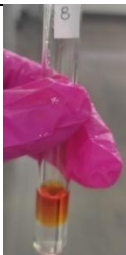
Figure 20 Screening for Phytochemical Analysis

Table 2 Phytochemical analysis of cinnamon bark extract

SECONDARY METABOLITE	TEST	RESULT	FIGURE
NA	Cinnamon bark extract		
Flavonoids	Concentrated H_2SO_4 Test	Positive as the solution turned orange-red.	
	Shinoda's Test	Negative	--
Phenols	Iodide test	Negative	--
	Ferric Chloride Test	Negative	--
Tanins	10% NaOH test	Negative	--
	Braymer's Test	Negative	--
Coumarins	NaOH Test	Negative	--
Alkaloids	Dragendroff's Test	Positive as evident by the change of color.	
	Wagner's Test	Positive result, as evidenced by the formation of precipitate.	
Carbohydrates	Lugol's Test	Negative	--
Proteins	Biuret Test	Negative	--
Ammonium		Positive	

4.2 Silver nanoparticles characterization

UV-Vis spectroscopy

The change in coloration from colorless to orange in the colloidal dispersion obtained when AgNPs-c are prepared, evidences the formation of silver nanoparticles. The inset in Figure 21 shows a vessel containing the AgNPs-c obtained, from which that coloration can be noted. To confirm the presence of silver nanoparticles, an UV-Vis spectrum was recorded and it is shown in Figure 21, from which an absorption band is observed at 427.5 nm, indicating the characteristic plasmonic band of silver nanoparticles.

UV-Vis spectroscopy analysis allows us to confirm the presence of silver nanoparticles in addition to giving us an idea of the shape.[68] The term localized surface plasmon resonance (LSPR) refers to a particular type of SPR in which the electromagnetic field remains localized to a nanoscale patterned surface. The presence of shapes other than spherical nanoparticles can be observed with the red shift from 400 nm due to surface faceting.[94]
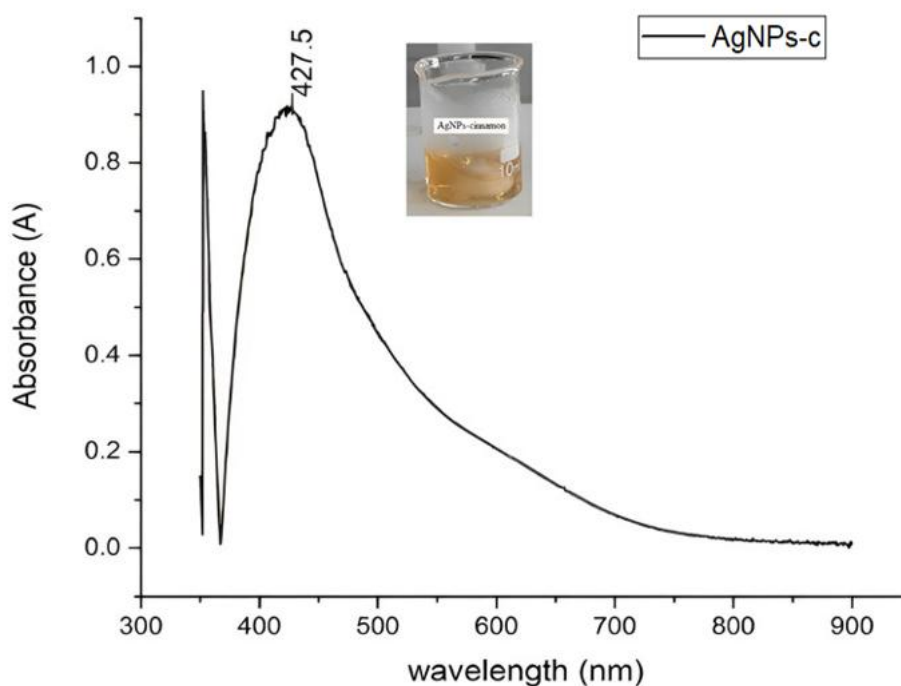
Figure 21 UV-Vis analysis of SPR of AgNPs-c

FT-IR spectroscopy

Due to reduction of silver ions, the cinnamaldehyde present in the cinnamon extract undergoes oxidation to form cinnamic acid. The chemical reaction associated with this redox process is indicated in Figure 22. The FTIR analysis confirms the cinnamaldehyde oxidation to cinnamic acid by comparing the spectra of the cinnamon extract (containing a significant amount of cinnamaldehyde) with that of the resulting colloidal dispersion containing the silver nanoparticles. This comparison is shown in Figure 23, in which some differences are evident, such as the appearance of the peak at 3263 cm^{-1}, which could indicate the presence of O-H associated with the carboxylic acid, the attenuation, and even disappearance of the peaks at 2813 and 2742 cm^{-1} related to the C-H of aldehydes, as well as the appearance of the peak at 1148 cm^{-1} corresponding to the stretching of C-O. These mentioned differences are important to demonstrate the formation of the carboxylic acid, and therefore, the effectiveness of silver reduction. It is also important to mention the presence of double peaks at 1623-1571, 1373-1309, and 1062, and 1022 cm^{-1} that are closely related to the symmetric and asymmetric tensions of carboxylates, inferring the interaction of the silver nanoparticles.[67,74] The bimodal bands suggests different size and shape distributions of the silver nanoparticles. Lastly, we can observe a single peak at 695.87 cm^{-1} associated with the aromatic C-H bending.
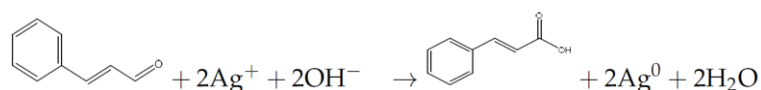
Figure 22 Chemical Reaction: silver reduction and cinnamaldehyde oxidation
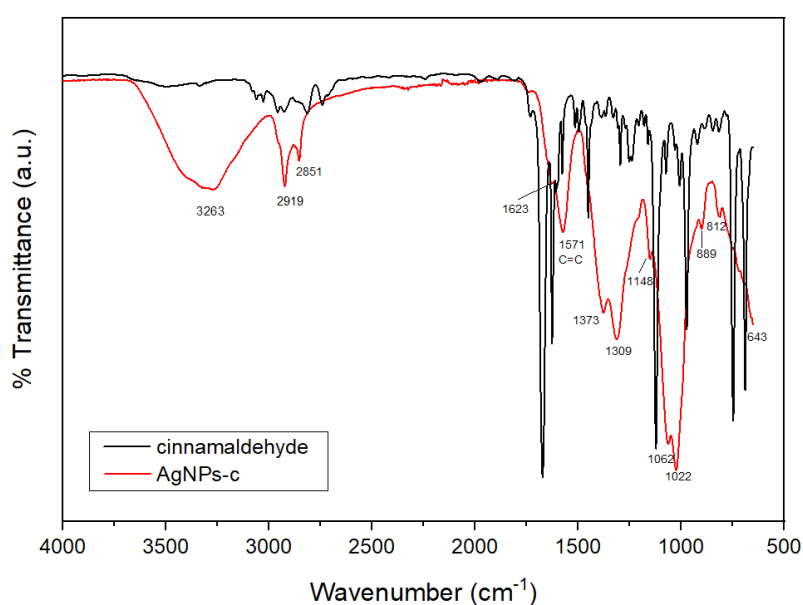
Figure 23 FT-IR spectra of cinnamon bark extract and AgNPs-c colloidal dispersion

42

Electron Microscopy: Scanning Electron Microscopy and Transmission Electron Microscopy

By obtaining TEM and SEM micrograph images of the synthesized silver nanoparticles, the sizes of AgNPs-c, which range from 5.9 to 31.7 nm, can be determined, as shown in Figure 24. In Figure 24A, it can observe the TEM micrograph illustrating the presence of different shapes of AgNPs-c, mostly spherical and of various sizes. The SEM micrograph showing spherical structures can be seen in Figure 24B, which is corroborated by surface plasmon resonance at 427.5 nm.
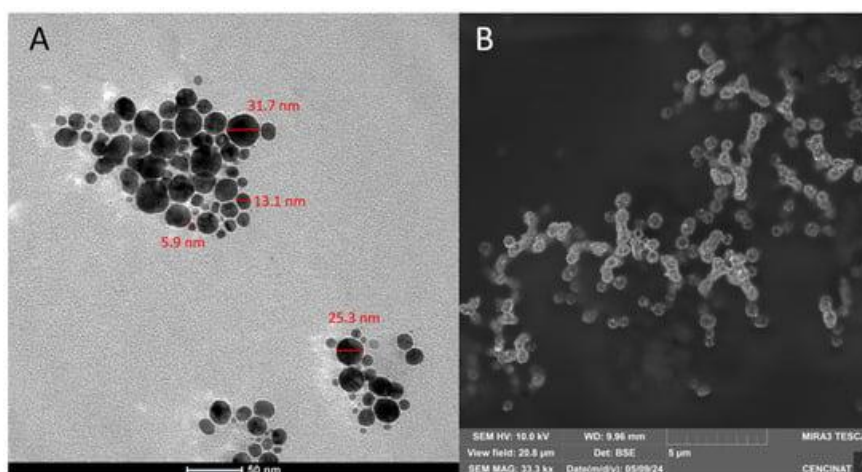
Figure 24 Electron micrographs: (A) TEM image of AgNPs-c, (B) SEM image for AgNPs-c obtained from cinnamon bark extract

Figure 25 shows a STEM micrograph of the silver nanoparticles. In these images, various shapes of silver nanostructures can be observed, such as prisms, cylinders, tetrahedrons, and spheres. Additionally, the different sizes of these nanostructures are also evidenced: 9 nm, 21 nm and 73 nm.
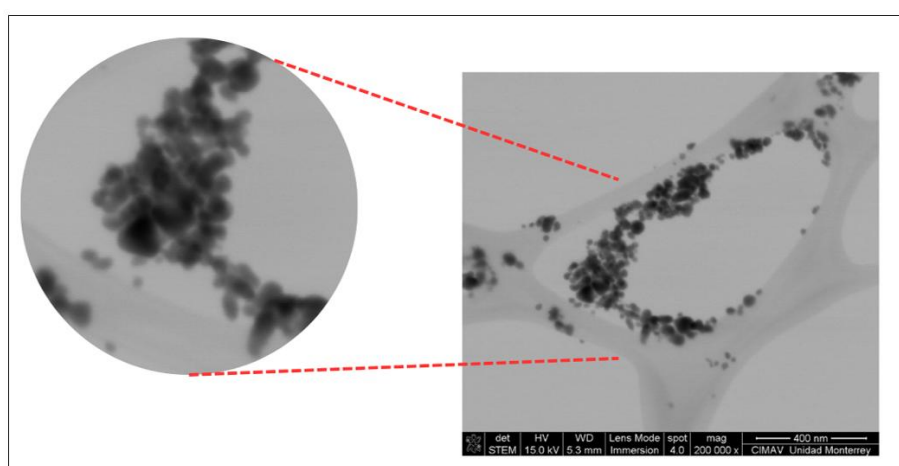
Figure 25 STEM Image of Silver Nanoparticles AgNPs-c

Dynamic Light Scattering

The different sizes (with their respective intensities) of the AgNPs-c obtained are graphically represented by the DLS analysis as shown in Figure 26A. Here three peaks are identified, each with a different percentage of intensity. The peaks at 2.94 nm, 8.7 and 65.1 nm are closely related to the dimensions of the silver nanoparticles obtained, these sizes are consistent with the plasmonic band shown in Figure 21. These AgNPs-c have an effective diameter of 44.8 nm with a polydispersity distribution of 0.356, which infers a polydispersity in the nanoparticles, this was also evidenced with the STEM analysis and is also suggested by the FTIR spectrum, which shows the presence of nanostructures with different shape.

With the results of the ζ-potential, it is possible to examine the potential associated with the surface of the nanoparticles, as well as confirm their stability, as long as the ζ-potential values range between −30 mV and 30 mV. This analysis is presented in Figure 26B, where it can be observed that the AgNPs-c have a negative surface charge of −13.6 mV. This surface potential value indicates the stability of the AgNPs-c, which is also demonstrated by the absence of noticeable changes in the appearance of the nanoparticles after several months.
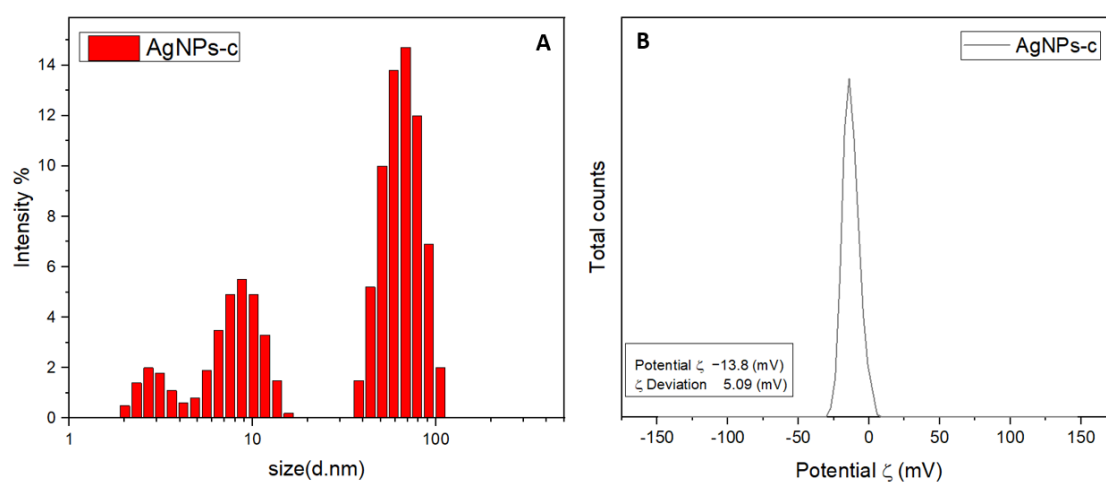
Figure 26 Characterization results of AgNPs-c (A) DLS analysis, and (B) ζ-potential

Antibacterial Analysis of Silver Nanoparticles

To determine the antibacterial properties of silver nanoparticles synthesized from cinnamon bark extract (AgNPs-c), both the Kirby-Bauer and broth microdilution methods were carried out. The results of the bactericidal activity analysis for AgNPs-c and their precursors are presented in Figure 27 and Figure 29 respectively. The Kirby-Bauer

method clearly shows the inhibition zones formed by AgNPs-c at various concentrations, with halo diameters comparable to that produced by the antibiotic ampicillin (Amp) used in the test. Table 3 details the diameters of the inhibition zones for the different concentrations of AgNPs-c tested.
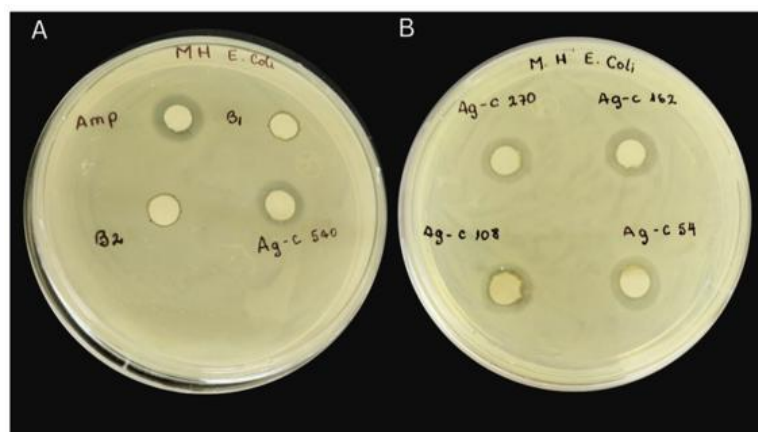
Figure 27 Disk diffusion assay results of the evaluation of different concentration of AgNPs-c where B1 is AgNO₃, B2 is cinnamon bark extract, and Amp is ampicillin antibiotic

Table 3 Inhibition zone of the AgNPs-c against of Gram positive and Gram negative bacteria obtained by Kirby-Bauer method.

Zone of inhibition (mm)				
Sample	**C7230**	**PE52**	**AN54**	**29213**
B1: AgNO₃	5.2	5.1	5.1	5.2
B2: Cinnamon bark extract	6	6	6	6
AgNPs-c 54 µg/mL	7	9	6	6
AgNPs-c 108 µg/mL	15	10	7	6
AgNPs-c 162 µg/mL	13	10	7	7
AgNPs-c 270 µg/mL	16	14	14	10
AgNPs-c 540 µg/mL	15	15	14	10

The precursors silver nitrate and cinnamon extract, as well as the blank sample, Table 3 show low inhibition zones values, indicating they have a slight antibacterial capacity against Gram-positive and Gram-negative bacteria evaluated. With silver nanoparticles, inhibition zones can be distinguished even at lowest concentrations of AgNPs-c. As the concentration of AgNPs-c increases, larger diameter inhibition zones are observed, indicating an increase in its bactericidal capacity. For example, the AgNPs-c system at 540 µg/mL causes inhibition zones of up to 15 mm in diameter for PE52, for AN54 14mm, for C7230 15 mm, and 10 mm for the 29213 bacteria. It is interesting to note that by increasing the concentration of AgNPs-c from 270 µg/mL to 540 µg/mL, the values of the inhibition halos remain almost constant, suggesting that the maximum

antibacterial capacity of the evaluated system is reached. Overall, the antibacterial analysis shows that AgNPs-c have bactericidal properties that vary with concentration.

The viability of the AgNPs-c against bacteria is also implied using a bacterial strain of *E. coli*. For this determination, bacteria were seeded in Petri dishes and 10 uL of AgNPs-c at different concentrations were directly added. After 12 hours of incubation, the viability of the nanoparticles at each concentration could be observed, evidenced by an evident region of inhibition shown in Figure 28.

Figure 28 Viability of AgNPs-c against E.coli

In the broth microdilution method, the appearance of turbidity after the incubation period implies bacterial growth in strains, or even more, the proliferation of colonies. From the results obtained by this method, presented in Figure 29A and Figure 29B a marked antibacterial activity is observed in the wells containing AgNPs-c, for all the bacteria analyzed, since no bacterial growth was detected. Regarding the activity of precursors, except for *Pseudomonas aeruginosa* bacteria, whose growth was inhibited by the cinnamon extract, no notable antibacterial activity is perceived.

Table 4 Results for the broth microdilution analysis of AgNPs-c against of sensible and resistant bacteria

Sample	KpE52	KpLC1	C7230	DH5	PAO1	PE52	AN2	AN54	2913
Medium and Inoculum	-	-	-	-	-	-	-	-	-
Cinnamon bark extract	-	-	-	-		-	-	-	-
AgNPs-c	+	+	-	+	+	+	+	+	+

The antibacterial activity of AgNPs-c against the bacteria *E. coli* was evaluated by measuring the changes in absorbance at 630 nm, relative to a standard. The growth kinetics of *E. coli* are shown in Figure 29B. Different growth stages are identified,

although the decline stage is not reached, since both live and dead bacterial cells absorb at 630 nm.[95] It is observed that higher concentrations of silver nanoparticles significantly inhibit bacterial growth. Silver nitrate (B1) acts as a bacteriostatic agent, achieving a constant stationary phase of bacterial growth after 12 hours, while cinnamon bark extract (B2) does not achieve this phase. The presence of AgNPs-c notably affects bacterial growth. At a concentration of 54 μg/ml, AgNPs-c cause a decrease in absorbance, indicating a reduction in the number of live bacterial cells. Furthermore, a higher concentration of AgNPs (108 μg/ml) results in even higher bacteriostatic behavior.
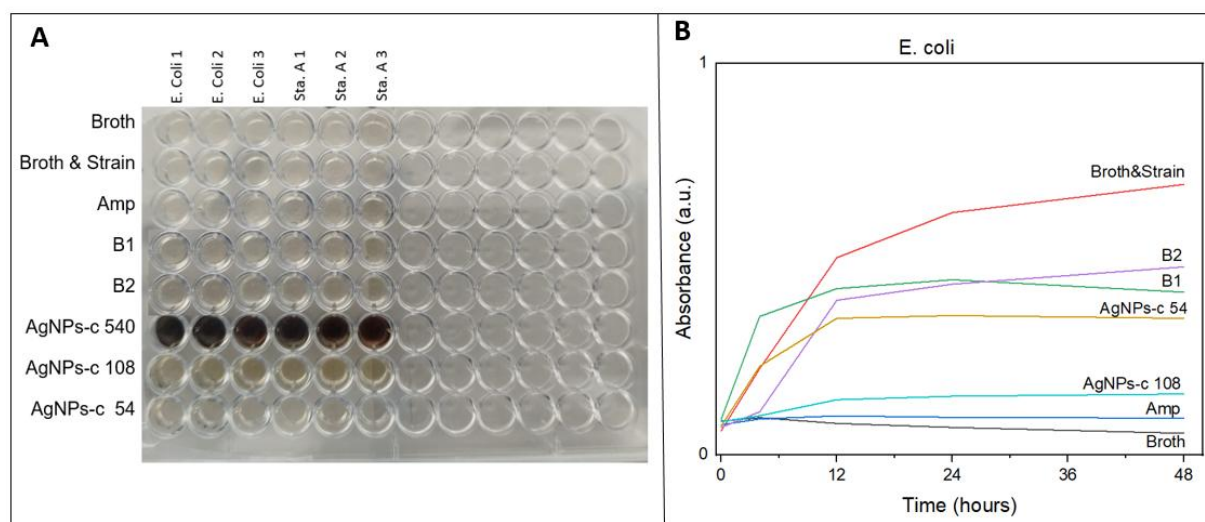
Figure 29 A: Broth Microdilution essay of AgNPS-c. B: Bacterostatic analysis graph

4.3 Nanocomposites Characterization

XRD X- Ray Diffraction

With the purpose of evaluating the structure of the biopolymer precursors of the biopolymer-based coating films prepared, X-ray diffraction tests were carried out, and the diffractograms obtained are shown in Figure 30.

The diffractogram of carboxymethyl cellulose shows the characteristic peak of CMC at approximately 22° showing the crystalline section of cellulose, a small difference can be seen in the intensity and shape of the peaks of the samples depending on the chemical additives and conditions processing used.
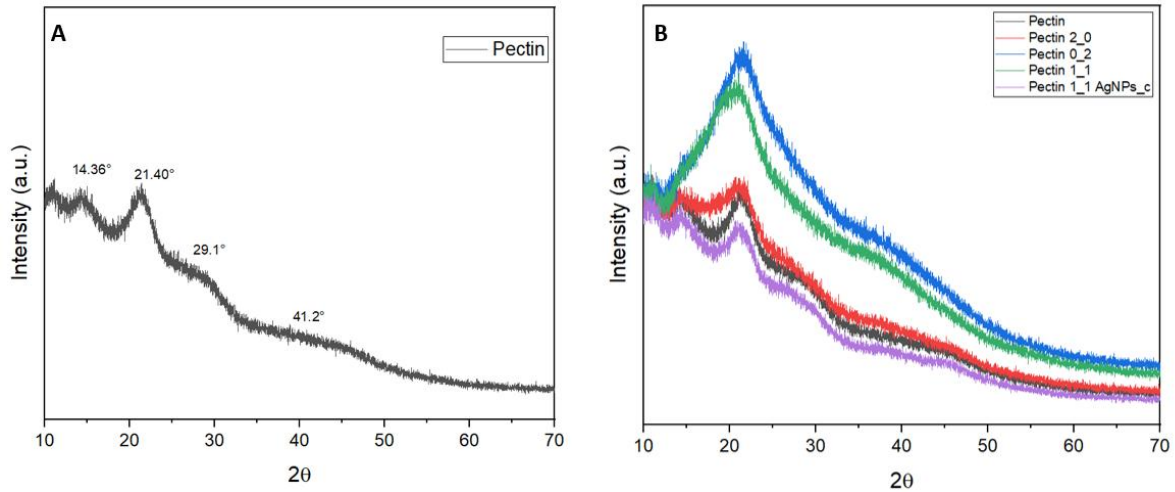
Figure 30 DRX Analysis of films of A: Pectin film and B: Pectin formulation films

The X-ray diffraction analysis shows the diffraction patterns of the pectin samples. The sample containing only pectin Figure 30A Since pectin is an amorphous material, the diffractogram will generate broad, low-intensity peaks. Pectin has a predominantly amorphous structure with certain semicrystalline phases, semicrystalline peaks at 21° and 40°.

The intensity and definition of the peaks are the lowest among the three samples, suggesting that the addition of additives in this proportion significantly affects the crystalline organization of the pectin. As can be seen in Figure 30B, the peaks of the samples containing egg albumin increase the semi-crystalline characteristic of the material.
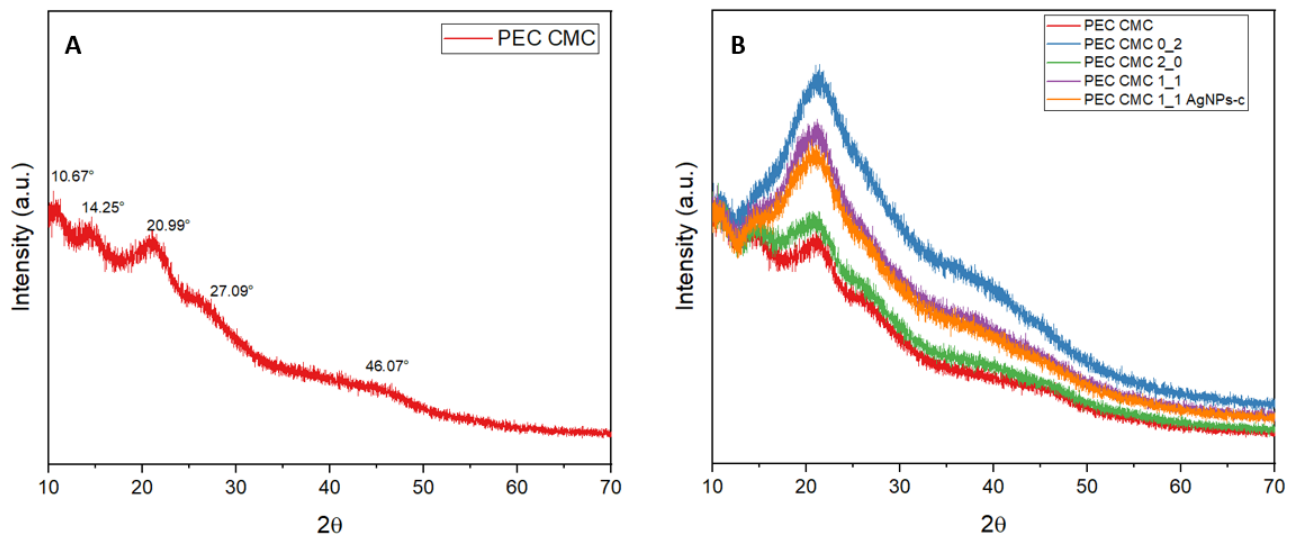
Figure 31 DRX Analysis of films of A: PEC CMC film and B: PEC CMC formulation films

When combining pectin with CMC, various peaks are observed in the spectrum, with the pectin peaks standing out, which show a slight shift. In particular, the 41° peak shifts to 46°.

When adding additives, variations in the intensity of these peaks can be observed. The highest peaks correspond to the samples containing egg albumin.

FTIR

In Figure 32, the FTIR spectrum of pectin is presented, where the main vibrational modes characteristic of this biopolymer can be identified. A band at 3326 cm^{-1} corresponds to the stretching of the O-H bond, indicating the presence of hydroxyl groups in the pectin structure. The presence of the band at 2928 cm^{-1} is attributed to the stretching of the C-H bond. At 1728 cm^{-1}, a characteristic peak of the stretching of the carbonyl group (C=O) present in the carboxylic groups of galacturonic acid is observed.[22] Can see a band at 1622 cm^{-1} , which corresponds to the stretching of the N-H bond of the amide group; this group may be present in certain types of pectin,[96] as seen in Figure 32, which proposes a structure for pectin. The stretching of the C-O bond is observed at 1224 cm^{-1}, this band is characteristic of ester bonds in the methoxyl groups of methylated pectin.
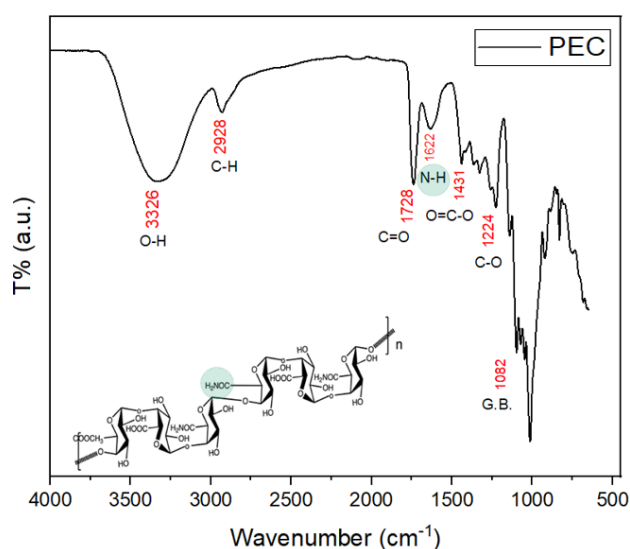
Figure 32 FTIR spectrum of Pectin

The inclusion of additives modifies the infrared spectrum in a certain way. When adding glycerol, the bands do not seem to change extremely, however when including the combination of glycerol and egg albumin some differences can be seen. The changes occur mainly at approximately 1600 cm^{-1} where the amide bands present in the egg albumin are accentuated. By including silver nanoparticles in the polymer, we can see the

interaction and amidation that is taking place Figure 33. Figure 33B shows a magnification of the region 1900-1450 cm^{-1}.
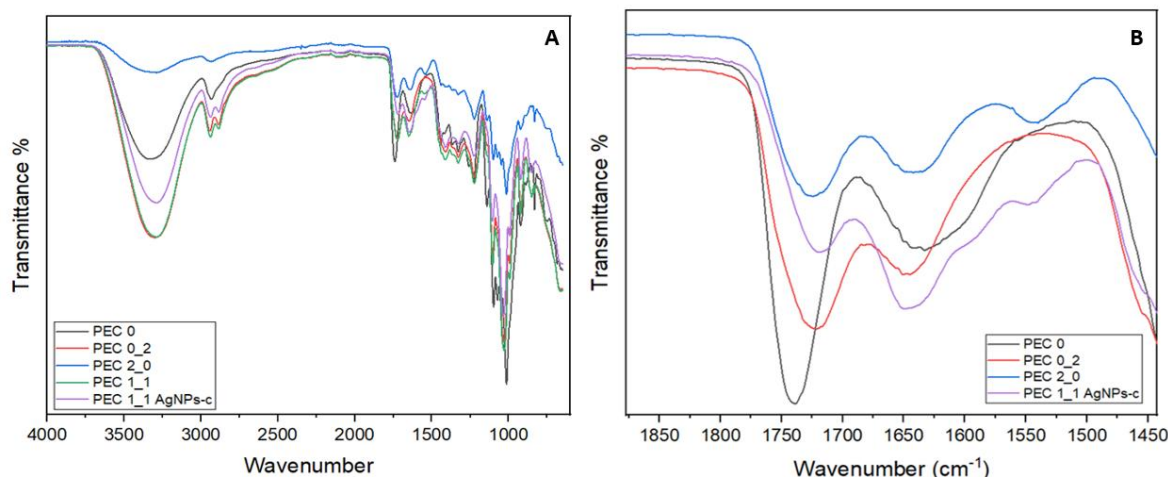
Figure 33: A FTIR spectra of pectin samples. B zone of changes of spectra

Figure 34 shows the FTIR spectra of carboxymethyl cellulose film and the G/EW/CMC films. In the CMC powder spectra Figure 34A, the strongest absorption around 3338 cm^{-1} corresponds to the vibration of intra-chain and inter-chain hydrogen-bonded hydroxyl groups (-OH). Absorption around 2910 cm^{-1} was caused by vibration of C-H bond. The bands from 1413 to 1327 cm^{-1} comes from C─H and O─H groups and in the fingerprint zone, the peak of ester groups (1054 cm^{-1}) is clearly present.
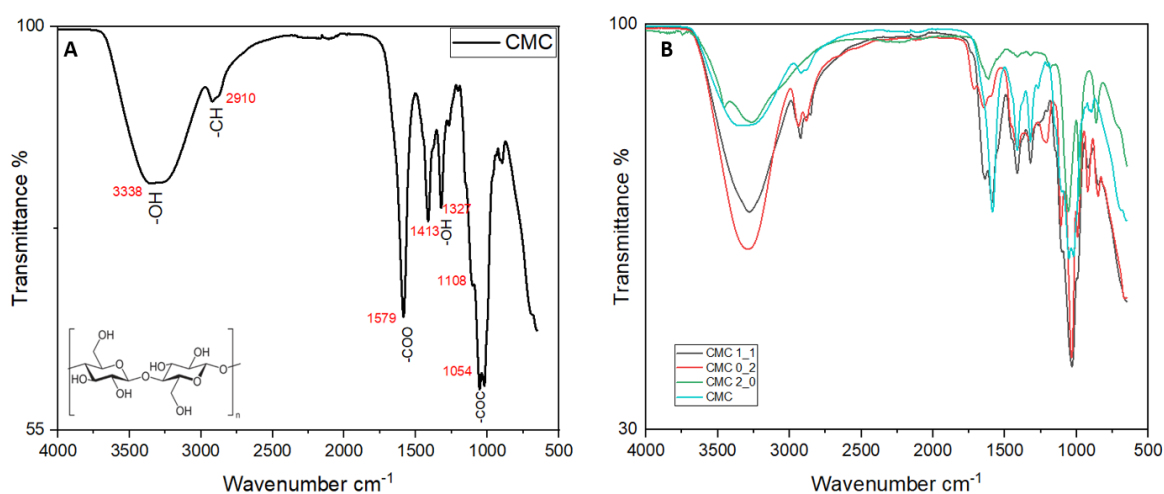
Figure 34 CMC Spectra: A CMC film B CMC formulation films
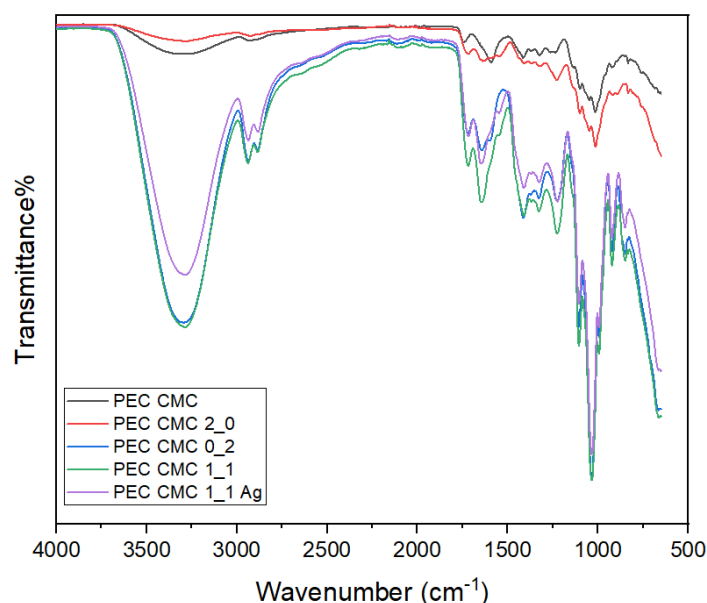
Figure 35 FTIR spectra of PEC CMC films

In the Figure 35, FTIR spectra of CMC/PEC film is presented. This spectrum shows the characteristic bands of both pectin and CMC. However, they were slightly displaced or less intense, showing good cross-linking and miscibility of biopolymers. Strong broadband of –OH was observed at 3489 cm^{-1}, and the bands at 1034 cm^{-1} and 1628 cm^{-1} suggested that CMC's carboxyl groups (–COOH) were present in the films after cross-linking. The results indicated a successful formation of the PEC-CMC-1_1 AgNPs-c film.

TGA
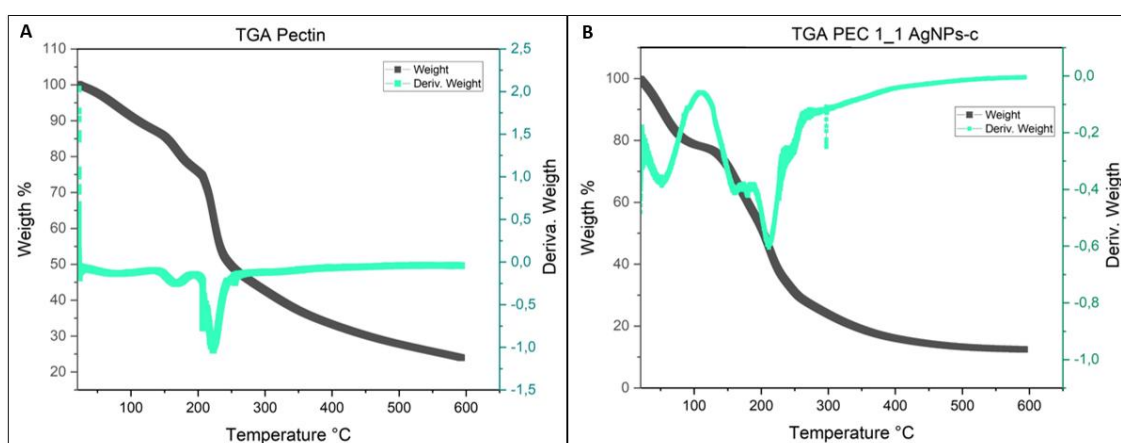
Figure 36 TGA analysis for pectin films

Figure 36A shows the thermogravimetric analysis (TGA) of pectin, where several stages of degradation are observed. The initial stage occurs between 50 and 160 °C and it is characterized by a broad band observed in the thermogram, which is related to the

evaporation of the residual water from the pectin preparation. The second stage, between 160 and 204 °C, is attributed to the decomposition of impurity of the sample. Between 240 and 350 °C, a weight loss is observed corresponding to the degradation of the main pectin skeleton. Finally, between 350 and 500 °C, we see another stage that is associated with the degradation of the carbons of the pectin ring.[97]

The TGA analysis of the PEC 1_1 AgNPs-c film Figure 36B shows four stages of degradation, the first from 50 to 109 °C due to the evaporation of residual water. The second stage of 160 to 181 °C is attributed to the degradation of glycerol and other volatile components of pectin sample. At 211-249 °C, a third degradation stage can be determined, which is attributed to the degradation of the main pectin skeleton. A slight stabilization of the structure can be observed due to the presence of the additives but especially the silver nanoparticles as suggested Shankar and co-workers[46] in their research. The degradation of the carbons of the pectin ring occurs in a fourth stage at 350 and 500 °C.
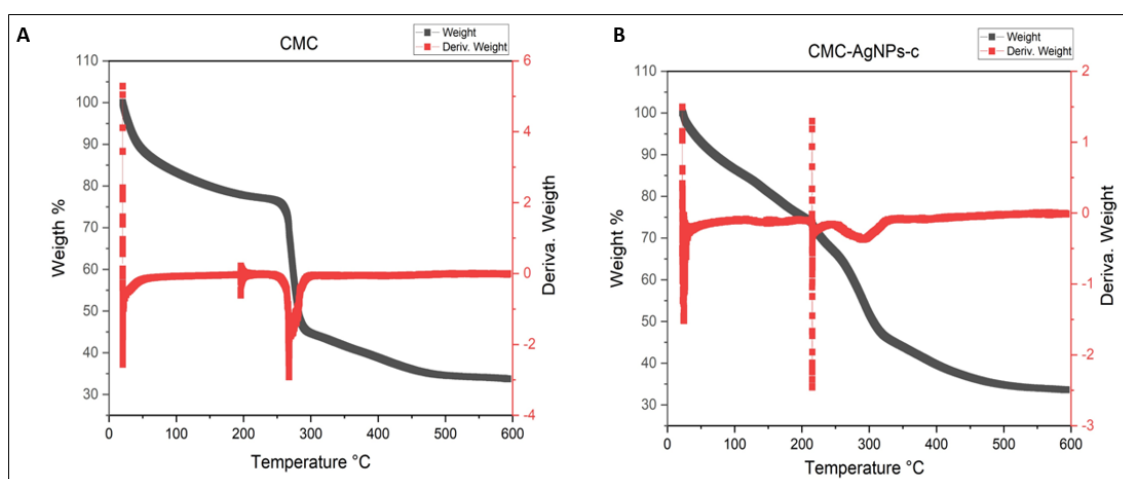
Figure 37 A: TGA for CMC film. B: TGA for CMC with AgNPs-c films

The TGA analysis for the pristine CMC sample is shown in Figure 37A, in which we can see a stage of weight loss begins at 50 °C, mainly this corresponds to the weight loss due to water evaporation which continues until 250 °C approximately. From 260 °C until 290 °C, the weight loss is drastic, for the loss of the degradation of the main structure of cellulose and from 290 until 480 °C a weight a less minus pronounced weight loss that could occur due to the thermal decomposition of cellulose by decarboxylation through dehydration.[98]

Figure 37B shows the thermogravimetry of the CMC-AgNPs-c analysis, where the initial decomposition of the nanocomposite due to water loss can be seen from 40 to approximately 125 °C. Above this temperature, a significant weight loss occurs, due to the decomposition of less stable components of the CMC-AgNPs-c, which could be the egg albumin and cinnamic acid used in the preparation of the silver nanoparticles. from 214 to 259 °C a degradation stage of the pectin structure, finally a last stage from 317 to 490 °C. This analysis demonstrates that the addition of AgNPs-c and egg albumin improves the thermal stability of CMC. Silver nanoparticles act as thermal stabilizers, reducing the degradation rate.[99] The improvement in thermal stability can be attributed to the interaction between the AgNPs-c and the polymer matrix, which provides a structure that is more resistant to thermal decomposition.[100]
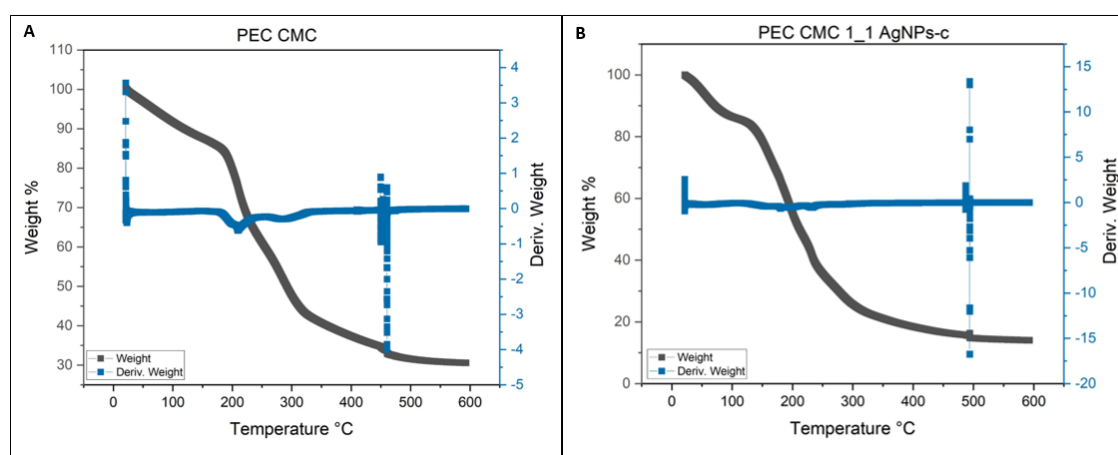
Figure 38 TGA graphs of A:PEC-CMC and B:PEC CMC 1_1 AgNPs-c

In the TGA analysis for PEC CMC sample Figure 38A, four stages can be observed: from 20 °C to 180 °C, a weight loss corresponding to the loss of absorbed water; up to about 320 °C, a second stage corresponding to the thermal decomposition of pectin, represented by a significant drop in weight; from 350 °C to 450 °C, a third phase corresponding to the degradation of the CMC polymer chain; and, from 450 °C onwards, a final, small stage that could correspond to the carbonization of organic residues.

Figure 38B shows the TGA of the PEC CMC sample with silver nanoparticles. The degradation stages do not differ significantly from the sample without silver nanoparticles. However, what is most notable is that the degradation rate of the polymers is more gradual, as the slope is not steep. This could imply that the addition of silver

nanoparticles   improves   the   thermal   stability   of   the   material.
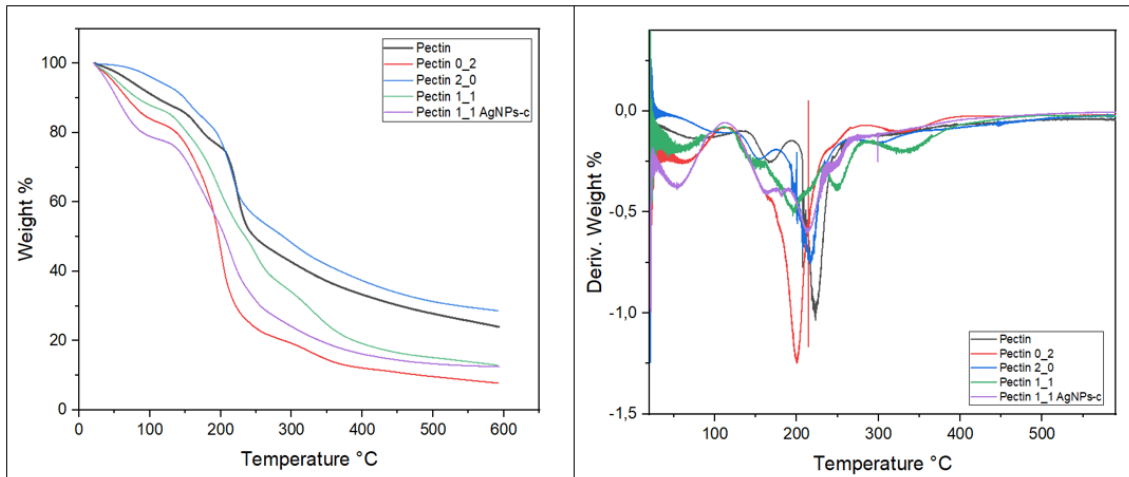
Figure 39 TGA of Pectin films
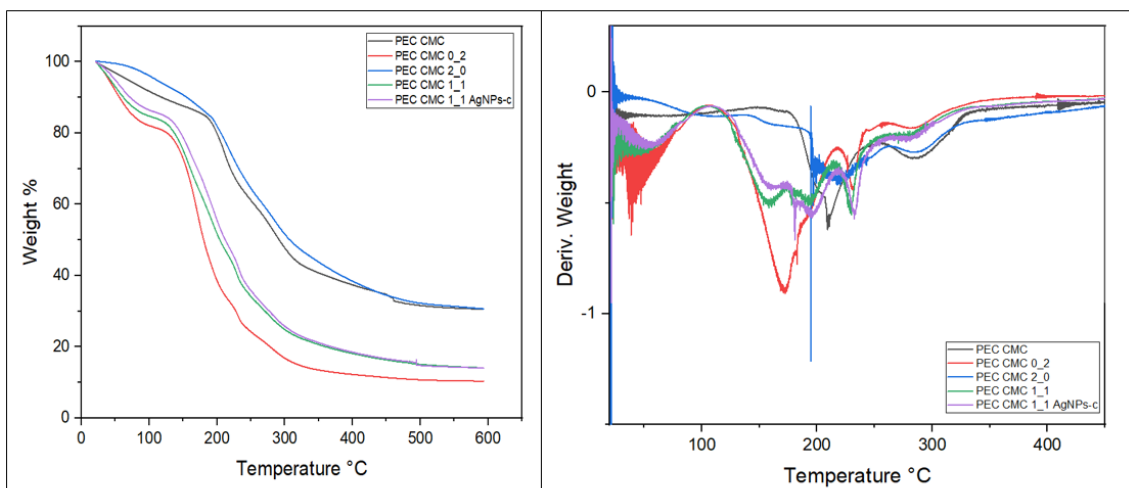
Figure 40 TGA PEC CMC Films

In Figure 39 and Figure 40 it is possible observed that the addition of glycerol to film formulations has the main function of providing them with greater softness and flexibility, thus increasing their plasticity, which is beneficial for the prepared material. However, thermogravimetric analyses reveal that this addition also leads to a reduction in the thermal stability of the biopolymers. This justifies the incorporation of egg albumin, which increases the thermal stability of the glycerol-containing biopolymer, something that is not achieved by the addition of citric acid alone.

Although the presence of silver nanoparticles has a significant impact on the thermal stability of CMC, as mentioned above in relation to Figure 37A and Figure 37B,

54

this effect is not reflected in the thermal stability of the films formed by the PEC-CMC combination.
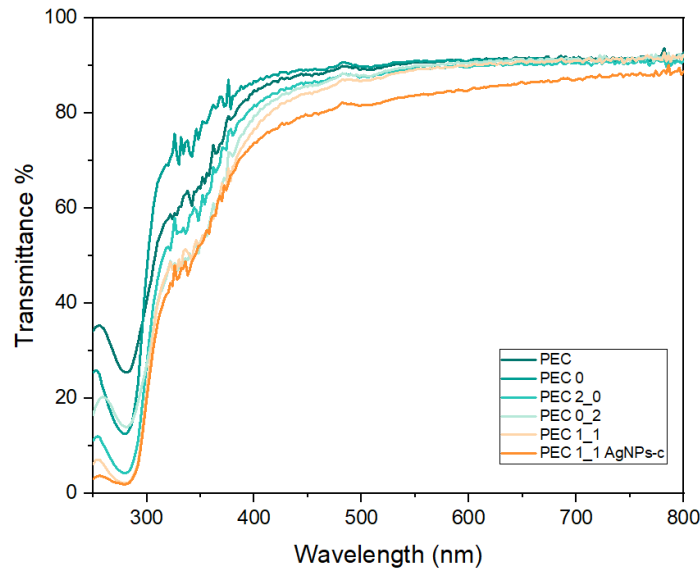
Figure 41 Transmittance of PEC films

Transmittance analyses of pectin films (Figure 41) reveal important data on the transparency of the different formulations. At 280 nm, the transmittance percentage is observed to decrease as additives are added. Films with all additives PEC 1_1 and those containing silver nanoparticles PEC 1_1 AgNPs-c present the lowest transmittance percentages. These results at this wavelength demonstrate that PEC 1_1 AgNPs-c films offer an excellent barrier against UV light. Between 365 and 450 nm, corresponding to UV radiation that penetrates deeper into the material, the lowest transmittance is observed in the pectin film containing all additives, including AgNPs-c silver nanoparticles, as represented by the orange line in the Figure 41. It is worth noting that the combination of components in the proposed formulation significantly reduces the amount of radiation passing through the material. The transmittance percentage of pectin films at 660 nm decreases with the incorporation of additives. Formulation PEC 1_1 AgNPs-c presents the lowest value, indicating that the addition of silver nanoparticles reduces the transparency of the material, thus improving its capacity as a barrier against visible light.
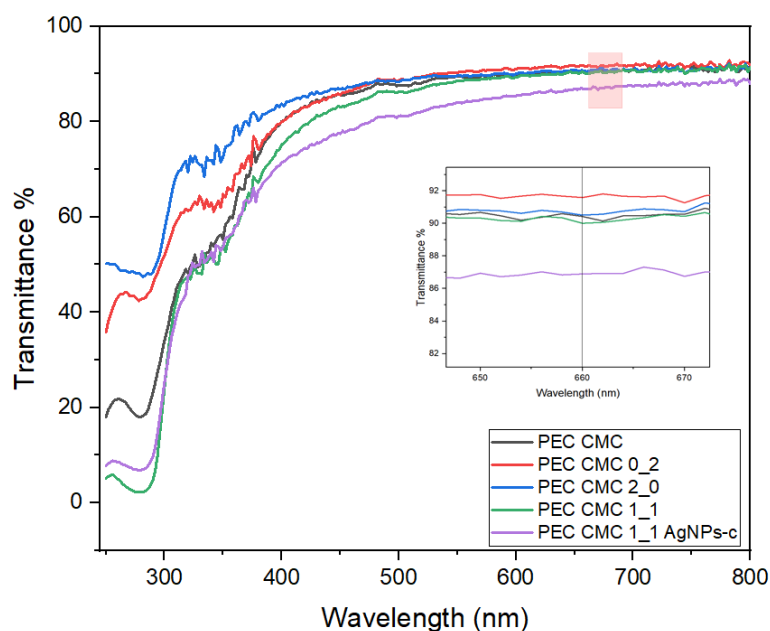
Figure 42 Transmittance of PEC CMC films

The light barrier properties of the Pectin and CMC films are shown in Figure 42. The transmittance at 280 nm is observed, where differences between the different films can be seen. The PEC CMC 2_0 films show the highest transmittance percentage, even higher than the transmittance of the PEC CMC films. The films that include all the components show a notable decrease in this transmittance, indicating a good barrier against UV light. From 365 nm onwards, it can be observed in Figure 42 that the transmittance values vary depending on the additives present in the polymer. The samples with the lowest transmittance percentages correspond to those containing the combination of additives and silver nanoparticles, denotes as PEC CMC 1_1 AgNPs-c in Figure 42. At 660 nm, the highest transmittance percentages are the PEC CMC 0_2 films, while the PEC CMC 2_0 and PEC CMC films show very similar transmittance values. The PEC CMC 1_1 films with all the additives show a slight decrease in the transmittance percentage value, but by adding AgNPs-c, this value drops considerably, indicating that these films offer a better barrier against visible light.

4.4 Mechanical Properties

The results of Tensile strength (TS), elongation at break (EAB) and Young's modulus are shown in Table 5 for pectin-based. These films have thicknesses varying between 0.1146 mm and 0.4382 mm. The thicker films contain glycerol only as an additive PEC 0_2, while the thinner films contain the complete mixture of additives PEC 1_1. The tensile strength values (TS) of this polymer present differences according to the

different formulations. The film PEC 0_2 shows the highest (TS) 20.20 MPa, while the PEC 2_0 film, formed with egg albumin, shows the lowest (TS) 1.42MPa. For polymeric materials with the characteristics for desired application, intermediated tensile strength values are preferred, meaning that the material has a certain ability to deform under an applied force.

The percentage of elongation at break (EAB) is highest for the film samples containing the combination of egg albumin and glycerol PEC 1_1, with 37.46% of EAB. This indicates greater flexibility of the film, which is suitable for food packaging applications. On the other hand, PEC 2_0 and pectin PEC 0 have the lowest values of elongation at break, with percentages lower than 10%.

The most notable difference between the formulations is the Young's modulus values. The film PEC 2_0 has the highest value of YM, with 772.13 MPa, which indicates that the film has great fragility. The lowest value of YM corresponds to the PEC 0_2 formulations with 4.01 MPa. These low values of Young Modulus are desirable for films used in food packaging.

Table 5 Mechanical properties (thickness), (TS) (EAB) and (YM) of Films

MECHANICAL PROPERTIES OF FILMS				
Sample	Thickness (mm)	TS (MPa)	EAB %	YM (MPa)
PEC 0	0.1241	19.96	9.83	412.28
PEC 0_2	0.4382	20.20	9.54	772.13
PEC 1_1	0.1146	2.55	37.46	9.66
PEC 2_0	0.1954	1.42	31.08	4.01

Figure 43 shows contour maps that show how the mechanical properties of the films vary depending on the percentage of glycerol (G%) and the percentage of egg albumin (EW%). For a film intended for fruit packaging, intermediate tensile strength values are required, which are in the green area of the contour map. According to Figure 43A, this combination is achieved with a higher percentage of egg albumin and a low concentration of glycerol.

For this type of polymers, the elongation at break must be high. The map in Figure 43B shows that this is achieved with a higher amount of glycerol and egg albumin. The combination of these additives significantly improves this property. The appropriate formulation to obtain low values of elastic modulus, and therefore, less brittle materials,

is with a higher concentration of glycerol and an intermediate or low concentration of egg albumin; as shown in the blue area of the contour map in Figure 43B.
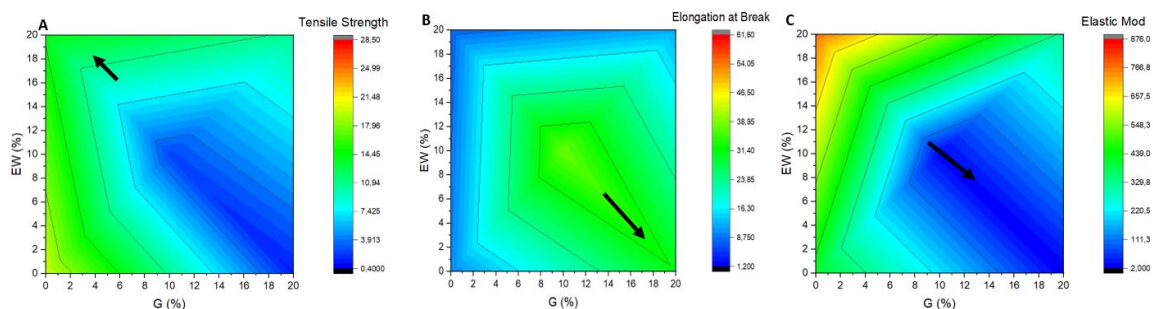
Figure 43 (A) Tensile Strength, (B) Elongation at Break and (C) Elastic Modulus analysis of pectin films

Table 6 Statistical Analysis ANOVA for films formulation containing a combination of glycerol and egg albumin.

TENSILE STRENGTH				
	Sum of Squares	**Mean Square**	**F Value**	**P Value**
G	906.0377	453.0189	15.6217	3.48832E-4
EW	109.3145	54.65726	1.8847	0.19109
Model	1223.7979	305.9495	10.5502	4.94196E-4
Error	376.9912	28.99933		
Corrected Total	1600.7892			
ELONGATION AT BREAK				
	Sum of Squares	**Mean Square**	**F Value**	**P Value**
G	1130.9852	565.4926	6.80631	0.0095
EW	11.72777	5.86389	0.07058	0.93221
Model	2958.20566	739.55141	8.9013	0.00109
Error	1080.08619	83.08355		
Corrected Total	4038.29184			
ELASTIC MODULUS				
	Sum of Squares	**Mean Square**	**F Value**	**P Value**
G	443299.87793	221649.93897	32.75871	8.3821E-6
EW	269371.90616	134685.95308	19.90588	1.10378E-4
Model	1567349.71978	391837.42994	57.91153	3.71294E-8
Error	87959.79442	6766.13803		
Corrected Total	1655309.5142			

Tensile Strenght: At the 0.05 level, the population means of G (Glycerol) are significantly different. At the 0.05 level, the population means of EW (Egg Albumin) are not significantly different

Elongation at Break: At the 0.05 level, the population means of G (Glycerol) are significantly different. At the 0.05 level, the population means of EW (Egg Albumin) are not significantly different

Young Modulus: At the 0.05 level, the population means of G (Glycerol) are significantly different. At the 0.05 level, the population means of EW (Egg Albumin) are significantly different

ANOVA analysis indicates that there is no significant difference in the tensile strength values when changing the concentration of egg albumin. Instead, there is a significant difference in the tensile strength values when modifying the concentration of glycerol. Similarly, this is the case for the elongation at break values for both the egg albumin and glycerol concentrations.

With the values of the elastic modulus, it can be observed that there is a significant difference when varying both the concentration of egg albumin and that of glycerol.

4.5 **Antibacterial Analysis of Films preparation**

The analysis by diffusion per well are showed in Figure 44 and Table 7. In these results, it is feasible to observe that the largest zone of inhibition (13 mm) is presented by the sample of the combination of PEC CMC 1_1 AgNPs-c. The next value is given by PEC 1_1 AgNPs-c and the lowest value is for CMC EW AgNPs-c, this indicates the antimicrobial property that these films possess.

Figure 44 Diffussion per well analysis of film forming solution

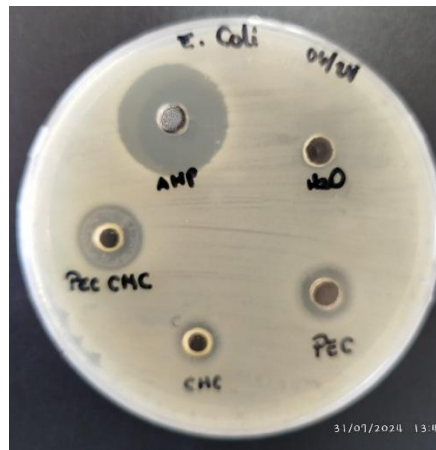Table 7 Zones of Inhibition of the films tested against E. Coli

Zones of Inhibition (mm)	
Sample	**E. Coli**
Ampicillin	22
H_2O	0
PEC 1_1 AgNPs	10
CMC EW AgNPs	8
PEC CMC 1_1 AgNPs	13

4.6 Water Vapor Permeability

Water vapor permeability (WVP) provides key information on moisture transfer and interactions with biopolymers in edible films. In fruit packaging, a balanced WVP allows for humidity control, preventing condensation and the growth of microorganisms. Furthermore, adequate oxygen (O_2) and carbon dioxide (CO_2) permeability is vital for fruit respiration, which maintains its freshness and quality, avoiding dehydration or the accumulation of gases that could shorten its shelf life.[101] Two prepared films: PEC 1_1 AgNPs-c, PEC CMC 1_1 AgNPS-c were analyzed to determine their WVP. To apply the equation mentioned above to determine WVP equation (2), the parameters Δm (changes in cup mass), t (film exposure time to humidity or moisture), L (film thickness) and ΔP (partial pressure difference of water vapor inside and outside the cup) are required. The first three parameters were easily determined from experiments. However, assigning a value to ΔP required a detailed analysis of the system to accurately determine the respective pressure difference on both sides of the film.

According to the thermodynamics of the system, the pressure of a gas (p_i) diffusing in a medium can be related to its concentration (c_i), as described by Henry's Law: $c_i = k_H\, p_i$. Under certain conditions, Henry's constant (k_H) can be considered a measure of the solubility of the gas in the medium in which it diffuses. Furthermore, as is well known, the water vapor transfer can be determined by the difference in the chemical potential of water on both sides of the coating film. This difference is directly proportional to the water vapor concentration gradient across the film. This relationship suggests applying Fick's Law of Diffusion equation (3), which connects the mass flux density (J_m) with the concentration gradient through the diffusion coefficient (or diffusivity). By combining Henry's Law and Fick's Law, the resulting expression relates the mass flux density to a pressure gradient, mediated by a coefficient (£), which is the product of solubility and diffusivity.

$$(3)\ J_m = -D\,\frac{\partial c_i}{\partial x} = -k_H\, D\,\frac{\partial P_i}{\partial x} = -£\,\frac{\partial P_i}{\partial x}$$

Mass flux density is defined as the amount of mass transferred per unit area per unit time across a surface, as indicated in equation Jm. This term is also commonly referred to in the literature as water vapor transfer rate (WVTR)[13].

$$(4)\ J_m = \frac{\Delta m}{A\,\Delta t} = WVTR$$

The £ coefficient is defined precisely as permeability (WVP), and from equation (4), it can be determined using equation (5), in which the approximation of a very thin film thickness has been maintained.

$$(5) \quad WPV = £ = \frac{J_m L}{\Delta P} = \frac{(WVTR)\,L}{\Delta P}$$
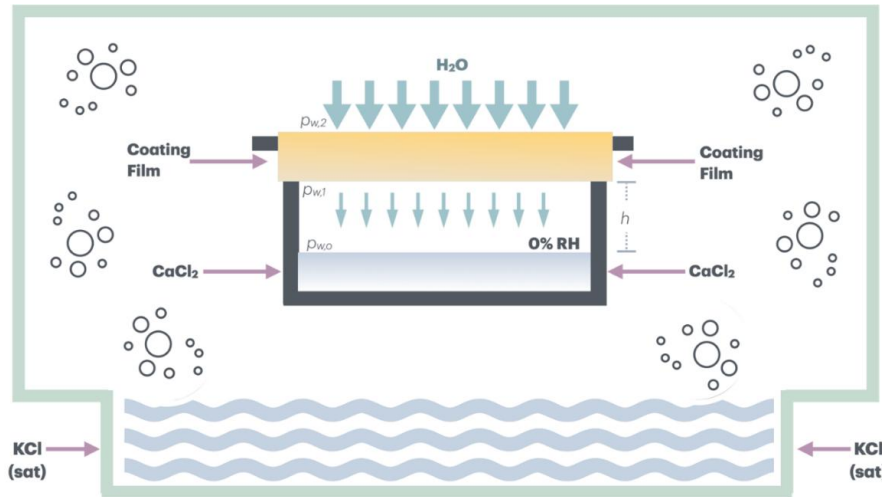
Figure 45 Schematic representation of WVP experiment

In Figure 45 a representative scheme describing the process of water vapor transfer through coating film is shown. The partial pressures of water vapor, inside and outside the cup, are represented by p_{wo} and p_{w2}, respectively. Due to the presence of the desiccant ($CaCl_2$), p_{wo} is zero, while p_{w2} is the partial pressure of water vapor corresponding to the relative humidity (RH) associated with the saturated KCl solution. The air space (h) between the bottom of the film and the surface of the desiccant is considered necessary to avoid contact of the film with the desiccant while handling of cup. The pressure difference: $\Delta p = p_{w2} - p_{wo}$, provides the driving force for the flow of water vapor through the film. Knowing ΔP, as well as the weight gain of the cup recorded during a certain time interval ($\Delta m/\Delta t$), and the area of the exposed film (area of the open mouth of the cup), WVP of the film can be determined according to the equation (5). However, this method applies only to films containing high amounts of lipid materials, which are good water vapor barriers with a low WVT.

Polysaccharide-based coating films generally result in being sensitive to humidity and they are characterized by a high WVT, for which the resistance provided by the stagnant air in the gap (h) is significant. For this case, the pressure difference, the driving force for the flow of water vapor through the film, results in $\Delta p_{film} = p_{w2} - p_{w1}$, due to the pressure inside cup is p_{w1}. The determination of this pressure p_{w1} involves using an

61

expression that relates the pressure as a function of the distance to the film. Empirically, it has been proposed that:

$$(6)\ p_{w1} = p_{ref}\, e^{-\frac{h}{H}}$$

where p_{ref} corresponds to a reference pressure. From associated with the system under study, h is the air gap, and H is a characteristic length of the system. For the system under study, H can be determined according to Fick's law using the characteristic values for water vapor of diffusivity and concertation:

$$(7)\ H = -\frac{D\,c}{J_m}$$

Thus, the pressure p_{w1} results in:

$$(8)\ p_{w1} = p_{atm} - (p_{atm} - p_{wo})e^{\frac{J_m\,h}{D\,\Delta c}}$$

where p_{atm} is the atmospheric pressure. From the expression for p_{w1}, the pressure difference Δp_{film} can be determined, and finally WVP according to the equation (5) which adapted to the terms defined above results in equation (2). In *Table 8* the data for the films evaluated are presented.

$$\text{WVP(g mm/m}^2\text{h kPa)} = \frac{\Delta m\,x\,\text{L}}{\text{A}\,x\,t\,x\,\Delta\text{P}}$$

$\Delta m = m_{final} - m_{initial}$

$A = \pi r^2$ (r=0.01m)

t=168 hours

$\Delta p_{film} = p_{w2} - p_{w1}$

Table 8 Data of the films to calculate the WVP

RH = 85%	p_w(T) = 3.17 kPa
T = 25 °C	p_{atm} = 77.6 kPa
D_{H2O}(T) = 0.25 cm^2/s	p_{wo} = 2.66 kPa
c_{H2O} = 4.25x10^{-5}	p_{w2} = (RH/100)*pw = 2.693 kPa

FILMS	Δm (g)	L (mm)	r (m)	WVP(g. mm/m^2. h. kPa)
PEC 1_1 AgNPs-c	0.5808	0.1882	0.01	3.0728
PEC CMC 1_1 AgNPs-c	0.4521	0.1958	0.01	2.4974

The WVP results shown in Table 8 Figure 46 indicate that for the pectin film the WVP is 3.0728 (g mm/m^2 h kPa), while the pectin and CMC nanocomposite has a lower value of 2.4979 (g mm/m^2 h kPa). which shows that the combination of the polymers improves the barrier properties of the nanocomposite. These values obtained are compared with research carried out for Acai packaging that report WVP values between 2.56 and 3.55 (g mm/m^2 h kPa) [13] for pectin-based films. On the other hand, Seslija and co-workers,[33,56] and others studies made by team research of Ghanbarzadeh[56].

Figure 46 WVP of films Pectin PEC 1_1AgPs-c and CMC 1_1 AgNPs-c

Figure 46 shows an image of one of the containers (cup) containing CaCl$_2$ before and after the test to determine the WVP, to show the mass gain that the desiccant experienced during the test.

4.7 Test of Shelf life of fruits

The test to shelf life of fruits Figure 47 shows a noticeable change in the appearance of fruits without the coating, with some damage caused by microorganisms. Meanwhile, during the first 7 days, the coated fruits remain completely fresh and free from any microorganism damage. On day 10, we can see that the uncoated fruits are more deteriorated, while the coated fruits still appear fresh and undamaged by microorganisms. On day 21 the coated fruit start to show damage and the uncoated fruit are completely deteriorated. This study indicates that the coating formulation significantly extends the shelf life of fruits.
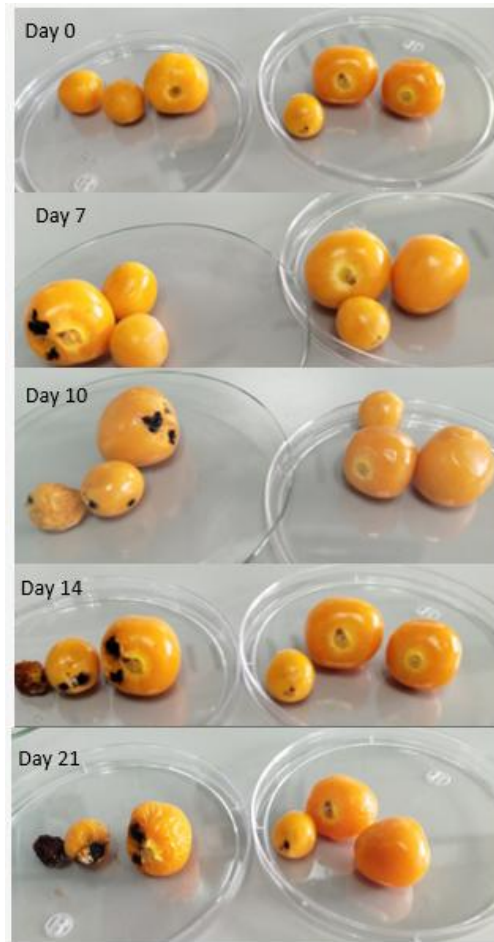
Figure 47 Test to shelf life of fruits applied to golden berries

5 CONCLUSIONS

- Formulations of pectin and CMC films were successfully developed, showing improved mechanical properties. These formulations exhibited adequate strength and flexibility, making them suitable for use in food packaging. The incorporation of reinforcing additives significantly contributed to the enhancement of these properties.

- It was feasible to synthesize silver nanoparticles using cinnamon bark extract as a reducing and capping agent. These nanoparticles exhibited suitable morphological properties and notable antibacterial activity, confirming the efficacy of the green chemistry method used.

- Silver Nanoparticles synthesized with cinnamon extract showed excellent bactericidal and bacteriostatic properties against resistant and sensitive bacteria. According to the data obtained in the Kirby Bauer and broth dilution tests

- It was possible to develop a useful nanocomposite for fruit packaging from pectin and carboxymethyl cellulose (CMC) improved with silver nanoparticles (AgNPs). This made it clear that the addition of silver nanoparticles and egg albumin significantly improved the thermal stability of the films, according to TGA analyses, where films with AgNPs showed greater resistance to thermal degradation.

- The nanocomposites obtained by the combination of pectin and CMC presented better mechanical and barrier properties compared to pure pectin films. Specifically, lower water vapor permeability (WVP) was achieved in the blended films, indicating a better moisture barrier.

- The ability of the films to extend the shelf life of fruits during storage was confirmed, keeping them fresh and free from damage by microorganisms for a longer period compared to uncoated fruits.

6   REFERENCES

1. Cardona, M. B. Paraísos de vida: los países más biodiversos de planeta. *Viajes* (2024).
2. Mestanza-Ramón, C. *et al.* In-situ and ex-situ biodiversity conservation in ecuador: A review of policies, actions and challenges. *Diversity* **12**, (2020).
3. Ministerio de Producción, C. E. I. y P. Boletines de Comercio Exterior 2024 – Ministerio de Producción Comercio Exterior Inversiones y Pesca. (2024).
4. Macieja, S. *et al.* Bioactive Carboxymethyl Cellulose (CMC)-Based Films Modified with Melanin and Silver Nanoparticles (AgNPs)—The Effect of the Degree of CMC Substitution on the In Situ Synthesis of AgNPs and Films' Functional Properties. *Int. J. Mol. Sci.* **23**, (2022).
5. Akyüz, G., Kaymazlar, E., Ay, H., Andaç, M. & Andaç, Ö. Use of Silver Nanoparticles Loaded Locust Bean Gum Coatings to Extend the Shelf-Life of Fruits. *Biointerface Res. Appl. Chem.* **13**, 1–16 (2023).
6. Kwon, H., Hong, S., Park, S. & Lee, C. W. Characterization of acid-modified polyvinyl alcohol and its application to barrier-coated paper for eco-friendly food packaging. *Food Packag. Shelf Life* **43**, 101271 (2024).
7. Moustafa, M. *et al.* New blends of acrylamide / chitosan and potato peel waste as improved water absorbing polymers for diaper applications. **30**, 1–9 (2022).
8. Perera, K. Y., Jaiswal, A. K. & Jaiswal, S. Biopolymer-Based Sustainable Food Packaging Materials : *Foods* 1–59 (2023).
9. R. Pramila. Biodegradation of low density polyethylene (LDPE) by fungi isolated from marine water– a SEM analysis. *African J. Microbiol. Res.* **5**, 5013–5018 (2011).
10. He, Y., Li, H., Fei, X. & Peng, L. Carboxymethyl cellulose/cellulose nanocrystals immobilized silver nanoparticles as an effective coating to improve barrier and antibacterial properties of paper for food packaging applications. *Carbohydr. Polym.* 117156 (2020) doi:10.1016/j.carbpol.2020.117156.
11. Dehnad, D., Mirzaei, H., Emam-djomeh, Z. & Jafari, S. Thermal and antimicrobial properties of chitosan – nanocellulose films for extending shelf life of ground meat. *Carbohydr. Polym.* **109**, 148–154 (2014).
12. Fang, Y. & Wakisaka, M. A Review on the Modified Atmosphere Preservation of Fruits and Vegetables with Cutting-Edge Technologies. 1–16 (2021).
13. Otoni, C. G. *et al.* Recent Advances on Edible Films Based on Fruits and Vegetables—A Review. *Compr. Rev. Food Sci. Food Saf.* **16**, 1151–1169 (2017).
14. Nair, S. S., Trafiałek, J. & Kolanowski, W. applied sciences Edible Packaging : A Technological Update for the Sustainable Future of the Food Industry. (2023).
15. FoodTech. El año en packaging: Tendencias y transformaciones en 2023. *Food Tech* https://thefoodtech.com/insumos-para-empaque/el-ano-en-packaging-tendencias-y-transformaciones-en-2023/ (2023).
16. Teixeira-Costa, B. E. & Andrade, C. T. Chitosan as a valuable biomolecule from seafood industry waste in the design of green food packaging. *Biomolecules* **11**, (2021).
17. Panahirad, S. *et al.* Applications of carboxymethyl cellulose- and pectin-based active edible coatings in preservation of fruits and vegetables: A review. *Trends Food Sci. Technol.* **110**, 663–673 (2021).
18. Ghosh, I. N. *et al.* Synergistic action of cinnamaldehyde with silver nanoparticles against spore-forming bacteria: A case for judicious use of silver nanoparticles for antibacterial applications. *Int. J. Nanomedicine* **8**, 4721–4731 (2013).

19. Solano-doblado, L. G., Alamilla-beltrán, L. & Jiménez-martínez, C. Películas y recubrimientos comestibles funcionalizados. **21**, 30–42 (2018).

20. Shah, S. *et al.* Thermal and ultrasound foam control in biotechnology : a mini - review. *Discov. Chem. Eng.* (2022) doi:10.1007/s43938-022-00016-z.

21. Dai, L., Zhang, J. & Cheng, F. Cross-linked starch-based edible coating reinforced by starch nanocrystals and its preservation effect on graded Huangguan pears. *Food Chem.* 125891 (2019) doi:10.1016/j.foodchem.2019.125891.

22. Kavitha, S., Vijaya, N., Pandeeswari, R. & Premalatha, M. Vibrational, electrical and optical studies on pectin-based polymer electrolyte. *Int. Res. J. Eng. Technol.* **3**, 1385–1390 (2016).

23. Kong, J. *et al.* Progress in Polymer Science Polymer-based composites by electrospinning : Preparation & functionalization with nanocarbons. *Prog. Polym. Sci.* **86**, 40–84 (2018).

24. Matloob, A. *et al.* A Review on Edible Coatings and Films : Advances , Composition , Production Methods , and Safety Concerns. (2023) doi:10.1021/acsomega.3c03459.

25. Jayakumar, R., Menon, D., Manzoor, K., Nair, S. V. & Tamura, H. Biomedical applications of chitin and chitosan based nanomaterials - A short review. *Carbohydr. Polym.* **82**, 227–232 (2010).

26. Lam, S., Indira, L. & Barrera, C. Potential Use of Vacuum Impregnation and High-Pressure Homogenization to Obtain Functional Products from Lulo Fruit. (2021).

27. Duan, C. *et al.* Chitosan as A Preservative for Fruits and Vegetables: A Review on Chemistry and Antimicrobial Properties. *J. Bioresour. Bioprod.* **4**, 11–21 (2019).

28. Meghana, M. C., Nandhini, C., Benny, L., George, L. & Varghese, A. *A Road Map on Synthetic Strategies and Applications of Biodegradable Polymers*. *Polymer Bulletin* vol. 80 (Springer Berlin Heidelberg, 2023).

29. Kamdem, D. P., Shen, Z. & Nabinejad, O. Development of biodegradable composite chitosan-based films incorporated with xylan and carvacrol for food packaging application. *Food Packag. Shelf Life* **21**, 100344 (2019).

30. Tavker, N., Gaur, U. K. & Sharma, M. Agro-waste extracted cellulose supported silver phosphate nanostructures as a green photocatalyst for improved photodegradation of RhB dye and industrial fertilizer effluents. *Nanoscale Adv.* **2**, 2870–2884 (2020).

31. Caló, E. & Khutoryanskiy, V. V. Biomedical applications of hydrogels: A review of patents and commercial products. *Eur. Polym. J.* **65**, 252–267 (2015).

32. Groh, K. J. *et al.* Overview of known plastic packaging-associated chemicals and their hazards. *Sci. Total Environ.* **651**, 3253–3268 (2019).

33. Šešlija, S. *et al.* Pectin/Carboxymethylcellulose Films as a Potential Food Packaging Material. *Macromol. Symp.* **378**, 1–5 (2018).

34. Caner, C. The effect of edible eggshell coatings on egg quality and consumer perception. *J. Sci. Food Agric.* **85**, 1897–1902 (2005).

35. Díaz-Montes, E. & Castro-Muñoz, R. Edible films and coatings as food-quality preservers: An overview. *Foods* **10**, 1–26 (2021).

36. Shulga, O., Gribkov, S. & Shulga, S. Ecological packaging materials for bakery and confectionery products based on a new pectin modification. *Ukr. Food J.* **11**, 390–402 (2022).

37. Chandra, H., Kumari, P., Bontempi, E. & Yadav, S. Medicinal plants: Treasure

trove for green synthesis of metallic nanoparticles and their biomedical applications. *Biocatal. Agric. Biotechnol.* **24**, 101518 (2020).

38. Srinivasa, P. C., Ramesh, M. N., Kumar, K. R. & Tharanathan, R. N. Properties of chitosan films prepared under different drying conditions. **63**, 79–85 (2004).

39. Yildirim-Yalcin, M., Tornuk, F. & Toker, O. S. Recent advances in the improvement of carboxymethyl cellulose-based edible films. *Trends Food Sci. Technol.* **129**, 179–193 (2022).

40. Fernández-Santos, J., Valls, C., Cusola, O. & Roncero, M. B. Composites of cellulose nanocrystals in combination with either cellulose nanofibril or carboxymethylcellulose as functional packaging films. *Int. J. Biol. Macromol.* **211**, 218–229 (2022).

41. Yossef, M. A. Comparison of Different Edible Coatings Materials For Improvement of Quality And Shelf Life of Perishable Fruits. *Middle East J. Appl. Sci.* **4**, 416–424 (2014).

42. Khan, S., Zahoor, M., Sher, R. & Ikram, M. Heliyon The impact of silver nanoparticles on the growth of plants : The agriculture applications. *Heliyon* **9**, e16928 (2023).

43. Simbine, E. O. *et al.* Application of silver nanoparticles in food packages: A review. *Food Sci. Technol.* **39**, 793–802 (2019).

44. Anaya-Esparza, L. M. *et al.* Funcionalización de los recubrimientos a base de quitosano para la conservación postcosecha de frutas y hortalizas. *TIP Rev. Espec. en Ciencias Químico-Biológicas* **23**, 1–14 (2020).

45. Hasan, K. M. F. *et al.* Functional silver nanoparticles synthesis from sustainable point of view: 2000 to 2023 – A review on game changing materials. *Heliyon* **8**, (2022).

46. Niño, K. A. *et al.* Películas biodegradables a partir de residuos de cítricos : propuesta de empaques activos. *Arévalo al., 2010. Rev Latinoam Biotecnol Amb Algal 1(2)124-134* **1**, 124–134 (2010).

47. Yildirim-Yalcin, M., Tornuk, F. & Toker, O. S. Recent advances in the improvement of carboxymethyl cellulose-based edible films. *Trends Food Sci. Technol.* **129**, 179–193 (2022).

48. Dhall, R. K. Advances in Edible Coatings for Fresh Fruits and Vegetables: A Review. *Crit. Rev. Food Sci. Nutr.* **53**, 435–450 (2013).

49. He, Y., Ye, H., You, T. & Xu, F. Sustainable and multifunctional cellulose-lignin films with excellent antibacterial and UV-shielding for active food packaging. **137**, 1–9 (2023).

50. Al-Tayyar, N. A., Youssef, A. M. & Al-hindi, R. Antimicrobial food packaging based on sustainable Bio-based materials for reducing foodborne Pathogens: A review. *Food Chem.* **310**, 125915 (2020).

51. Atsani, F., Indiarto, R. & Utama, G. Edible Film Casting Techniques and Materials and Their. (2023).

52. Kurečič, M. *et al.* A green approach to obtain stable and hydrophilic cellulose-based electrospun nanofibrous substrates for sustained release of therapeutic molecules. *RSC Adv.* **9**, 21288–21301 (2019).

53. Elbaz, M. Effect of carob germ extract on properties of new formulated light mayonnaise. (2018).

54. T.Heinze. Etherification of Cellulose. in *Cellulose Derivatives* (ed. Springer) 429–472 (2018).

55. Toğrul, H. & Arslan, N. Extending shelf-life of peach and pear by using CMC from sugar beet pulp cellulose as a hydrophilic polymer in emulsions. *Food*

Hydrocoll. **18**, 215–226 (2004).

56.   Ghanbarzadeh, B., Almasi, H. & Entezami, A. A. Physical properties of edible modified starch/carboxymethyl cellulose films. *Innov. Food Sci. Emerg. Technol.* **11**, 697–702 (2010).

57.   Tongdeesoontorn, W., Mauer, L. J., Wongruong, S., Sriburi, P. & Rachtanapun, P. Effect of carboxymethyl cellulose concentration on physical properties of biodegradable cassava starch-based films. *Chem. Cent. J.* **5**, 1–8 (2011).

58.   Ardjoum, N., Shankar, S., Chibani, N., Salmieri, S. & Lacroix, M. In situ synthesis of silver nanoparticles in pectin matrix using gamma irradiation for the preparation of antibacterial pectin/silver nanoparticles composite films. *Food Hydrocoll.* **121**, 107000 (2021).

59.   Moalemiyan, M., Ramaswamy, H. S. & Maftoonazad, N. Pectin-based edible coating for shelf-life extension of Ataulfo mango. *J. Food Process Eng.* **35**, 572–600 (2012).

60.   Thakhiew, W., Devahastin, S. & Soponronnarit, S. Effects of drying methods and plasticizer concentration on some physical and mechanical properties of edible chitosan films. *J. Food Eng.* **99**, 216–224 (2010).

61.   Salleh, A. *et al.* The potential of silver nanoparticles for antiviral and antibacterial applications: A mechanism of action. *Nanomaterials* **10**, 1–20 (2020).

62.   Rosero, A., Espinoza-montero, P. & Fernández, L. RECUBRIMIENTOS COMESTIBLES CON MATERIALES MICRO / NANOESTRUCTURADOS PARA LA CONSERVACIÓN DE FRUTAS Y VERDURAS : UNA REVISIÓN EDIBLE COATINGS WITH MICRO / NANOSTRUCTURED MATERIALS FOR FRUITS AND VEGETABLES PRESERVATION : A REVIEW. 149–178 (2020) doi:10.26807/ia.vi.180.

63.   Zhao, X. *et al.* Effect of cinnamaldehyde incorporation on the structural and physical properties, functional activity of soy protein isolate-egg white composite edible films. *J. Food Process. Preserv.* **45**, 1–12 (2021).

64.   Huopalahti, R. *et al.* Bioactive egg compounds. *Bioact. Egg Compd.* 1–298 (2007) doi:10.1007/978-3-540-37885-3.

65.   Duda-Chodak, A., Tarko, T. & Petka-Poniatowska, K. Antimicrobial Compounds in Food Packaging. *Int. J. Mol. Sci.* **24**, (2023).

66.   Menichetti, A., Mavridi-printezi, A., Mordini, D. & Montalti, M. Effect of Size , Shape and Surface Functionalization on the Antibacterial Activity of Silver Nanoparticles. (2023).

67.   Granja Alvear, A. *et al.* Synergistic Antibacterial Properties of Silver Nanoparticles and Its Reducing Agent from Cinnamon Bark Extract. *Bioengineering* **11**, 1–15 (2024).

68.   Granja, L. A. *et al.* Polyvinyl Alcohol Films Loaded with Silver Nanostructures with Different Sizes and Shapes with Tuneable Plasmonic and Electric Properties. A Spectroscopic Study. *Mater. Res.* **25**, (2022).

69.   Yaqoob, A. A., Umar, K. & Ibrahim, M. N. M. Silver nanoparticles: various methods of synthesis, size affecting factors and their potential applications–a review. *Appl. Nanosci.* **10**, 1369–1378 (2020).

70.   Singh, D. K., Singh, S. & Singh, P. *Nanomaterials: Advances and Applications. Nanomaterials: Advances and Applications* (2023). doi:10.1007/978-981-19-7963-7.

71.   Balaji, D. S. *et al.* Extracellular biosynthesis of functionalized silver nanoparticles by strains of Cladosporium cladosporioides fungus. *Colloids*

Surfaces B Biointerfaces **68**, 88–92 (2009).

72. Ahmed, O. *et al.* Plant Extract-Synthesized Silver Nanoparticles for Application in Dental Therapy. *Pharmaceutics* **14**, 1–26 (2022).

73. Nie, P., Zhao, Y. & Xu, H. Synthesis, applications, toxicity and toxicity mechanisms of silver nanoparticles: A review. *Ecotoxicol. Environ. Saf.* **253**, 114636 (2023).

74. Singh, N. B. Green synthesis of nanomaterials. *Handb. Microb. Nanotechnol.* 225–254 (2022) doi:10.1016/B978-0-12-823426-6.00007-3.

75. Alahmad, A. *et al.* Green Synthesis of Silver Nanoparticles Using Hypericum perforatum L. Aqueous Extract with the Evaluation of Its Antibacterial Activity against Clinical and Food Pathogens. *Pharmaceutics* **14**, (2022).

76. Castillo-Henríquez, L. *et al.* Green synthesis of gold and silver nanoparticles from plant extracts and their possible applications as antimicrobial agents in the agricultural area. *Nanomaterials* **10**, 1–24 (2020).

77. Fatima, F. *et al.* Green synthesized silver nanoparticles using tridax procumbens for topical application: Excision wound model and histopathological studies. *Pharmaceutics* **13**, (2021).

78. Chen, C. *et al.* Ångstrom-scale silver particle – embedded carbomer gel promotes wound healing by inhibiting bacterial colonization and inflammation. (2020).

79. Wang, Z. *et al.* Ångstrom-Scale Silver Particles as a Promising Agent for Low-Toxicity Broad-Spectrum Potent Anticancer Therapy. **1808556**, 1–15 (2019).

80. Ashenhurst, J. UV-Vis Spectroscopy: Absorbance of Carbonyl. *Chemistry, Master Organic* https://www.masterorganicchemistry.com/2016/09/26/uv-vis-spectroscopy-absorbance-of-carbonyls/ (2021).

81. Canales, D. *et al.* Fungicides films of low-density polyethylene (LDPE)/inclusion complexes (Carvacrol and Cinnamaldehyde) against botrytis cinerea. *Coatings* **9**, 1–17 (2019).

82. Rastogi, L. & Arunachalam, J. Sunlight based irradiation strategy for rapid green synthesis of highly stable silver nanoparticles using aqueous garlic (Allium sativum) extract and their antibacterial potential. *Mater. Chem. Phys.* **129**, 558–563 (2011).

83. Mulvaney, P. Surface Plasmon Spectroscopy of Nanosized Metal Particles. 788–800 (1996) doi:10.1021/la9502711.

84. Mohammad Jafari Eskandri, R. G. and M. A. A. Transmission Electron Microscopy of Nanomaterials. in *Book Electronic Cristallography* (ed. IntechOpen) doi:http://dx.doi.org/10.5772/intechopen.92212.

85. Bunsell, A. R. & Thionnet, A. Quantifiable analysis of the failure of advanced carbon fibre composite structures leading to improved safety factors. *Prog. Mater. Sci.* **123**, 100753 (2022).

86. Jia, Z., Li, J., Gao, L., Yang, D. & Kanaev, A. Dynamic Light Scattering : A Powerful Tool for In Situ Nanoparticle Sizing. (2023).

87. Filippov, S. K. *et al.* Materials Horizons Dynamic light scattering and transmission electron microscopy in drug delivery : a roadmap for correct characterization of nanoparticles and interpretation of results. 5354–5370 (2023) doi:10.1039/d3mh00717k.

88. Cai, T. Polarized imaging of dynamic light scattering to measure nanoparticle size , morphology , and distributions. 1–4 (2023).

89. Gajic, I. *et al.* Antimicrobial Susceptibility Testing: A Comprehensive Review of Currently Used Methods. *Antibiotics* **11**, 1–26 (2022).

90. Hudzicki, J. Kirby-Bauer Disk Diffusion Susceptibility Test Protocol Author

Information. *Am. Soc. Microbiol.* 1–13 (2012).

91. ASTM E1131-08 2008. Astm E1131-08. 8–10 (2008) doi:10.1520/E1131-08.2.
92. Katiyar, V. & Ghosh, T. *Nanotechnology in Edible Food Packaging*. (2021).
93. Ramasamy, M., Lee, J. H. & Lee, J. Direct one-pot synthesis of cinnamaldehyde immobilized on gold nanoparticles and their antibiofilm properties. *Colloids Surfaces B Biointerfaces* **160**, 639–648 (2017).
94. Wiley, B., Sun, Y., Mayers, B. & Xia, Y. Shape-controlled synthesis of metal nanostructures: The case of silver. *Chem. - A Eur. J.* **11**, 454–463 (2005).
95. Bruna, T., Maldonado-Bravo, F., Jara, P. & Caro, N. Silver nanoparticles and their antibacterial applications. *Int. J. Mol. Sci.* **22**, (2021).
96. Effendi, A. D., Md Yusof, M. A., Abd Mutalib, N. F. & Sia, C. W. Amidated Pectic Polysaccharides (Pectin) as Methane Hydrate Inhibitor at Constant Cooling and Isobaric Condition. *Polymers (Basel).* **15**, (2023).
97. Shankar, S., Tanomrod, N., Rawdkuen, S. & Rhim, J. W. Preparation of pectin/silver nanoparticles composite films with UV-light barrier and properties. *Int. J. Biol. Macromol.* **92**, 842–849 (2016).
98. Manjubala, G. P. U. N. I. Thermal behavior of carboxymethyl cellulose in the presence of polycarboxylic acid crosslinkers. *J. Therm. Anal. Calorim.* **2**, (2019).
99. Coetzee, D., Venkataraman, M., Militky, J. & Petru, M. Influence of Nanoparticles on Thermal and Electrical Conductivity of Composites. (2020).
100. Trotta, F. *et al.* Silver Bionanocomposites as Active Food Packaging : Recent Advances & Future Trends Tackling the Food Waste Crisis. 1–32 (2023).
101. Souza, Victor G.L. Carolina Rodriguez, I. C. *Permeation of Oxygen and Carbon Dioxide Through Food Packaging Materials*. (Humana, New York, NY, 2024). doi:https://doi.org/10.1007/978-1-0716-3613-8_12.

Article

Synergistic Antibacterial Properties of Silver Nanoparticles and Its Reducing Agent from Cinnamon Bark Extract

Araceli Granja Alvear [1], Nayely Pineda-Aguilar [2], Patricia Lozano [3], Cristóbal Lárez-Velázquez [4], Gottfried Suppan [1], Salomé Galeas [5], Alexis Debut [6], Karla Vizuete [6], Lola De Lima [1], Juan Pablo Saucedo-Vázquez [1], Frank Alexis [7,*] and Floralba López [1,*]

1 CATS Research Group, School of Chemical Sciences Engineering, Yachay Tech University, Urcuquí 100119, Ecuador; lgranja@yachaytech.edu.ec (A.G.A.); gott.suppan@hotmail.com (G.S.); ldelima@yachaytech.edu.ec (L.D.L.); jsaucedo@yachaytech.edu.ec (J.P.S.-V.)
2 Centro de Investigación de Materiales Avanzados CIMAV-Monterrey, Monterrey 64630, Mexico; nayely.pineda@cimav.edu.mx
3 Centro de Investigaciones en Ciencias Microbiológicas, Instituto de Ciencias, Universidad Autónoma de Puebla, Puebla 72570, Mexico; patricia.lozano@correo.buap.mx
4 Laboratorio de Polímeros, Departamento de Química, Facultad de Ciencias, Universidad de Los Andes, Mérida 5101, Venezuela; clarez@ula.ve
5 Laboratorio de Nuevos Materiales (LANUM), Escuela Politécnica Nacional, Quito 170143, Ecuador; salome.galeas@epn.edu.ec
6 Centro de Nanociencia y Nanotecnología, Universidad de las Fuerzas Armadas ESPE, Sangolqui 171523, Ecuador; apdebut@espe.edu.ec (A.D.); ksvizuete@espe.edu.ec (K.V.)
7 Departamento de Ingeniería Química, Colegio de Ciencias e Ingeniería, Instituto de Energía y Materiales, Instituto de Microbiología, Universidad San Francisco de Quito (USFQ), Quito 170901, Ecuador
* Correspondence: falexis@usfq.edu.ec (F.A.); flopez@yachaytech.edu.ec (F.L.)

Abstract: Synthesis of silver nanoparticles with antibacterial properties using a one-pot green approach that harnesses the natural reducing and capping properties of cinnamon (*Cinnamomum verum*) bark extract is presented in this work. Silver nitrate was the sole chemical reagent employed in this process, acting as the precursor salt. Gas Chromatography-Mass Spectroscopy (GC-MS), High-Performance Liquid Chromatography (HPLC) analysis, and some phytochemical tests demonstrated that cinnamaldehyde is the main component in the cinnamon bark extract. The resulting bio-reduced silver nanoparticles underwent comprehensive characterization by Ultraviolet–Vis (UV-Vis) and Fourier Transform InfraRed spectrophotometry (FTIR), Dynamic Light Scattering (DLS), Transmission Electron Microscopy, and Scanning Electron Microscopy suggesting that cinnamaldehyde was chemically oxidized to produce silver nanoparticles. These cinnamon-extract-based silver nanoparticles (AgNPs-cinnamon) displayed diverse morphologies ranging from spherical to prismatic shapes, with sizes spanning between 2.94 and 65.1 nm. Subsequently, the antibacterial efficacy of these nanoparticles was investigated against *Klebsiella*, *E. Coli*, *Pseudomonas*, *Staphylococcus aureus*, and *Acinetobacter* strains. The results suggest the promising potential of silver nanoparticles obtained (AgNPs-cinnamon) as antimicrobial agents, offering a new avenue in the fight against bacterial infections.

Keywords: silver nanoparticles; nanomaterials; green synthesis; antibacterial properties; cinnamaldehyde

1. Introduction

In recent years, significant scientific advances in nanotechnology have led to the development of many nanomaterials with customized properties for applications in various domains. These applications span biotechnology, catalysis, optics, electronics, textiles, and the food industry [1–7]. Silver nanoparticles have attracted considerable attention in the field of nanomaterials due to their widely documented outstanding optical, magnetic, and electrical properties, which emerge from the peculiar behavior exhibited by matter at the nanometer scale [8–11]. Specifically, the well-documented antibacterial activity

associated with silver has prompted the incorporation of silver nanoparticles in various applications, with the purpose of addressing the challenges arising in the post-antibiotic era. This phenomenon has stimulated the development of new agents capable of combating pathogenic microorganisms without promoting the emergence of additional resistance mechanisms [12–19].

Unlike physical methods, which usually require specialized equipment, chemical synthesis methods offer a more accessible and less demanding alternative in terms of experimental requirements. These approaches involve meticulous formulation design that requires the selection of chemical reagents and precise control of experimental parameters to achieve control of the desired size and shape through assembly or self-assembly [20–23]. However, some of these chemical reagents are expensive and pose a risk to the environment. To address these drawbacks and take advantage of the inherent chemical structures of biological systems, green synthesis methods have gained appeal as an alternative to produce silver nanostructures [24–36]. Methods using plant extracts (roots, leaves, stems, fruits), microbial cells (yeasts, bacteria, fungi), or biopolymers as reducing agents have been investigated. This strategy offers the additional advantage of potentially conferring antibacterial activity to the resulting nanomaterials [37–43]. The higher stability and efficiency observed in bio-assisted nanostructures are attributed to the intricate chemical structures of the bioagents involved, which lead to more complex mechanisms in the reduction and limitation processes [25].

Several natural extracts have been evaluated for their potential to reduce silver ions and facilitate the formation of nanomaterials with diverse sizes and morphologies, suggesting favorable synthesis routes for obtaining silver nanoparticles [25]. Extracts derived from *Cinnamomum zeylancium*, *Acorus calamus*, Tea, Cocous and *Nelumbo nucifera*, *Pistacia atlantic*, *Premna herbacea*, *Centella asiatica*, *Acalypha indica*, *Allium sativum* leaves and *Citrus sinensis*, *Vitex negundo* [30,39,44–46] have been used as reducing agents, giving rise to spherical silver nanoparticles with diameters ranging from 8 to 50 nm. On the other hand, Aloe Vera extract [28], *Memecylon edule,* or *Eclipta prostrate* [47] extracts have also produced silver nanoparticles with triangular and hexagonal shapes, ranging from 25 to 80 nm in size. Furthermore, the *Datura metel* extract yielded quasi-linear superstructures with sizes between 16 and 40 nm [27,48]. However, conventional agents from natural extract only reduce the number of agents without additional bioactivity.

Medical applications of silver nanoparticles range from antimicrobial and anticancer treatments to wound healing, bone repair, vaccine adjuvants, anti-diabetic agents, and biosensors [43]. It is notable that the biological activity of silver particles is enhanced at subnanometer scales (silver Angstrom particles, AgAPs), opening the research landscape in the applications of AgNPs and sub-AgNPs [49,50]. Recently, Khan et. al. published a review of applications of AgNPs in agriculture, acting as antivirals, antibacterials, antifungals, and even as nano-pesticides. Interestingly, they improve seed germination and plant growth and also improve the quantum efficiency of the photosynthetic process [51]. In the field of material science, silver nanoparticles are recognized for their versatility in applications in biomolecule sensing, diagnostic in healthcare systems, optics, and electronics applications. A particular example of the use of AgNPs in optics is the development of metasurfaces formed of self-assembled silver nanocubes (AgNCs) immobilized on a thick layer of gold, generating a new generation of dynamically controlled optical components [52].

Many studies have demonstrated the effective bactericidal capacity of silver nanoparticles (AgNPs), which operate through several simultaneous mechanisms of action. Some promising results have shown that smaller nanoparticles exhibit greater bactericidal activity [14,48,53,54], mainly attributed to their greater surface area available for interaction with bacterial membranes. This interaction leads to membrane disruption, protein dysfunction, oxidative stress, and DNA damage within bacteria, altering essential functions such as permeability and respiration [3,55–58], ultimately resulting in bacterial death. The proposed mechanisms for DNA modification suggest the participation of silver ions, which can hinder protein synthesis, deactivate respiratory enzymes, and generate reactive oxygen

species, thereby interfering with adenosine triphosphate (ATP) production. Nanostructures with smaller sizes and spherical or quasi-spherical shapes are more prone to release silver ions due to their larger surface area [8,59].

Incorporating phytochemical agents, such as organic compounds or antibiotics, in conjunction with silver nanomaterials has demonstrated a synergistic effect against pathogenic bacteria [14,60]. This innovative approach of combining phytochemicals and metallic nanomaterials has emerged as a promising strategy to address the challenge of multidrug resistance technology (MDR) and meet the pressing need for effective antibacterial agents [61,62]. Using nanostructures improves the bioavailability of phytochemical agents, facilitating their controlled release at the desired target site or tissue and improving the stability, antimicrobial efficacy, and reduced toxicity to the host [63–65]. Cinnamaldehyde, the main chemical component extracted from cinnamon bark and its essential oil, belonging to the Cinnamomum genus of the Lauraceae family, has a wide range of beneficial properties, including analgesic, antiseptic, insecticidal, and parasiticidal effects. Due to its exceptional antimicrobial efficacy against various infections [61,66], cinnamaldehyde can be considered a promising phytochemical agent. When used as a reducing and capping agent during the synthesis of silver nanostructures, a redox reaction, as depicted in Equation (1), is expected to occur, converting cinnamaldehyde into cinnamic acid. By synergistically combining the phytochemical activity of cinnamaldehyde with the antimicrobial properties of silver nanoparticles, the combined system exhibits enhanced antibacterial efficacy [67–69].

$$\text{(cinnamaldehyde)} + 2Ag^+ + 2OH^- \longrightarrow \text{(cinnamic acid)} + 2Ag^0 + 2H_2O \tag{1}$$
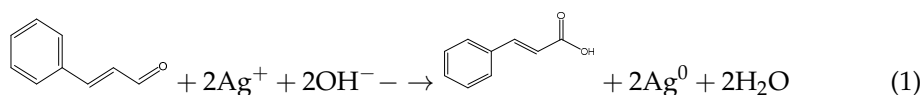
In this work, a one-pot method of green synthesis was employed to produce silver nanoparticles, only involving two reagents, namely a silver nitrate solution and an emulsified cinnamon bark extract. The extract derived from cinnamon bark served as a sustainable and natural source of phytochemical compounds, acting as reducing and capping agents during the formation of the silver nanoparticles. The morphological, structural, and chemical features of the resulting silver nanostructures were evaluated, as well as their bactericidal activity against different resistant and sensitive Gram-negative and Gram-positive bacteria. This simple synthesis method represents a promising alternative for generating nanocomposites with significant applications in the food and biotechnology industry.

2. Materials and Methods

Silver nitrate (AgNO$_3$) was purchased from Sigma Aldrich (99.5%) and used as obtained without further purification. The cinnamon barks were purchased from local stores, and its extract was acquired by steam distillation for 2 h, maintaining a 1:9 (*w:v*) ratio of crushed cinnamon bark mass and distilled water volume. The cinnamaldehyde was extracted by (steam) distillation and then stored for later use and analysis.

Bacterial strains used: *Klebsiella pneumoniae* (KpCL17), *Escherichia coli* (DH5α), *Pseudomonas aeruginosa* (PAO1), *Acinetobacter haemolyticus* (AN54), *Klebsiella pneumoniae* (KpE52), *Escherichia coli* (C7230), *Pseudomonas aeruginosa* (PE52), *Acinetobacter* (AN2) and *Staphylococcus aureus* (29213), came from the Pediatric Hospital of the city of Puebla in Mexico.

2.1. Preparation of Silver Nanoparticles from Cinnamon Bark Extract (AgNPs-Cinnamon)

Silver nanostructures were prepared by mixing the cinnamaldehyde extracted with a 1 mM AgNO$_3$ solution, maintaining a 1:1 (*v:v*) ratio. The mixture was stirred for 20 min at 40 °C. The onset of the reaction was evidenced by a light yellow/pink color After preparation, the resulting colloidal dispersion was carefully stored for later use.

2.2. Characterization of Silver Nanoparticles (AgNPs-Cinnamon)

FTIR spectroscopy analysis was carried out to identify specific functional groups of cinnamaldehyde from the extract and the resultant AgNPs-cinnamon, from which it is

possible to assess the structure chemical alterations experienced by cinnamaldehyde after the oxidation process during silver reduction. FTIR spectra were obtained using a Perkin Elmer/100 FTIR spectrophotometer (San Miguel de Urcuquí, Ecuador), operating in a range between 500 and 4500 cm^{-1}.

GC-MC analysis to confirm the presence of cinnamaldehyde was performed with a SYNAPT-G2Si Waters mass spectrometer (San Miguel de Urcuquí, Ecuador) coupled to an Agilent 7290A Gas Chromatography (San Miguel de Urcuquí, Ecuador) equipped with an Agilent DB5-MS (San Miguel de Urcuquí, Ecuador), 30 m length, 0.25 mm I.D., 0.25 μm (5% phenyl and 95% polydimethylsiloxane) column. The carrier gas was Helium (1.5 mL/min), and a temperature gradient of 70 °C to 300 °C (5 °C/min) was used for the analysis. Furthermore, the analysis of cinnamon bark extract involved various phytochemical tests aimed at identifying the presence of proteins, phenols, and flavonoids. The detailed methodologies for these tests and the spectroscopic characterization of cinnamaldehyde can be found in the Supplementary Materials (S1).

The formation of nanoparticles was tracked through observation of the Surface Plasmon Resonance (SPR) phenomenon by UV Vis spectroscopy. This phenomenon generates signals in the visible region that can be recorded in the UV-Vis spectrum. A Perkin Elmer/LAMBDA 1050 UV/Vis spectrophotometer (175 to 3300 nm, San Miguel de Urcuquí, Ecuador) with a quartz cuvette was used for recording spectra and evaluating wavelengths between 300 and 800 nm with a scan speed of 5 nm/s and a resolution of 1 nm.

The shape and structure of the AgNPs-cinnamon were determined by Transmission Electron Microscopy (TEM) using a microscope model Tecnai G2 Spirit Twin (Sangolquí, Ecuador) equipped with an Eagle 4k HR camera (Sangolquí, Ecuador). Briefly, the solid samples were resuspended in absolute ethanol. 5 μL of each suspension was placed on a Copper F/C TEM grid. Images were acquired at different magnifications by operating the microscope at 80 kV. Additional morphology evaluation was performed using a TESCAN model MIRA 3 field emission scanning electron microscope FEG-SEM. Images were obtained at various magnifications operating at 10 kV. Each of the samples was placed on a scanning electron microscopy pin fixed with a double layer of double-sided carbon tape.

Dynamic Light Scattering (DLS) was performed on nanoparticles suspended in a liquid phase to determine their size distribution. For this analysis, MALVERN, Zetasizer ZS90 automatized equipment (Coatzacoalcos, Veracruz, México) with DTS0012 cells (Malvern Panalytical, Coatzacoalcos, Veracruz, México) was used. ζ-potential of the obtained nanostructures was additionally evaluated on the same equipment. From these measurements, it is possible to determine the stability of the prepared nanoparticle system.

2.3. Bactericidal Activity Analysis

The AgNPs-cinnamon bactericidal activity was evaluated for Gram-negative and Gram-positive bacteria of resistant and sensitive types using both disk diffusion methods, commonly referred to as the Kirby Bauer method, and the microdilution in broth method. The disk diffusion method was performed by inoculating a standard quantity of microorganisms on a plate with the Muller Hinton Broth (MHB) base, forming bacterial turf. This method implies the determination of the generated zone of inhibition (ZI), in which the effectiveness of antibiotics or bactericides against specific bacterial strains is estimated from measurements of that inhibition zone [42]. ZI is the area around an antibiotic- or bactericide-impregnated disk where bacterial growth is visibly inhibited. Therefore, this method provides a qualitative assessment of the bacterial susceptibility of the tested substance. The disk diffusion method is widely used and provides a quick way to determine the effectiveness of various antibiotics and bactericides against different bacterial strains. The resistant bacterial cultures *Pseudomonas aeruginosa* (PE52), *Acinetobacter haemolyticus* (AN54), *Escherichia coli* (C7230), and *Staphylococcus aureus* (29213), which came from the Pediatric Hospital of the city of Puebla in Mexico, were used to evaluate the antibacterial properties of AgNPs-cinnamon.

Under appropriate conditions, sensi-disks were prepared by impregnating 1 cm diameter filter paper discs with 10 µL of various antibacterial agent samples, including silver nitrate solution and cinnamon extract, denoted below as Blank 1 and Blank 2, respectively, and AgNPs-cinnamon suspensions concentrated 2, 3, 5 and 10 times their initial concentration. These impregnated discs were placed in Petri dishes containing inoculated bacteria and incubated at 37 °C. In all the cases, a disk containing 10 mg of ampicillin was included as a growth inhibitor reference. Three replicates were conducted for each sample.

Mueller Hinton Broth (MHB) method was followed as previously described [70]. Briefly, in a 38 g/L MHB culture medium, the bacteria were inoculated. The Sensi-disks impregnated with the bactericidal agent samples were placed on the inoculated culture medium, and the agar was gently pressed to ensure that they were sufficiently impregnated on the surface. After an incubation process at 37 °C for 18 to 24 h, the disks were removed, and the inhibition halos were measured.

The broth microdilution method involves creating a liquid broth with varying antimicrobial agent concentrations. Microorganisms were introduced, and after incubation, growth was monitored. During this method, the bacterial strains were standardized to 0.5 McFarland [70]. 100 µL of Luria-Bertani (LB) culture medium was poured into the appropriately labeled wells, adding 100 µL of respective AgNPs-cinnamon samples and 10 µL of bacteria inoculum. The incubation process at 37 °C took 20 h. Gram-negative sensitive bacteria *Klebsiella pneumoniae* (KpCL17), *Escherichia coli* (DH5α), *Pseudomonas aeruginosa* (PAO1), and *Acinetobacter haemolyticus* (AN54), as well as the Gram-negative resistant bacteria *Klebsiella pneumoniae* (KpE52), *Escherichia coli* (C7230), *Pseudomonas aeruginosa* (PE52) and *Acinetobacter* (AN2) were used to evaluate the antibacterial capacities of the AgNPs-cinnamon by this method.

3. Results and Discussion

3.1. Phytochemical Tests of Cinnamon Extract Cinnamon

The phytochemical tests presented in the Supplementary Materials (Figure S1) indicate that the extract obtained from the steam distillation of cinnamon bark mainly comprises cinnamaldehyde with a small quantity of flavonoids and alkaloids. Unlike other previously reported works such as that of Ahmad et al. in which the reducing and capping agents of silver ions are attributed to the presence of phenols [39]. The silver nanoparticles system was prepared from hydro-distilled steam distillation, containing mainly cinnamaldehyde.

3.2. FTIR and GC-MS Characterization of Cinnamon Extract and AgNPs-Cinnamon

Following the separation of the oily phase from the semi-transparent white microemulsion obtained from the steam distillation of cinnamon bark, FTIR spectroscopy analysis was directly carried out to the obtained distillate, as well as to the purified and decanted aqueous phase. The resulting FTIR spectrum for purified cinnamaldehyde is presented in Figure 1A. The most prominent peaks in the spectrum can be attributed to the distinctive features of cinnamaldehyde. At 3028, 3062, and 3069 cm^{-1} due to the aromatic and olefinic stretching vibration of C-H groups. Additionally, at 2813 and 2742 cm^{-1}, the Fermi resonance of the C-H of the aldehyde is observed. The peak at 1673 cm^{-1} corresponds to the stretching of the conjugated carbonyl group C=O of the aldehyde, while the peak at 1625 cm^{-1} is associated with the stretching C=C of the conjugated olefin. The peak at 973 cm^{-1} is characteristic of C-H out-of-plane (oop) bending of a disubstituted trans-olefin group. The peaks between 1605 and 1451 cm^{-1} are associated with the vibrations of C=C in the aromatic structure. Furthermore, the peaks at lower wavenumbers at 744 and 688 cm^{-1} indicate a monosubstituted benzene's aromatic structure. Finally, a peak at 1121 cm^{-1} due to the stretching of the alpha carbon–aldehydic carbon C-C bond is also indicated. In addition, HPLC and GC-MS of the microemulsion were developed to evaluate the composition of the extract; both chromatograms are presented in the Supplementary Materials (Figures S2 and S3). The mass spectrum taken from the peak at 22.3 min of retention time of the GC-MC chromatogram is shown in Figure 1B, demonstrating the high purity of

cinnamaldehyde by the presence of their characteristic fragmentation pattern (m/z = 131, 103, 77, and 51) with the molecular ion and base peak at m/z = 131 as has been reported before [45].
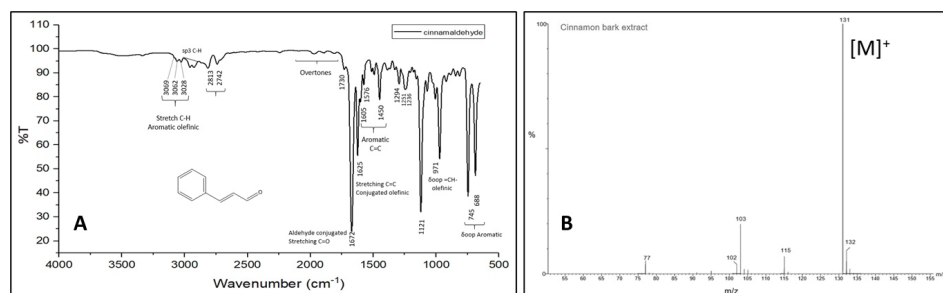

Figure 1. (**A**) FTIR spectrum and (**B**) GCMS spectrum of cinnamaldehyde extracted from cinnamon bark.

Figure 2 shows a comparison between the FTIR spectra of the extracted cinnamaldehyde and the solution resulting from the preparation of silver nanoparticles to explain the oxidation of cinnamaldehyde to cinnamic acid. Some differences in the spectra can be observed, i.e., the appearance of the peak at 3263 cm^{-1}, which could evidence the presence of O-H associated with the carboxylic acid, the disappearance or attenuation of the peaks at 2813 and 2742 cm^{-1} related to the C-H of aldehydes, as well as the appearance of the peak at 1148 cm^{-1} corresponding to stretching of C-O. These differences are clear evidence of the presence of carboxylic acid and that the cinnamaldehyde acts as a reducing agent in the formation of AgNPs-cinnamon. Additionally, it is important to highlight the presence of the double peaks related to the symmetrical and asymmetrical tensions of the carboxylates occurring at 1623–1571, 1373–1309, and 1062, and 1022 cm^{-1}, which explains their interaction with silver nanoparticles. The bimodal shape of these peaks suggests different size and shape distributions of silver nanoparticles. These results agree with what was previously reported by Premkumar et al. [71]. However, for the low energy bands, Premkumar's work reported several peaks in the region of 520 cm^{-1} that were assigned to vibrations of carbon halides (C-Cl, C-Br, C-I). In contrast, we observed a single broad peak at 695.87 cm^{-1} associated with the C-H aromatic bending as mentioned above.
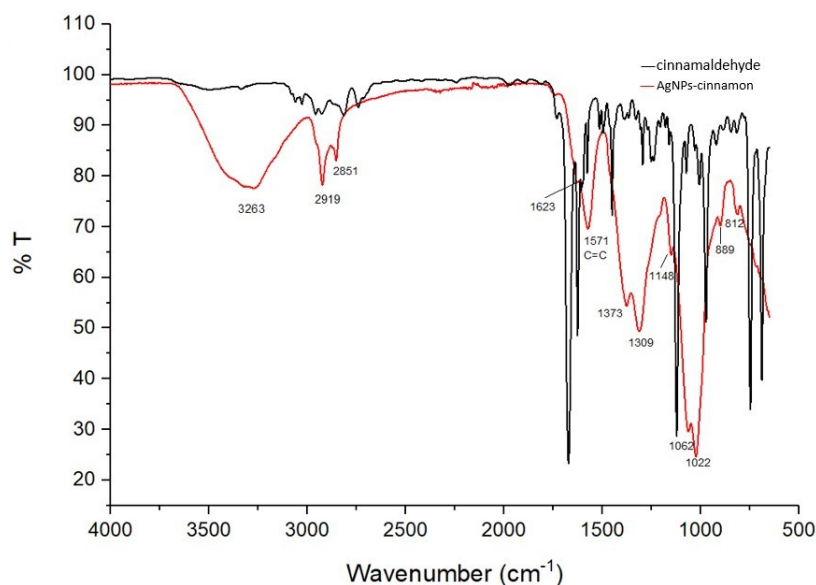

Figure 2. FTIR spectra of cinnamaldehyde extracted from cinnamon bark (black line) and the colloidal dispersion of synthesized silver nanoparticles, AgNPs-cinnamon (red line).

3.3. Surface Plasmon Resonance Analysis by UV-Vis Spectroscopy

The formation of the silver nanoparticles could be evidenced by the change in coloration presented by the colloidal dispersion obtained, as represented in Figure 3. This was further confirmed by the appearance of strong absorption bands 427.5 nm in the UV-Vis spectrum, as is shown in Figure 4, due to the collective oscillations of the conduction electrons of metal nanoparticles that come into resonance with the electromagnetic radiation with which the AgNPs are excited. This phenomenon of Surface Plasmon Resonance (SPR) can be considered as the signature optical property of noble metal nanoparticles [22,23,65]. The UV-Vis spectroscopy analysis allows not only the confirmation of the presence of silver nanoparticles but also the estimation of their shape [8,71]. In some cases, when describing nanoparticles, the term Localized Surface Plasmon Resonance refers to a particular kind of SPR in which the electromagnetic field remains localized in a nanoscale pattern surface [72]. The redshift from 400 nm implies the presence of shapes other than spherical nanoparticles due to surface faceting [5,71–73].

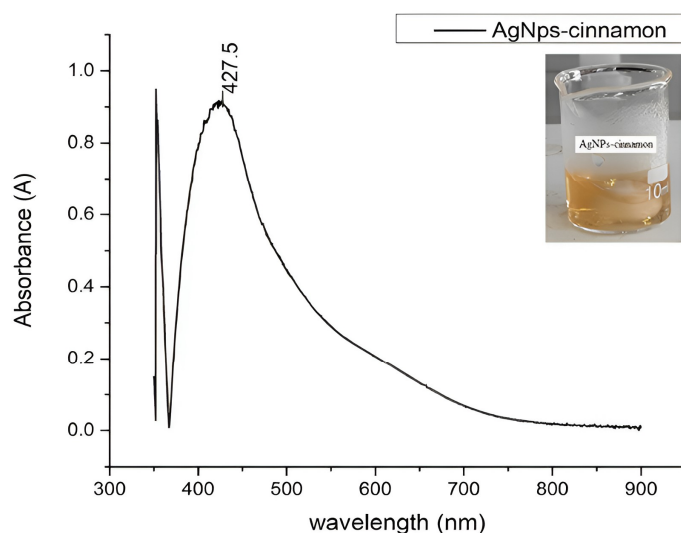**Figure 3.** Scheme of synthesis of silver nanoparticle from cinnamon bark extract.

Figure 4. UV-Vis spectrum of the product of the green synthesis of AgNPs-cinnamon.

In addition, a subtle shoulder can be distinguished at higher wavelengths, suggesting the existence of bigger silver nanoparticles with different shapes, showing the ability of the cinnamaldehyde extracted as a reducing and capping agent [8].

3.4. Morphological Analysis

TEM and SEM micrograph images of the synthesized AgNPs are displayed in Figure 5A and 5B, respectively. According to the shown image, the particle sizes of AgNPs ranged from approximately 5.9 to 31.7 nm. Figure 5A displays TEM micrographs illustrating the presence of AgNPs-cinnamon of different shapes, mostly spherical particles, of varying sizes. SEM image in Figure 5B shows structures beyond the spherical shape, confirming the red shift of the surface plasmon resonance (427.5 nm). The formation of silver nanoparticles confirms the reducing activity of cinnamaldehyde, the primary constituent of cinnamon bark extract, as discussed earlier.
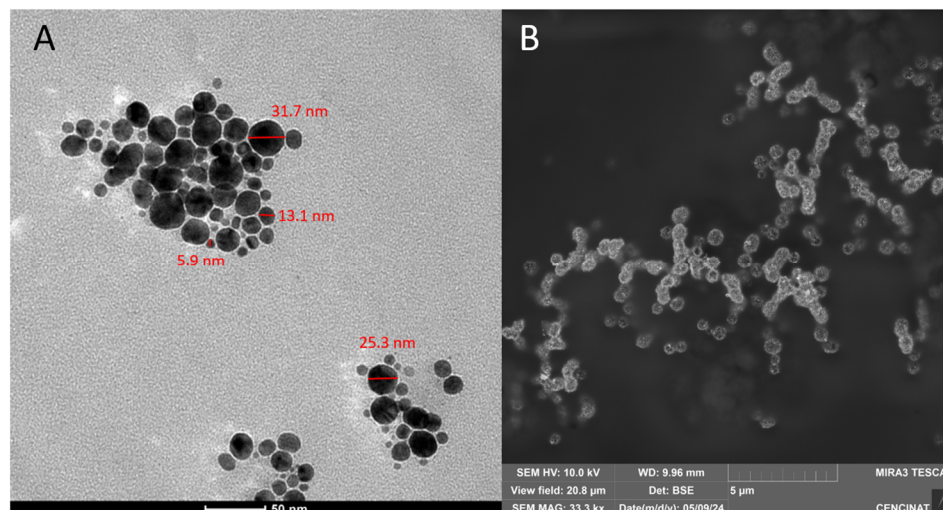
Figure 5. (**A**) TEM and (**B**) SEM images of AgNPs prepared from the cinnamon bark extract.

The shape of silver nanoparticles has been recognized as a critical factor influencing their bactericidal activity [74–76]. This phenomenon can be attributed to the shape-dependent disruption of cell membranes in Gram-negative bacteria, such as *E. coli* [77,78]. Alshareef et al. [79] have reported that silver nanoparticles in both spherical and rod shapes exhibit strong antimicrobial properties. However, Cheon et al. [80] observed variations in the bactericidal effectiveness of silver nanoparticles following this sequence: spherical > disc > triangular nanoparticles. In this regard, the presence of a combination of different shapes of AgNPs-cinnamon, as seen in Figure 5, could offer advantages in terms of bactericidal activity. This is because different shapes of nanoparticles may interact with bacterial cells in diverse ways, potentially leading to multiple mechanisms of cell disruption.

DLS analysis provides a graphical representation of the different sizes of the AgNPs-cinnamon obtained, along with their corresponding intensities. This illustration is shown in Figure 6A, in which three peaks can be distinguished, each with a different percentage of intensity. Each of these peaks, occurring at 2.94 nm, 8.7 nm, and 65.1 nm, are related to variable dimensions of silver nanoparticles in the sample. The effective diameter corresponds to 44.8 nm for a distribution polydispersity of 0.356. These results reveal a polydispersity in the nanoparticles, as observed by electron microscopy analysis and suggested by the FTIR spectroscopic analysis, supporting the idea of the presence of nanoparticles of different shapes.
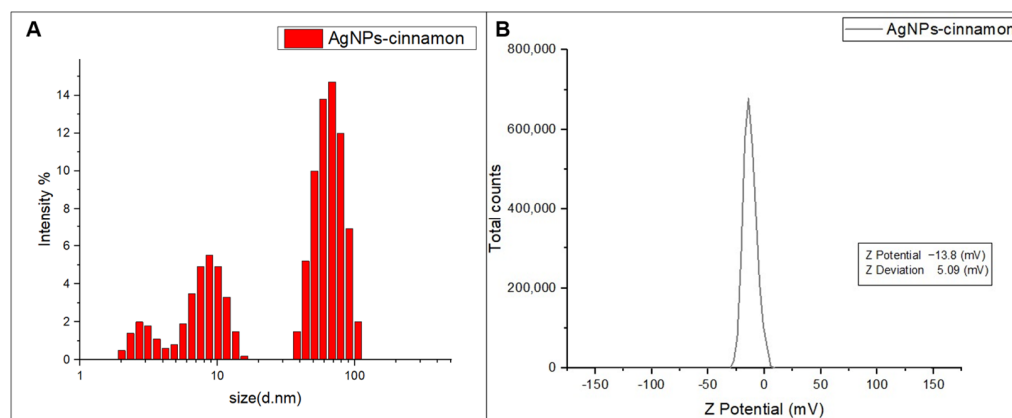

Figure 6. (**A**) Size of AgNPs-cinnamon measured by Dynamic Light Scattering, and (**B**) ζ−Potential determined for AgNPs-cinnamon.

By analyzing the $\zeta-$potential, it is possible to examine the potential associated with the surface of nanoparticles, as well as to attest to the stability of the nanoparticles, as long as the $\zeta-$potential values range between -30 mV and 30 mV [81]. The results obtained from this analysis are shown in Figure 6B, from which it is feasible to see that the AgNPs-cinnamon has a negative surface charge of -13.6 mV. This surface electrical potential value indicates the stability of AgNPs-cinnamon, as evidenced by the observed absence of noticeable changes in these systems after several months.

3.5. Evaluation of Antibacterial Properties

Results of the study of the bactericidal activity of the AgNPs-cinnamon and their precursors are shown in Figure 7 and in Table 1, the diameters of the inhibition zones are indicated. The control samples; silver nitrate (Blank 1) and cinnamon extract (Blank 2), show small zones of inhibition, suggesting a slight bactericidal capacity against Gram-negative and Gram-positive bacteria of silver ions and cinnamon extract.
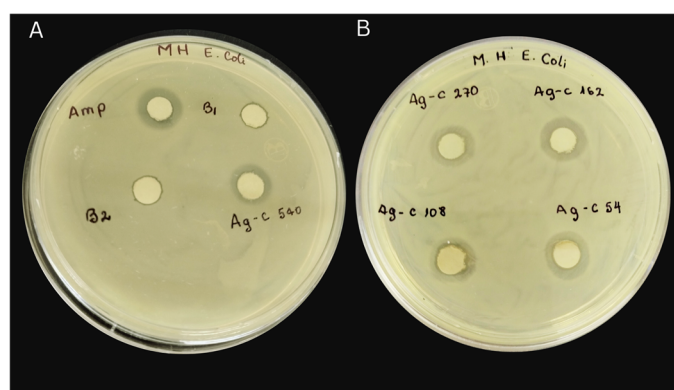

Figure 7. Disk diffusion assay results evaluating the effect of concentration of AgNPs on bacterial growth after incubation at 37 °C for 24 h on agar plates. (**A**) Amp = 10 µg ampicilin, B1 = 1.7 µg AgNO$_3$, B2 = 20 µL cinnamon bark extract, AgC-540 = AgNPs-cinnamon 540 µg/mL. (**B**) AgC-270 = AgNPs-cinnamon 270 µg/mL, AgC-162 = AgNPs-cinnamon 162 µg/mL, AgC-108 = AgNPs-cinnamon 108 µg/mL, AgC-54 = AgNPs-cinnamon 54 µg/mL.

Table 1. Results for antibacterial activity tests of AgNPs-cinnamon dispersions at different concentrations, silver nitrate (Blank 1), and cinnamon extract (Blank 2).

	Zone of Inhibition (mm)			
Sample	**C7230**	**PE52**	**AN54**	**29213**
Blank 1: AgNO$_3$	5.2	5.1	5.1	5.2
Blank 2: Cinnamon bark extract	6	6	6	6
AgNPs-cinnamon 54 µg/mL	7	9	6	6
AgNPs-cinnamon 108 µg/mL	15	10	7	6
AgNPs-cinnamon 162 µg/mL	13	10	7	7
AgNPs-cinnamon 270 µg/mL	16	14	14	10
AgNPs-cinnamon 540 µg/mL	15	15	14	10

Inhibition halos are present even at the lowest concentrations of AgNPs-cinnamon (54 µg/mL). As the concentration of the nanoparticles increases two and three times from its initial concentration, halos of greater diameter are observed (Table 1), indicating an increase in their bactericidal capacity (see Figure 7). This effect is further accentuated at higher concentrations of AgNPs showing inhibition halos that reach notable sizes, for example, the system AgNPs-cinnamon 540 µg/mL cause inhibition zones up to 15 mm in diameter for PE52, 14 mm for AN54, 15 mm for C7230, and 10 mm for 29213 bacteria. It is interesting to note that by increasing the AgNPs-cinnamon concentration from 270 µg/mL to 540 µg/mL, the values of the inhibition halos remain almost constant, suggesting that

the maximum antibacterial capacity of the evaluated system is reached. In summary, these results reveal that silver nanoparticles synthesized from cinnamon extract have bactericidal properties that vary with the AgNPs concentration, reaching their maximum efficacy at moderate concentrations, beyond which no substantial increase in bacterial inhibition is observed.

The result of the broth microdilution method is shown in Figure 8A for analysis of the antibacterial properties of AgNPs-cinnamon. By introducing the different sensitive and resistant bacteria tested into the wells, bacterial growth is clearly observed (Figure S5 in Supplementary Materials). In addition, the appearance of turbidity is distinguished, which indicates the proliferation of colonies. A similar phenomenon of bacterial growth is evident in the case of cinnamon extract, except for PE52 Pseudomonas bacteria, whose growth is inhibited by the cinnamon extract. However, as is detailed in Table 2, a marked antibacterial activity is appreciated for all of the tested bacteria in the wells with AgNPs-cinnamon since no bacterial growth is observed in any way. Li et al. examined the activity of AgNPs against *P. aeruginosa*, *S. epidermidis*, and *E. coli*, demonstrating that AgNPs are more active against *E. coli* than *P. aeruginosa* and *S. epidermidis* [82]. However, it is important to consider the dependence of antibacterial activity on the concentration of silver nanoparticles. From the various studies on MDR bacteria, AgNPs are effective against pathogenic bacteria such as *E. coli*, *S. Typhi*, *S. epidermidis*, and *S. aureus*, *P. aeruginosa* [70,82–85].
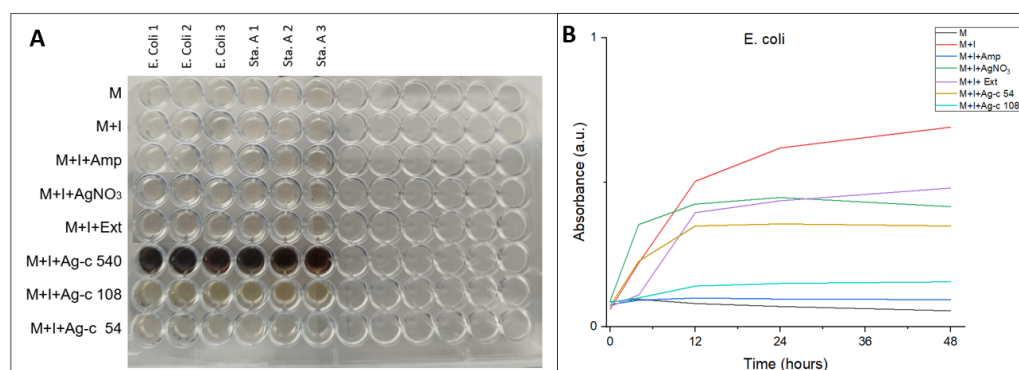

Figure 8. ELISA microplates of microdilution in broth assays (**A**) of AgNPs-cinnamon against *S. aureus* as a function of time (**B**). Different AgNPs concentration: 54 μg/mL and 108 μg/mL were evaluated. (M = medium, I = Inoculum, Amp = Ampicillin, Ext = Cinnamon bark extract).

Table 2. Antibacterial activity of cinnamon bark extract and AgNPs-cinnamon dispersions. Symbols '−' and '+' denote no antibacterial activity and high antibacterial activity, respectively.

Sample	KpE52	KpLC1	C7230	DH5α	PAO1	PE52	AN2	AN54	29213
Medium and Inoculum	−	−	−	−	−	−	−	−	−
Cinnamon bark extract	−	−	−	−	−	+	−	−	−
AgNPs-cinnamon	+	+	−	+	+	+	+	+	+

To evaluate the dependence of concentration on antibacterial activity, broth microdilution. Three different concentrations of silver nanoparticles were tested: Ag-c 54, Ag-c 108 and Ag-cc 540. The antibacterial activity was evaluated by measuring absorbance at a wavelength of 630 nm during 48 h, whose results are shown in Figure 8B. It is observed that silver nanoparticles with higher concentrations significantly inhibit bacterial growth.

The effect of AgNPs-cinnamon on the growth kinetics of *S. aureus* is shown in Figure 8B. Different growth stages can be identified, while the decline stage cannot be attained because the living and dead bacterial cells show absorbance at 630 nm [86]. The silver nitrate (Blank 1) acts as a bacteriostatic agent, attaining a constant stationary phase of bacteria growth at 12 h, while the cinnamon bark extract (Blank 2) does not reach it. On the other hand, the presence of AgNPs-cinnamon notably affects the growth of bacteria. The sample Ag-c

54, corresponding to 54 µg/mL AgNPs, exhibits a decrease in the absorbance, implying a decrease in the number of live bacterial cells. Furthermore, a higher concentration of AgNPs (108 µg/mL) results in a higher bacteriostatic behavior.

4. Conclusions

In this work, the synthesis of silver nanoparticles with antibacterial activity using cinnamon bark extract as a reducing and capping agent was successfully achieved. The process involved mixing the cinnamon extract, mainly composed of cinnamaldehyde, with a silver nitrate solution in a specific ratio, leading to the generation of silver nanoparticles (AgNPs-cinnamon). The formation process of AgNPs-cinnamon is mainly attributed to the interaction between silver nitrate and cinnamaldehyde and not with other constituents present in the cinnamon extract. This conclusion arises from phytochemical and spectroscopic analyses of the cinnamon extract, which consistently yielded negative results for the presence of protein and phenol compounds. These results are consistent with the GC-MS and HPLC analysis that confirm the high purity of cinnamaldehyde. However, the presence of a small content of flavonoids and alkaloids was confirmed, providing the appropriate conditions for the reduction of silver and the subsequent formation of silver nanoparticles. FTIR analysis revealed chemical modifications that occur in the cinnamaldehyde during the silver reduction process, with the appearance of carboxylic acid groups, supporting the proposed oxidation of cinnamaldehyde to cinnamic acid and their interaction with the silver nanoparticles. In addition, UV-Vis spectroscopy corroborated the presence of silver nanoparticles by detecting surface plasmon resonance (SPR) signals within the visible spectrum. The spectrum also suggests the coexistence of various shapes and sizes of nanoparticles.

The shape and size of AgNPs-cinnamon, analyzed by DLS, TEM, and SEM imaging, confirmed their morphological diversity. This variety of forms could potentially exert an influence on its bactericidal activity. Meanwhile, the DLS measurements indicated a polydispersity in the size of the nanoparticles, with several peaks corresponding to different dimensions. ζ-potential analysis indicates that AgNPs-cinnamon possesses a high enough surface charge, implying good stability.

An evaluation of the antibacterial properties of AgNPs-cinnamon was carried out through two different methodologies: disk diffusion and broth microdilution methods. It is important to mention that AgNPs-cinnamon showed bactericidal activity against various Gram-negative and Gram-positive, drug-sensitive, and drug-resistant bacteria. The bactericidal efficacy was directly correlated with the concentrations of AgNP-cinnamon. By contrast, cinnamon extract alone had minimal impact on bacterial growth. The morphological diversity exhibited by AgNPs-cinnamon is potentially important for improving its efficacy against different bacterial strains.

Supplementary Materials: The following supporting information can be downloaded at: https://www.mdpi.com/article/10.3390/bioengineering11050517/s1, Figure S1. UV-Vis spectrum of cinnamon bark extract. Figure S2. Chromatogram of cinnamon bark extract on the HILIC column. Peak 1 represents cinnamaldehyde and peaks 2 and 3 represent two minor components of the extract. Figure S3. GC chromatogram showing the characteristic base peak of cinnamaldehyde m/z = 131 at a retention time of 22.3 min. Table S1. Results of the determination of secondary metabolites in the cinnamon bark. Figure S4 Phytochemical screening of qualitative tests to secondary metabolites. Figure S5 ELISA microplate of broth microdilution method to analyze the antimicrobial activity of silver nanoparticles for the tested bacteria. Figure S6 Bacterial viability at 54, 108, and 540 µg/mL of AgNPs-cinnamon. Figure S7 Temporal progress of the AgNPs formation evaluated by the absorbance at plasmonic band wavelength. Figure S8 Plasmonic band of AgNPs-cinnamon as a function of silver nitrate concentration.

References

1. Mansoori, G.A.; Brandenburg, K.S. A Comparative Study of Two Folate-Conjugated Gold Nanoparticles for Cancer Nanotechnology Applications. *Cancers* **2010**, *2*, 1911–1928. [CrossRef] [PubMed]
2. Becker, R.O. Silver ions in the treatment of local infections. *Met. Based Drugs* **1999**, *6*, 311–314. [CrossRef] [PubMed]
3. More, P.R.; Pandt, S.; Filippis, A.; Franci, G.; Mijakovic, I.; Galdiero, M. Silver Nanoparticles: Bactericidal and Mechanistic Approach against Drug Resistant Pathogens. *Microorganisms* **2023**, *11*, 369. [CrossRef] [PubMed]
4. Giri, A.K.; Jena, B.; Biswal, B.; Pradhan, A.K.; Arakha, M.; Acharya, S.; Acharya, L. Green synthesis and characterization of silver nanoparticles using Eugenia roxburghii DC. extract and activity against biofilm-producing bacteria. *Sci. Rep.* **2022**, *12*, 8383.
5. Yaqoob, A.A.; Umar, K.; Ibrahim, M.N.M. Silver nanoparticles: Various methods of synthesis, size affecting factors and their potential applications—A review. *Appl. Nanosci.* **2020**, *10*, 1369–1378. [CrossRef]
6. Putta, S.; Sharma, R.K.; Khandelwal, P. Metal Nanoparticles: Synthesis, Characterization, and Biomedical Applications. In *Nanomaterials Advanced and Applications*; Singh, D., Singh, S., Singh, P., Eds.; Springer: Singapore, 2013; pp. 85–102.
7. Tavker, N.; Gaur, U.; Sharma, M. Agro-waste extracted cellulose supported silver phosphate nanostructures as a green photocatalyst for improved photodegradation of RhB dye and industrial fertilizer effluents. *Nanoscale Adv.* **2020**, *2*, 2870–2884. [CrossRef] [PubMed]
8. Granja, L.A.; Pineda-Aguilar, N.; Saucedo-Vázquez, J.P.; Suppan, G.; Lárez-Velázquez, C.; Galeas, S.; González, G.; López, F. Polyvinyl Alcohol Films Loaded with Silver Nanostructures with Different Sizes and Shapes with Tunable Plasmonic and Electric Properties. A Spectroscopic Study. *Mater. Res.* **2022**, *25*, e20210574. [CrossRef]
9. Hornyak, G.L.; Tibbals, H.F.; Dutta, J.; Moore, J.J. *Introduction to Nanoscience Nanotechnology*; CRC Press: Boca Raton, FL, USA, 2009.
10. Beyene, H.D.; Werkneh, A.A.; Bezabh, H.K.; Ambaye, T.G. Synthesis paradigm and applications of silver nanoparticles (AgNPs), a review. *Sustain. Mater. Technol.* **2017**, *13*, 18–23. [CrossRef]
11. Sudarman, F.; Shiddiq, M.; Armynah, B.; Tahir, D. Silver nanoparticles (AgNPs) synthesis methods as heavy-metal sensors: A review. *Int. J. Environ. Sci. Technol.* **2023**, *20*, 9351–9368. [CrossRef]
12. Menichetti, A.; Mavridi-Printezi, A.; Mordini, D.; Montalti, M. Effect of Size, Shape and Surface Functionalization on the Antibacterial Activity of Silver Nanoparticles. *J. Funct. Biomater.* **2023**, *14*, 244. [CrossRef]
13. Silva, L.P.; Silveira, A.P.; Bonatto, C.C.; Reis, I.G.; Milreu, P.V. Silver Nanoparticles as Antimicrobial Agents: Past, Present, and Future. In *Nanostructures for Antimicrobial Therapy: Nanostructures in Therapeutic Medicine Series*; Ficai, A., Grumezescu, A.M., Eds.; Elsevier: Amsterdam, The Netherlands, 2017; pp. 577–596.
14. Bruna, T.; Maldonado-Bravo, F.; Jara, P.; Caro, N. Silver Nanoparticles and Their Antibacterial Applications. *Int. J. Mol. Sci.* **2021**, *22*, 7202. [CrossRef]
15. Betts, J.W.; Hornsey, M.; La Ragione, R.M. Novel Antibacterials: Alternatives to Traditional Antibiotics. *Adv. Microb. Physiol.* **2018**, *73*, 123–169. [PubMed]
16. Natan, M.; Banin, E. From Nano to Micro: Using nanotechnology to combat microorganisms and their multidrug resistance. *FEMS Microbiol. Rev.* **2017**, *41*, 302–322. [CrossRef]
17. Lee, N.Y.; Ko, W.C.; Hsueh, P.R. Nanoparticles in the treatment of infections caused by multidrug-resistant organisms. *Front. Pharmacol.* **2019**, *10*, 1153. [CrossRef] [PubMed]
18. Prasastha, R.V.; Yasur, J.; Abishad, P.; Unni, V.; Purushottam, D.; Nishanth, M.A.D.; Niyeditha, P.; Vergis, J.; Singh, S.V.; Kullaiah, B.; et al. Antimicrobial Efficacy of Green Synthesized Nanosilver with Entrapped Cinnamaldehyde against Multi-Drug Resistant Enteroaggregative Escherichia coli in Galleria mellonella. *Pharmaceutics* **2022**, *14*, 1924. [CrossRef]

19. Nie, P.; Zhao, Y.; Xu, H. Synthesis, applications, toxicity and toxicity mechanisms of silver nanoparticles: A review. *Ecotoxicol. Environ. Saf.* **2023**, *253*, 114636. [CrossRef] [PubMed]

20. Kang, Z.; Asanithi, P.; Chaiyakun, S.; Limsuwan, P. Growth of Silver Nanoparticles by DC Magnetron Sputtering. *J. Nanomater.* **2012**, *2012*, 963909.

21. Davis, P.; Morrisey, C.P.; Tuley, S.M.V.; Bingham, C.I. Synthesis and Stabilization of Colloidal Gold Nanoparticle Suspensions for SERS. In *Nanoparticles: Synthesis, Stabilization, Passivation, and Functionalization*; Nagarajan, R., Alan Hatton, T., Eds.; ACS Symposium Series; ACS Division of Colloid and Surface Chemistry: Washington, DC, USA, 2008.

22. Tao, A.; Sinsermsuksakul, P.; Yang, P. Polyhedral Silver Nanocrystals with Distinct Scattering Signatures. *Angew. Chem. Int. Ed.* **2006**, *45*, 4597–4601. [CrossRef]

23. Wiley, B.; Sun, Y.; Mayers, B.; Xia, Y. Shape-Controlled Synthesis of Metal Nanostructures: The Case of Silver. *Chem. Eur. J.* **2005**, *11*, 454–463. [CrossRef]

24. Rastogi, L.; Arunachalam, J. Sunlight based irradiation strategy for rapid green synthesis of highly stable silver nanoparticles using aqueous garlic (*Allium sativum*) extract and their antibacterial potential. *Mater. Chem. Phys.* **2011**, *129*, 558–563. [CrossRef]

25. Hasan, H.; Liu, X.; Zhou, S.; Horváth, P.G.; Bak, M.; Bejó, L.; Sipos, G.; Alpár, T. Functional silver nanoparticles synthesis from sustainable point of review: 2000 to 2023-A review on game changing materials. *Heliyon* **2022**, *8*, e12322. [CrossRef] [PubMed]

26. Chandra, H.; Kumari, P.; Bontempi, E.; Yadav, S. Medicinal plants: Treasure trove for green synthesis of metallic nanoparticles and their biomedical applications. *Biocatal. Agric. Biotechnol.* **2020**, *24*, 101518. [CrossRef]

27. Ahmed, S.; Ahmad, M.; Swami, B.L.; Ikram, S. A Review on Plants Extract Mediated Synthesis of Silver Nanoparticles for Antimicrobial Applications: A Green Expertise. *J. Adv. Res.* **2016**, *7*, 17–28. [CrossRef] [PubMed]

28. Chandran, S.; Chaudhary, M.; Pasricha, R.; Ahmad, A.; Satry, M. Synthesis of Gold Nanotriangles and Silver Nanoparticles Using Aloe Vera Plant Extract. *Biotechnol. Prog.* **2008**, *22*, 577–583. [CrossRef] [PubMed]

29. Krishnaraj, C.; Jagan, E.G.; Rajasekar, S.; Selvakumar, P.; Kalaichelvan, P.T.; Mohan, N. Synthesis of silver nanoparticles using Acalypha indica leaf extracts and its antibacterial activity against water borne pathogens. *Colloids Surf. B Biointerfaces* **2010**, *76*, 50–56. [CrossRef] [PubMed]

30. Song, J.; Kim, B.S. Rapid biological synthesis of silver nanoparticles using plant leaf extracts. *Bioprocess Biosyst. Eng.* **2009**, *32*, 79–84. [CrossRef]

31. Li, S.; Shen, Y.; Xie, A.; Yu, X.; Qiu, L.; Zhang, L.; Zhang, Q. Green synthesis of silver nanoparticles using *Capsicum annuum* L. extract. *Green Chem.* **2007**, *9*, 852–858. [CrossRef]

32. MubarakAli, D.; Thajuddin, N.; Jeganathan, K.; Gunasekaran, M. Plant extract mediated synthesis of silver and gold nanoparticles and its antibacterial activity against clinically isolated pathogens. *Colloids Surf. B Biointerfaces* **2011**, *85*, 360–365. [CrossRef]

33. Kaviya, S.; Santhanalakshmi, J.; Viswanathan, B.; Muthumary, J.; Srinivasan, K. Biosynthesis of silver nanoparticles using citrus sinensis peel extract and its antibacterial activity. *Spectrochim. Acta Part A Mol. Biomol. Spectrosc.* **2011**, *79*, 594–598. [CrossRef]

34. Ghasemi, S.; Dabirian, S.; Kariminejad, F.; Koohi, D.E.; Nemattalab, M.; Majidimoghadam, S.; Zamani, E.; Yousefbeyk, F. Process optimization for green synthesis of silver nanoparticles using Rubus discolor leaves extract and its biological activities against multi-drug resistant bacteria and cancer cells. *Sci. Rep.* **2024**, *14*, 4130. [CrossRef]

35. Alburae, N.; Alshamrani, R.; Mohammed, A.E. Bioactive silver nanoparticles fabricated using Lasiurus scindicus and Panicum turgidum seed extracts: Anticancer and antibacterial efficiency. *Sci. Rep.* **2024**, *14*, 4162. [CrossRef] [PubMed]

36. Thirumoorthy, G.; Balasubramanian, B.; George, J.A.; Nizam, A.; Nagella, P.; Srinatha, N.; Pappuswamy, M.; Alanazi, A.M.; Meyyazhagan, A.; Rengasamy, K.R.R.; et al. Phytofabricated bimetallic synthesis of silver-copper nanoparticles using *Aerva lanata* extract to evaluate their potential cytotoxic and antimicrobial activities. *Sci. Rep.* **2024**, *14*, 1270. [CrossRef] [PubMed]

37. Balaji, D.S.; Basavaraja, S.; Deshpande, R.; Mahesh, D.B.; Prabhakar, B.K.; Venkataraman, A. Extracellular biosynthesis of functionalized silver nanoparticles by strains of Cladosporium cladosporioides fungus. *Colloids Surf. B Biointerfaces* **2009**, *68*, 88–92. [CrossRef] [PubMed]

38. Mustapha, T.; Misni, N.; Ithnin, N.R.; Daskum, A.M.; Unyah, N.Z. A Review on Plants and Microorganisms Mediated Synthesis of Silver Nanoparticles, Role of Plants Metabolites and Applications. *Appl. Microbiol. Biotechnol.* **2022**, *19*, 674. [CrossRef] [PubMed]

39. Ahmad, A.; Mushtaq, Z.; Saeed, F.; Afzaal, M.; Al Jbawi, E. Ultrasonic-assisted green synthesis of silver nanoparticles through cinnamon extract: Biochemical, structural, and antimicrobial properties. *Appl. Microbiol. Biotechnol.* **2023**, *26*, 1984–1994. [CrossRef]

40. de Carvalho, W.L.; Boriollo, M.F.G.; Tonon, C.C.; da Silva, J.J.; Cruz, F.M.; Martins, A.L.; Höfling, J.F.; Spolidorio, D.M.P. Antimicrobial effects of silver nanoparticles and extracts of Syzygium cumini flowers and seeds: Periodontal, cariogenic and opportunistic pathogens. *Arch. Oral Biol.* **2021**, *125*, 105101. [CrossRef] [PubMed]

41. Li, W.R.; Shi, Q.S.; Ouyang, Y.S.; Chen, Y.B.; Duan, S.S. Antifungal effects of citronella oil against Aspergillus niger ATCC 16404. *Appl. Microbiol. Biotechnol.* **2013**, *97*, 7483–7492. [CrossRef]

42. Furtado, G.; Medeiros, A. Single-Disk Diffusion Testing (Kirby-Bauer) of Susceptibility of *Proteus mirabilis* to Chloramphenicol: Significance of the Intermediate Category. *J. Clin. Microbiol.* **1980**, *12*, 550–553. [CrossRef] [PubMed]

43. Xu, L.; Wang, Y.Y.; Huang, J.; Chen, C.Y.; Wang, Z.X.; Xie, H. Silver nanoparticles: Synthesis, medical applications and biosafety. *Theranostics* **2020**, *10*, 8996–9031. [CrossRef]

44. Nabikhan, A.; Kandasamy, K.; Raj, A.; Alikunhi, N. Synthesis of antimicrobial silver nanoparticles by callus and leaf extracts forms saltmarsh plant, *Sesuvium portulacastrum* L. *Colloids Surf. B Biointerfaces* **2010**, *79*, 488–493. [CrossRef]

45. Tambe, E.; Gotmare, S. Mass Spectra Interpretation of Cinnamaldehyde Present in Whole and Powdered Cinnamon Oil. *Int. J. Recent Sci. Res.* **2022**, *13*, 1127–1129.

46. Mariselvan, R.; Ranjitsingh, A.L.; Usha, R.N.A.; Kalirajan, K.; Padmalatha, C.; Mosae, S.P. Green synthesis of silver nanoparticles from the extract of the inflorescence of *Cocos nucifera* (Family: Arecaceae) for enhanced antibacterial activity. *Spectrochim. Acta Part A Mol. Biomol. Spectrosc.* **2014**, *6*, 537–541. [CrossRef]

47. Elavazhagan, T.; Arunachalam, K.D. Memecylon edule leaf extract mediated green synthesis of silver and gold nanoparticles. *Int. J. Nanomed.* **2011**, *6*, 1265–1278. [CrossRef]

48. Loo, Y.Y.; Rukayadi, Y.; Nor-Khaizura, M.A.; Kuan, C.H.; Chieng, B.W.; Nishibuchi, M.; Radu, S. In Vitro Antimicrobial Activity of Green Synthesized Silver Nanoparticles Against Selected Gram-Negative Foodborne Pathogens. *Front. Microbiol.* **2018**, *9*, 1555. [CrossRef]

49. Chen, C.Y.; Yin, H.; Chen, X.; Chen, T.H.; Liu, H.M.; Rao, S.S.; Tan, Y.J.; Qian, Y.X.; Liu, Y.W.; Hu, X.K.; et al. Ångstrom-scale silver particle–embedded carbomer gel promotes wound healing by inhibiting bacterial colonization and inflammation. *Sci. Adv.* **2020**, *6*, eaba0942. [CrossRef] [PubMed]

50. Wang, Z.X.; Chen, C.Y.; Wang, Y.; Li, F.X.; Huang, J.; Luo, Z.W.; Rao, S.S.; Tan, Y.J.; Liu, Y.W.; Yin, X.; et al. Ångstrom-Scale Silver Particles as a Promising Agent for Low-Toxicity Broad-Spectrum Potent Anticancer Therapy. *Adv. Funct. Mater.* **2019**, *29*, 1808556. [CrossRef]

51. Khan, S.; Zahoor, M.; Khan, R.S.; Ikram, M.; Islam, N. The impact of silver nanoparticles on the growth of plants: The agriculture applications. *Heliyon* **2023**, *9*, e16928. [CrossRef] [PubMed]

52. Petronella, F.; Madeleine, T.; De Mei, V.; Zaccagnini, F.; Striccoli, M.; D'Alessandro, G. Thermoplasmonic Controlled Optical Absorber Based on a Liquid Crystal Metasurface. *ACS Appl. Mater. Interfaces* **2023**, *15*, 49468–49477. [CrossRef]

53. Yin, I.X.; Zhang, J.; Zhao, I.S.; Mei, M.L.; Li, Q.; Chu, C.H. The Antibacterial Mechanism of Silver Nanoparticles and Its Application in Dentistry. *IJN* **2020**, *15*, 2555–2562. [CrossRef]

54. Kalwar, K.; Shan, D. Antimicrobial Effect of Silver Nanoparticles (AgNPs) and Their Mechanism—A Mini Review. *Micro Amp. Nano Lett.* **2018**, *13*, 277–280. [CrossRef]

55. Russell, A.D.; Hugo, W.B. Antimicrobial Activity and Action of Silver. In *Progress in Medicinal Chemistry*; Ellis, G.P., Luscombe, D.K., Eds.; Elsevier: Amsterdam, The Netherlands, 1994; Volume 31, pp. 351–370.

56. Adeyemi, O.S.; Shittu, E.O.; Akpor, O.B.; Rotimi, D.; Batiha, G. Silver Nanoparticles Restrict Microbial Growth by Promoting Oxidative Stress and DNA Damage. *EXCLI J.* **2020**, *19*, 492–500. [PubMed]

57. Ravichandiran, P.; Sheet, S.; Premnath, D.; Kim, A.R.; Yoo, D. 1,4-Naphthoquinone Analogues: Potent Antibacterial Agents and Mode of Action Evaluation. *Molecules* **2019**, *24*, 1437. [CrossRef]

58. Ravichandiran, P.; Masłyk, M.; Sheet, S.; Janeczko, M.; Premnath, D.; Kim, A.R.; Park, B.H.; Han, M.H.; Yoo, D. Synthesis and Antimicrobial Evaluation of 1,4-Naphthoquinone Derivatives as Potential Antibacterial Agents. *Chem. Open* **2019**, *8*, 589–600. [CrossRef] [PubMed]

59. Shanmuganathan, R.; MubarakAli, D.; Prabakar, D.; Muthukumar, H.; Thajuddin, N.; Kumar, S.S.; Pugazhendhi, A. An Enhancement of Antimicrobial Efficacy of Biogenic and Ceftriaxone-Conjugated Silver Nanoparticles: Green Approach. *Environ. Sci. Pollut. Res.* **2018**, *25*, 10362–10370. [CrossRef] [PubMed]

60. Gosh, I.N.; Patil, S.D.; Sharma, T.K.; Srivastava, S.K.; Pathania, R.; Navani, N.K. Synergistic action of cinnamaldehyde with silver nanoparticles against spore-forming bacteria: A case for judicious use of silver nanoparticles for antibacterial applications. *Int. J. Nanomed.* **2013**, *8*, 4721–4731.

61. Murugaiyan, J.; Kumar, P.A.; Rao, G.S.; Iskandar, K.; Hawser, S.; Hays, J.P.; Mohsen, Y.; Adukkadukkam, S.; Awuah, W.A.; Jose, R.A.M.; et al. Progress in Alternative Strategies to Combat Antimicrobial Resistance: Focus on Antibiotics. *Antibiotics* **2022**, *11*, 20. [CrossRef] [PubMed]

62. Weldick, P.J.; Wang, A.; Halbus, A.F.; Paunov, V.N. Emerging nanotechnologies for targeting antimicrobial resistance. *Nanoscale* **2022**, *14*, 4018–4041. [CrossRef] [PubMed]

63. Ahmad, R.; Srivastava, S.; Ghosh, S.; Khare, S.K. Phytochemical delivery through nanocarriers: A review. *Colloids Surf. B Biointerfaces* **2021**, *14*, 111389. [CrossRef] [PubMed]

64. Sweet, M.J.; Chessher, A.; Singleton, I. Metal-Based Nanoparticles; Size, Function, and Areas for Advancement in Applied Microbiology. In *Advances in Applied Microbiology*; Elsevier: Amsterdam, The Netherlands, 2012.

65. Majeed, M.; Hakeem, K.R.; Rehman, R.U. Synergistic effects of plant extract coupled silver nanoparticles in various therapeutic applications- present insights and bottlenecks. *Chemosphere* **2022**, *288*, 132527. [CrossRef]

66. Alkhathlan, A.H.; Al-Abdulkarim, H.A.; Khan, M.; Khan, M.; Alkholief, M.; Alshamsan, A.; Almomen, A.; Albekairi, N.; Alkhathlan, H.Z.; Siddiqui, M.R.H. Evaluation of the Anticancer Activity of Phytomolecules Conjugated Gold Nanoparticles Synthesized by Aqueous Extracts of *Zingiber officinale* (Ginger) and *Nigella sativa* L. Seeds (Black Cumin). *Materials* **2021**, *14*, 3368. [CrossRef]

67. van Liefferinge, E.; Forte, C.; Degroote, J.; Ovyn, A.; van Noten, N.; Mangelinckx, S.; Michiels, J. In vitro and in vivo antimicrobial activity of cinnamaldehyde and derivatives towards the intestinal bacteria of the weaned piglet. *Ital. J. Anim. Sci.* **2022**, *21*, 493–506. [CrossRef]

68. Al-Bayati, F.A.; Muthanna, J.M. Isolation, identification, and purification of cinnamaldehyde from Cinnamomum zeylanicum bark oil. An antibacterial study. *Pharm. Biol.* **2009**, *47*, 61–66. [CrossRef]

69. Ramasamy, M.; Lee, J.-H.; Lee, J. Direct one-pot synthesis of cinnamaldehyde immobilized on gold nanoparticles and their antibiofilm properties. *Colloids Surf. B Biointerfaces* **2017**, *160*, 639–648. [CrossRef] [PubMed]

70. Mattei, A.S.; Alves, S.H.; Severo, C.B.; Guazzelli Lda, S.; Oliveira Fde, M.; Severo, L.C. Use of Mueller-Hinton Broth and Agar in The Germ Tube Test. *Ins. Med. Trop.* **2014**, *56*, 483–485. [CrossRef]

71. Premkumar, J.; Sudhakar, T.; Dhakal, A.; Shrestha, J.B.; Krishnakumar, S.; Balashanmugam, P. Synthesis of silver nanoparticles (AgNPs) from cinnamon against bacterial pathogens. *Biocatal. Agric. Biotechnol.* **2018**, *15*, 311–316. [CrossRef]

72. Cruz, D.A.; Rodriguez, M. Nanoparticulas metalicas y plasmones de superficie: Una relacion profund. *Av. En Cienc. E Ing.* **2012**, *3*, 67–78.

73. Amendola, V.; Pilot, R.; Frasconi, M.; Marago, O.M.; Iatì, M.A. Surface plasmon resonance in gold nanoparticles: A review. *J. Phys. Condens. Matter* **2017**, *29*, 203002. [CrossRef] [PubMed]

74. Anker, J.N.; Hall, W.P.; Lyandres, O.; Shah, N.C.; Zhao, J.; van Duyne, R. Biosensing with plasmonic nanosensors. *Nat. Mater.* **2008**, *7*, 442–453. [CrossRef] [PubMed]

75. Dakal, T.C.; Kumar, A.; Majumdar, R.S.; Yadav, V. Mechanistic Basis of Antimicrobial Actions of Silver Nanoparticles. *Front. Microbiol.* **2016**, *7*, 1831. [CrossRef]

76. Raza, M.A.; Kanwal, Z.; Rauf, A.; Sabri, A.N.; Riaz, S.; Naseem, S. Size- and Shape-Dependent Antibacterial Studies of Silver Nanoparticles Synthesized by Wet Chemical Routes. *Nanomaterials* **2016**, *6*, 74. [CrossRef]

77. Acharya, D.; Singha, K.M.; Pandey, P.; Mohanta, B.; Rajkumari, J.; Singha, L.P. Shape Dependent Physical Mutilation and Lethal Effects of Silver Nanoparticles on Bacteria. *Sci. Rep.* **2018**, *8*, 201. [CrossRef] [PubMed]

78. Pal, S.; Tak, Y.K.; Song, J.M. Does the Antibacterial Activity of Silver Nanoparticles Depend on the Shape of the Nanoparticle. A Study of the Gram-Negative Bacterium *Escherichia coli*. *Appl. Environ. Microbiol.* **2007**, *73*, 1712–1720. [CrossRef] [PubMed]

79. Alshareef, A.; Laird, K.; Cross, R.B.M. Shape-dependent antibacterial activity of silver nanoparticles on Escherichia coli and Enterococcus faecium bacterium. *Appl. Surf. Sci.* **2017**, *424*, 310–315. [CrossRef]

80. Cheon, J.Y.; Kim, S.J.; Rhee, Y.H.; Kwon, O.H.; Park, W.H. Shape-dependent antimicrobial activities of silver nanoparticles. *Int. J. Nanomed.* **2019**, *14*, 2773–2780. [CrossRef] [PubMed]

81. Zhang, Y.; Chen, Y.; Westerhoff, P.; Hristovski, K.; Crittenden, J.C. Stability of commercial metal oxide nanoparticles in water. *Water Res.* **2008**, *42*, 2204–2212. [CrossRef] [PubMed]

82. Li, W.R.; Sun, T.L.; Zhou, S.L.; Ma, Y.K.; Shi, Q.S.; Xie, Z.B.; Huang, X.M. A comparative analysis of antibacterial activity, dynamics, and effects of silver ions and silver nanoparticles against four bacterial strains. *Int. Biodeterior. Biodegrad.* **2017**, *123*, 304–310. [CrossRef]

83. Ouda, M. Some Nanoparticles Effects on *Proteus* sp. *and KLebsiella sp. Isolated from Water*. *AJIDM* **2014**, *2*, 4–10.

84. Lara, H.H.; Ayala-Núñez, N.V.; Ixtepan, L.D.C.; Rodríguez, C. Bactericidal Effect of Silver Nanoparticles against Multidrug-Resistant Bacteria. *World J. Microbiol. Biotechnol.* **2010**, *26*, 615–621. [CrossRef]

85. Kora, A.J.; Arunachalam, J. Assessment of Antibacterial Activity of Silver Nanoparticles on *Pseudomonas aeruginosa* and Its Mechanism of Action. *World J. Microbiol. Biotechnol.* **2011**, *27*, 1209–1216. [CrossRef]

86. Chouhan, S.; Guleria, S. Green synthesis of AgNPs using *Cannabis sativa* leaf extract: Characterization, antibacterial, anti-yeast and a-amylase inhibitory activity. *Mater. Sci. Energy Technol.* **2020**, *3*, 536–544. [CrossRef]